Analysis of Bloch Formalism In Undamped And Damped Periodic Structures

A Thesis
Presented to
The Academic Faculty

by

Farhad Farzbod

In Partial Fulfillment
of the Requirements for the Degree
Doctor of Philosophy

George W. Woodruff School of Mechanical Engineering
Georgia Institute of Technology
December 2010

Analysis of Bloch Formalism In Undamped And Damped Periodic Structures

Approved by:

Professor Michael J. Leamy, Advisor
School of Mechanical Engineering
Georgia Institute of Technology

Professor Massimo Ruzzene
School of Aerospace Engineering
Georgia Institute of Technology

Professor Hamid Garmestani
School of Materials Science and Engineering
Georgia Institute of Technology

Professor Nader Sadegh
School of Mechanical Engineering
Georgia Institute of Technology

Professor Samuel Graham
School of Mechanical Engineering
Georgia Institute of Technology

Date Approved: November 10, 2010

ACKNOWLEDGEMENTS

I would like to express my sincere thanks to Dr. Michael J. Leamy, my advisor for his guidance, patience and support throughout my graduate study. Also I would like to thank Dr. Nader Sadegh for his guidance and support during the first few years of my graduate studies. Thanks are also due to the other committee members Dr. Massimo Ruzzene, Dr. Hamid Garmestani and Dr. Samuel Graham. I take this opportunity to express my gratitude to my friends and colleagues who made my stay here in Atlanta a joyful period of my life. I was blessed with their friendship and support.

Last but not least, I would like to express my deepest gratitude to my parents. My father's support and wisdom made my life's journey much more interesting and my mother's kindness and vision gave meaning to my childhood memories.

TABLE OF CONTENTS

LIST OF TABLES

LIST OF FIGURES

SUMMARY

Bloch analysis was originally developed by Felix Bloch to solve Schrödinger's equation for the electron wave function in a periodic potential field, such as that found in a pristine crystalline solid. His method has since been adapted to study elastic wave propagation in periodic structures. The absence of a rigorous mathematical analysis of the approach, as applied to periodic structures, has resulted in mistreatment of internal forces and misapplication to nonlinear media. In this thesis, we detail a mathematical basis for Bloch analysis and thereby shed important light on the proper application of the technique. We show conclusively that translational invariance is not a proper justification for invoking the existence of a "propagation constant," and that in nonlinear media this results in a flawed analysis. Next, we propose a general framework for applying Bloch analysis in damped systems and investigate the effect of damping on dispersion curves. In the context of Schrödinger's equation, damping is absent and energy is conserved. In the damped setting, application of Bloch analysis is not straight-forward and requires additional considerations in order to obtain valid results. Results are presented in which the approach is applied to example structures. These results reveal that damping may introduce wavenumber band gaps and bending of dispersion curves such that two or more temporal frequencies exist for each dispersion curve and wavenumber. We close the thesis by deriving conditions which predict the number of wavevectors at each frequency in a dispersion relation. This has important implications for the number of nearest neighbor interactions that must be included in a model in order to obtain dispersion predictions which match experiment.

CHAPTER I

INTRODUCTION

In this chapter we first provide motivation for studying periodic structures and then discuss wave propagation in these structures and our contribution in this regard. We close this chapter by providing a thesis overview.

1.1 Motivation

Structures with periodic features are found widely in nature and engineered systems (Fig.1). From an engineering perspective, the main interest in these structures stems from their ease of manufacture, significant impact and high temperature tolerance, and high strength-to-weight ratios [1]. For these properties, structures like the ones depicted in Fig.2 are being used abundantly in the aerospace industry.

Periodic assemblies can also be patterned in such a way that they show negative Poisson's ratio [9]-[11]. In addition, periodic structures provide advantageous wave propagation characteristics that are useful in wave guides and filters [12]. Due to their important role in industry, it is vital to model and understand wave phenomena in these structures. Another type of periodic structure, is the crystalline solid. Crystalline solids have been of interest for their electric and/or heat conductance properties. Carbon nanotubes, as an example, have been shown to have novel properties which make them a preferred choice in several applications of nanotechnology. In this thesis, we focus on the modelling of the engineering structures with macro-scale size. However, it is shown in Chapter 6 that the mass-spring model can characterize phononic band structures of crystals.

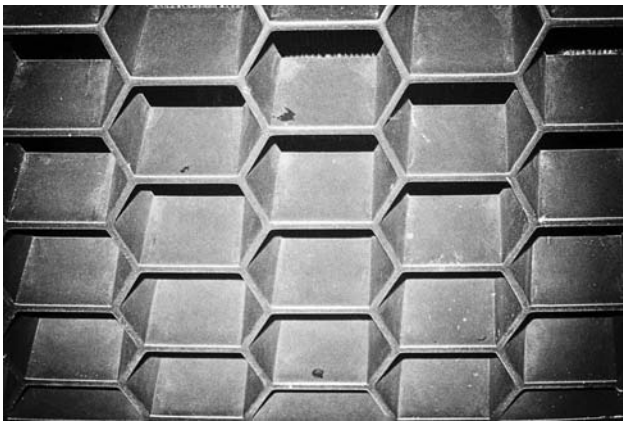

Figure 1: An example of a periodic structure [2].

1.2 Review of Wave Propagation in Undamped Periodic Structures

The modeling theories of periodic materials are not restricted to the engineering field. Wave propagation behavior in periodic media has been an area of interest for physicists and the like. Engineers are primarily interested in the wave characteristics of macroscopic periodic structures such as sandwich beams and honeycomb panels for airplane fuselages, while physicists study wave phenomena taking place in microscopic periodic medium, such as electron and phonon transport in crystals. These two approaches by engineers and physicists, developed independently and in parallel (until fairly recently) have both been referred to as Bloch analysis.

In the physical sciences, wave-like (hyperbolic) partial differential equations arise; these are parametrized by one or more periodic coefficients [28]. Generally, these equations take the form $\nabla^2\psi(\mathbf{r}) + \omega^2 F(\mathbf{r})\psi(\mathbf{r}) = 0$ in which $\psi(\mathbf{r})$ is a field vector at location $\mathbf{r}$ and $F(\mathbf{r})$ is a periodic function. Floquet studied this equation when stated in one-dimension and $F(\mathbf{r})$ is a cosine function (which yields Mathieu's equation). Bloch also solved a similar equation in quantum mechanics. Brillouin [28] used the Bloch theorem to solve the three dimensional wave equation. Since this time,

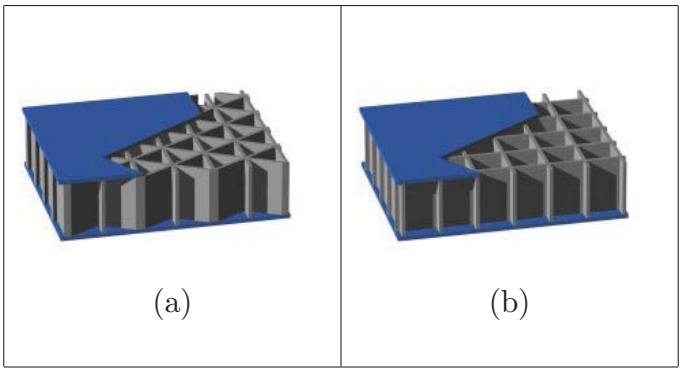

Figure 2: Schematic pictures of hexagonal (a) and square (b) honeycomb cores [7].

Bloch's method has been utilized in other physical sciences [29] as well as engineering applications, to include acoustics and the study of sonic crystals [30],[31].

In structural wave propagation, one of the early pioneers of the subject was Heckl [32]. He studied wave propagation in a beam with periodic discontinuities, such as in a grillage. In his work, Heckl assumed a thin-enough beam such that the usual linear differential equation for bending beams holds. Then, from translational invariance of the structure, he concluded the existence of the "propagation constant." He stated that in a single-frequency wave, displacements of two points q_1 and q_2 separated by a periodic length satisfy $q_2 = q_1.e^{\mu}$, where μ is the propagation constant. Another early pioneer of the field was Mead [33],[34], who applied Heckl's method for investigating harmonic wave propagation in periodic systems. He used the propagation constant to study both the displacements and the forces in a periodic system. His method reduces the size of the problem from the entire periodic structure to a single unit cell. Mead's work was followed by other researchers who analyzed a diverse variety of structures [35]-[45]. In his review paper [46], Mead addresses some of the relevant work which uses the propagation constant idea.

Advances in computation led to wide use of the finite element method in the study of wave propagation. The method transforms the equations governing a continuous

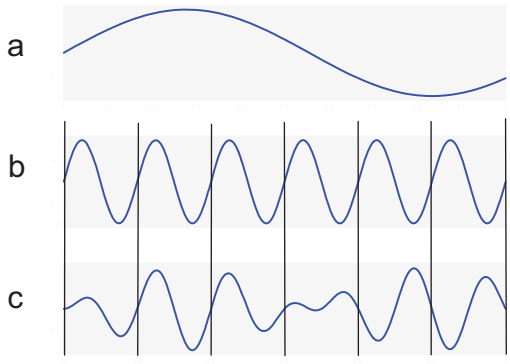

Figure 3: The envelope function, unit cell vibration and the product of them is depicted here for a 1-D case and some ω and $\mathbf{k}$. Graph (a) shows the external excitation exerted on the structure. In the graph b, the vertical lines are the cell boundary. The bottom graph (c) shows vibration of the lattice as the product of the envelope function (graph a) and the unit cell vibration (graph b).

medium to equations governing a finite degree-of-freedom system. In the finite element analysis of a structure, it is of great advantage if the equations of motion are written for a unit cell rather than the entire structure. However, as in any discrete treatment, the challenge is that the resulting equations of motion include internal forces on the right-hand side. Orris [47] used Mead's work to tackle this problem in investigating harmonic wave propagation in periodic structures. More recently, this method has been applied by Duhamel *et al.*[41] and Phani *et al.*[48] to investigate the acoustic band structure of example honeycomb structures. In these works and others, researchers exclusively use the fact that the equations of motion can be reduced to the minimum number of degrees of freedom (e.g., displacements) using Bloch analysis, and thus solve the wave equation on the boundary of the irreducible Brillouin zone. In their standard procedure, it has been assumed that the propagating wave through the structure has a sinusoidal envelope, which is defined by the propagation constant. This results in a Bloch relation between two consecutive lattice points or forces (see Fig. 3).

1.3 Contributions with Regards to Wave Propagation in Undamped Periodic Structures

Although the "propagation constant" method has been called Bloch analysis [48], there has been little effort to connect the two methods rigorously. This rigorous treatment is of particular concern since some researchers have applied the propagation constant technique in nonlinear cases [49], [50]. As is shown in Chapter III, we need the linearity of the differential equation of motion to prove the existence of a propagation constant; *i.e.,* the translational invariance in a structure is not a sufficient condition for the existence of a propagation constant. In this thesis, we develop a framework to rigorously connect Bloch analysis and the "propagation constant" technique. This framework also enables us to address other issues with wave propagation in periodic structures; in this regard, the contributions of the thesis are:

- We demonstrate that for any two- or three-dimensional periodic lattice, the forces on the boundary of the unit cell vanish upon the action of a linear transformation, and this results in an eigenvalue problem.
- Using the resulting eigenvalue problem, we rigorously link the previously used "propagation constant" technique to the Bloch analysis.
- Using the developed framework, we construct a simple counter-example to add to the growing evidence that considering only the boundary of the irreducible Brillouin zone may lead to erroneous calculations of the magnitude of band gaps.

1.4 Contributions with Regards to Damped Wave Propagation in Periodic Structures

As mentioned before, Bloch's method was originally developed by Felix Bloch [54] to solve Schrödinger's equation for the electron wave function in a periodic potential field, such as found in a pristine crystalline solid. Unlike electron wave functions, damping and energy dissipation mechanisms alter waves in periodic structures. Mead [34] provided an early discussion of damping in a 1-D infinite periodic structure. Mukherjee and Lee [77] investigated wave propagation in a viscoelastic composite. In their model, they assumed a real wavevector and complex temporal frequency; hence their analysis does not hold for the steady-state situation. Sprik and Wegdam [78] considered acoustic band gaps in composites of solids and viscous liquids. They considered both temporal and spatial attenuation in this special case only. Others [79]-[82] have investigated the effect of damping on limited numbers of layers and/or limited frequency damping models. Recently Hussein [83] studied the effect of damping on dispersion curves and band structures. In his paper, he restricted his investigation of band gap properties to the effect of Rayleigh-type damping. In our work, we address general linear damping for the steady state situation and our original contributions to this area include:

- We formulate Bloch analysis for generally damped periodic structures.
- We investigate the effect damping has on the range of admissible wavevectors and dispersion curves.
- We discuss phenomena which arise only in a damped periodic structure including:
  - Spatial frequency band gaps.

– Multiple frequencies for a given dispersion branch and wavevector.

1.5 Contributions with Regards to Phonon Dispersion

The mass-spring model as will be discussed in Chapter IV, also characterizes the force constant model of a crystalline material. Phonon dispersion curves of various crystals are obtained either by experiments or by *ab initio* calculations. The force constants are then calculated by fitting the mass-spring-model output into the experimental / *ab initio* results. The advantage of a force constant model is its simplicity and also the ease of application to similar materials. For example, the phonon dispersion curves of graphene are obtained by experiment, the force constants are next evaluated and then phonon dispersion curves of carbon nanotubes with any chiralities can be determined by the evaluated constants. Since there are several compounds that form layered structures similar to graphite, there exist several tubular nanostructures including nanotubes made out of BN [3], MoS_2 [4], BC_2N [5] and SiO_2 [6]. In the force constant model, there is a cut-off distance after which there is negligible interaction between atoms. Hence we need only to consider interaction between atoms up to, for example, the third nearest neighbor. There are models however, in which the forces between atoms are modeled by elastic beams [7], [8]. In these models, the interaction between the nearest neighbors are considered. In this thesis, by considering the number of wavevectors for each frequency in the dispersion relation, we derive conditions to check the validity of the nearest-neighbor-interaction model. This criterion is achieved by employing the framework we develop in the early chapters of the thesis. In short, our contribution in this regard is:

- We develop a framework to predict the maximum number of wavevectors for each frequency in the characterization of phonon dispersion.

1.6 Thesis Overview

We start by a short introduction of periodic structures and our contributions to this subject. In Chapter II, Bloch analysis is reviewed as we write about the origin of this theorem. We then detail a mathematical basis for invoking Bloch formalism in the analysis of periodic structures and connect Bloch analysis with the "Propagation constant" technique. In Chapter III, the treatment of forces in Bloch analysis is discussed. Chapter IV deals with the mathematical basis for Bloch analysis of damped structures. The validity of Bloch's theorem in these structures is explored and some new properties special to these structures are presented. In Chapter V, we investigate phonon dispersion curves of crystalline materials. It is shown that a mass-spring model is a useful tool by which we can reproduce experimental results. We then investigate the relation between the number of temporal frequencies and wavevectors. In Chapter VI, we propose follow-on research in this specific area.

CHAPTER II

MATHEMATICAL BASIS FOR BLOCH FORMALISM IN PERIODIC STRUCTURES

In this chapter, we first discuss Bloch analysis from its original perspective in quantum mechanics. Then we revisit Bloch analysis for discrete systems from a new perspective. We then address the role of asymmetry in investigating frequency band gaps. Most studies assume that the extremum of frequencies exclusively occur on the boundary of the irreducible Brillouin zone. While this is generally true in solid state physics, it is not strictly true in a general wave propagation problem [51], [52]. By constructing an asymmetrical counter-example, we add to growing evidence that this assumption might lead to erroneous conclusions about the extent of frequency band gaps. Finally, in Appendix A we show by example that invoking a propagation constant in nonlinear systems violates energy conservation.

2.1 Bloch Analysis

We first overview Bloch analysis as it has been applied to periodic structures. We then present the Bloch analysis in its original form as it arose in quantum mechanics. Finally, we rigorously demonstrate the Bloch relations (or propagation constants) for forces and displacements in periodic lattices.

2.1.1 Overview

Any lattice structure in a three dimensional space can be constructed by translating a repeating unit cell along three linearly independent - but not necessarily orthogonal - lattice vectors $\mathbf{a}_1, \mathbf{a}_2, \mathbf{a}_3$ [28]. Applying Lagrangian or Newtonian dynamics, the equations of motion for a unit cell take the following general form,

$$\mathbf{M}\ddot{\mathbf{q}}+\mathbf{K}\mathbf{q} = \mathbf{F}, \tag{1}$$

in which matrices $\mathbf{M}$ and $\mathbf{K}$ represent the global mass and stiffness matrices of the unit cell, $\mathbf{q}$ and $\ddot{\mathbf{q}}$ represents the (nodal) displacements and accelerations, and $\mathbf{F}$ denotes the (nodal) forces on that unit cell exerted by the neighboring cells in the structure. Bloch analysis starts with a harmonic solution for $\mathbf{q}$. As a result $\ddot{\mathbf{q}}$ can be replaced by $-\omega^2\mathbf{q}$, such that (1) takes the form:

$$(-\omega^2\mathbf{M} + \mathbf{K})\mathbf{q} = \mathbf{F}. \tag{2}$$

We denote the displacements of the cell located at $n_1\mathbf{a}_1+n_2\mathbf{a}_2+n_3\mathbf{a}_3$ by $\mathbf{q}(n_1, n_2, n_3)$. In Chapter 3 we demonstrate rigorously that solutions to (2) exist having the property:

$$\mathbf{q}(n_1, n_2, n_3) = e^{\mathbf{k}\cdot(n_1\mathbf{a}_1+n_2\mathbf{a}_2+n_3\mathbf{a}_3)}\mathbf{q}(0, 0, 0), \tag{3}$$

where $\mathbf{k}\cdot(n_1\mathbf{a}_1 + n_2\mathbf{a}_2 + n_3\mathbf{a}_3)$ is the general form of the propagation constant. As mentioned before, (3) has been used by most published works to reduce (2) to an eigenvalue problem. The resulting eigenvalue ω is the propagation frequency, and it is a function of $\mathbf{M}$ and $\mathbf{K}$ and wavevector $\mathbf{k}$. Each propagation mode of the entire lattice can be written as the product of an envelope harmonic function and the unit cell vibration; see Fig. 3 for an example.

2.1.2 Origins

Bloch theory was originally used to study the behavior of electrons in a crystal. The behavior of the electron wave function $\psi_k(\mathbf{r})$ with energy E_k follows the Schrödinger equation [53],

$$\left[-\frac{\hbar}{2m}\nabla^2 + V(\mathbf{r})\right]\psi_k(\mathbf{r}) = E_k\psi_k(\mathbf{r}) \ , \tag{4}$$

in which m is the mass of an electron and $\hbar$ is Planck's constant. For a single electron, *i.e.*, neglecting the magnetic effects, the potential energy from all other nuclei and electrons is periodic in the crystal: $V(\mathbf{r}) = V(\mathbf{r}+\mathbf{p})$ in which $\mathbf{p}$ is any lattice vector. In (4), the bracketed term is the Hamiltonian operator $\mathbf{H}(\mathbf{r})$. With this substitution, (4) can be restated in a more compact form as,

$$\mathbf{H}(\mathbf{r})\psi_k(\mathbf{r}) = E_k\psi_k(\mathbf{r}) \quad \text{and} \quad \mathbf{H}(\mathbf{r}) = \mathbf{H}(\mathbf{r}+\mathbf{p}). \tag{5}$$

It is well-known [54] that the solution to the eigenvalue problem of (5) takes the form:

$$\psi_k(\mathbf{r}+\mathbf{p}) = e^{i\mathbf{k}_e\cdot\mathbf{p}}\psi_k(\mathbf{r}), \tag{6}$$

in which $\mathbf{k}_e$ is the electron wavevector. In addition, due to the periodicity of the crystal, the probability of finding an electron would be the same at $\mathbf{r}+\mathbf{p}$ and $\mathbf{r}$:

$$\left|\psi_k(\mathbf{r}+\mathbf{p})\right|^2 = \left|\psi_k(\mathbf{r})\right|^2. \tag{7}$$

Here by substituting (6) into (7), we conclude $\left|e^{i\mathbf{k}_e\cdot\mathbf{p}}\right| = 1$ and hence that $\mathbf{k}_e\cdot\mathbf{p}$ is a real number.

Unlike the *inhomogeneous* equation of motion (2), the homogeneous wave equation in (5) is inherently an eigenvalue problem. Consequently, we cannot borrow Bloch's

analysis without proper justification. In other words, the existence of the propagation constant needs to be addressed within a proper mathematical treatment using (2).

2.2 Bloch Formalism in Periodic Structures

In this chapter we detail the mathematical basis for invoking Bloch formalism (3) in the analysis of periodic structures. In order to find the Bloch relation between the displacements, we presuppose a mapping which associates the displacements of a unit cell to the displacements of another unit cell without any assumption on its form or nature. This mapping holds for desired solutions to (2). Then with the use of symmetry in the system, we find the mathematical expression required for this mapping. To facilitate our goal, we first define a translation operator $\mathbf{T_V}$ for each lattice vector $\mathbf{V} = n_1\mathbf{a}_1 + n_2\mathbf{a}_2$ which upon operating on any function $f(\mathbf{r})$, shifts the argument by $\mathbf{V}$:

$$\mathbf{T_V} : f(\mathbf{r}) \longmapsto f(\mathbf{r} + \mathbf{V}). \tag{8}$$

For ease of notation, we associate x and y directions to $\mathbf{a}_1$ and $\mathbf{a}_2$ and identify translation operators $\mathbf{T}_x$, $\mathbf{T}_y$ and $\mathbf{T}_{xy}$ corresponding to $\mathbf{V}$'s equal to $\mathbf{a}_1$, $\mathbf{a}_2$, and $\mathbf{a}_1+\mathbf{a}_2$, respectively. We then consider a single unit cell in the lattice structure and define a minimal set of displacements. We denote them as $\mathbf{q}_i$ and $\widetilde{\mathbf{q}}$ for the internal and essential boundary displacements, respectively. The remaining nodal displacements in the unit cell can be determined by applying $\mathbf{T}_x$, $\mathbf{T}_y$ and $\mathbf{T}_{xy}$ on $\widetilde{\mathbf{q}}$; *i.e.*, by pushing $\widetilde{\mathbf{q}}$ forward in a combination of $\mathbf{a}_1$ and/or $\mathbf{a}_2$; see Fig. 4 for an example geometry. The relation between the minimum set of displacements $\mathbf{q}_i$, $\widetilde{\mathbf{q}}$ and the totality of unit cell displacements $\mathbf{q}$ is stated as [93]:

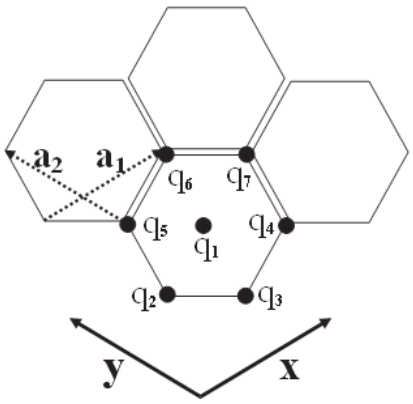

Figure 4: A honeycomb lattice, with the unit vectors $\mathbf{a}_1$and $\mathbf{a}_2$. The minimal set of displacements in a unit cell are $\mathbf{q}_i = [\mathbf{q}_1]$, $\widetilde{\mathbf{q}} = \begin{bmatrix} \mathbf{q}_2 & \mathbf{q}_3 \end{bmatrix}^T$. The rest of the displacements can be defined by pushing these minimal set in $\mathbf{a}_1$or/and $\mathbf{a}_2$ direction: $[\mathbf{q}_4] = \mathbf{T}_x(\widetilde{\mathbf{q}}) = \widetilde{\mathbf{q}}_x$, $[\mathbf{q}_5] = \mathbf{T}_y(\widetilde{\mathbf{q}}) = \widetilde{\mathbf{q}}_y$, $\begin{bmatrix} \mathbf{q}_6 & \mathbf{q}_7 \end{bmatrix}^T = \mathbf{T}_{xy}(\widetilde{\mathbf{q}}) = \widetilde{\mathbf{q}}_{xy}$.

$$\mathbf{q} = \mathbf{T}\widehat{\mathbf{q}}\,, \tag{9}$$

in which

$$\widehat{\mathbf{q}} = \begin{bmatrix} \mathbf{q}_i \\ \widetilde{\mathbf{q}} \end{bmatrix}, \mathbf{T} = \begin{bmatrix} \mathbf{I} & \mathbf{0} \\ \mathbf{0} & \mathbf{I} \\ \mathbf{0} & \mathbf{T}_x \\ \mathbf{0} & \mathbf{T}_y \\ \mathbf{0} & \mathbf{T}_{xy} \end{bmatrix}, \tag{10}$$

such that $\mathbf{q}$ and $\mathbf{F}$ take the form

$$\mathbf{q} = \begin{bmatrix} \mathbf{q}_i \\ \widetilde{\mathbf{q}} \\ \widetilde{\mathbf{q}}_x \\ \widetilde{\mathbf{q}}_y \\ \widetilde{\mathbf{q}}_{xy} \end{bmatrix}, \mathbf{F} = \begin{bmatrix} \mathbf{F}_i \\ \mathbf{F}_{\widetilde{\mathbf{q}}}^{n_1,n_2} \\ \mathbf{F}_{\widetilde{\mathbf{q}}x}^{n_1,n_2} \\ \mathbf{F}_{\widetilde{\mathbf{q}}y}^{n_1,n_2} \\ \mathbf{F}_{\widetilde{\mathbf{q}}xy}^{n_1,n_2} \end{bmatrix}. \tag{11}$$

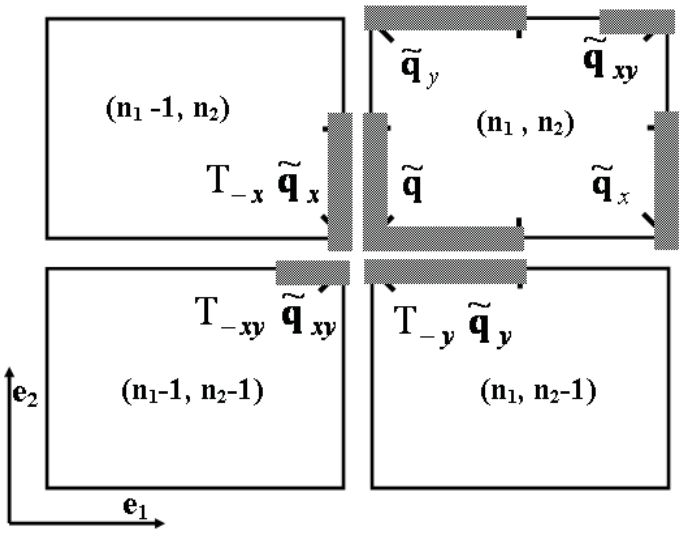

Figure 5: A schematic view of unit cell with its neighboring cells. In the cell (n_1, n_2), $\widetilde{\mathbf{q}}$ represents coordinates of the lower left shaded region. $\mathbf{T}_{-x}$ is an operator which pulls forces and displacements back in the x direction. The operators $\mathbf{T}_{-y}$ and $\mathbf{T}_{-xy}$ would do the same in their respective directions.

In (11), $\mathbf{F}^{n_1,n_2}_{\widetilde{\mathbf{q}}x}$ denotes the force located with $\widetilde{\mathbf{q}}_x$ and acting on the cell (n_1, n_2)[93]. Note that $\widetilde{\mathbf{q}}_x$ of the cell (n_1, n_2) is contained by $\widetilde{\mathbf{q}}$ of the cell (n_1+1, n_2). We can also define negative translation operators $\mathbf{T}^T_{-x}$, $\mathbf{T}^T_{-y}$ and $\mathbf{T}^T_{-xy}$. If $\mathbf{T}_x$ represents a pushing forward action in the x direction, then $\mathbf{T}^T_{-x}$ is a pulling back action in the same x direction (Fig. 5). Up to this point, we have not assumed the functional form of these mappings. The above conditions can be formally stated as:

$$\mathbf{T}^T_{-x}(\mathbf{F}^{n_1,n_2}_{\widetilde{\mathbf{q}}x}) = \mathbf{F}^{n_1-1,n_2}_{\widetilde{\mathbf{q}}x},\ \mathbf{T}^T_{-y}(\mathbf{F}^{n_1,n_2}_{\widetilde{\mathbf{q}}y}) = \mathbf{F}^{n_1,n_2-1}_{\widetilde{\mathbf{q}}y},\ \mathbf{T}^T_{-xy}(\mathbf{F}^{n_1,n_2}_{\widetilde{\mathbf{q}}xy}) = \mathbf{F}^{n_1-1,n_2-1}_{\widetilde{\mathbf{q}}x}. \quad (12)$$

Due to the equilibrium condition at $\widetilde{\mathbf{q}}$ (as can bee seen in the schematic shaded region in Fig. 6) we have the following result [93], [55]:

$$\begin{bmatrix} \mathbf{I} & \mathbf{0} & \mathbf{0} & \mathbf{0} & \mathbf{0} \\ \mathbf{0} & \mathbf{I} & \mathbf{T}^T_{-x} & \mathbf{T}^T_{-y} & \mathbf{T}^T_{-xy} \end{bmatrix} \mathbf{F} = \mathbf{0}. \quad (13)$$

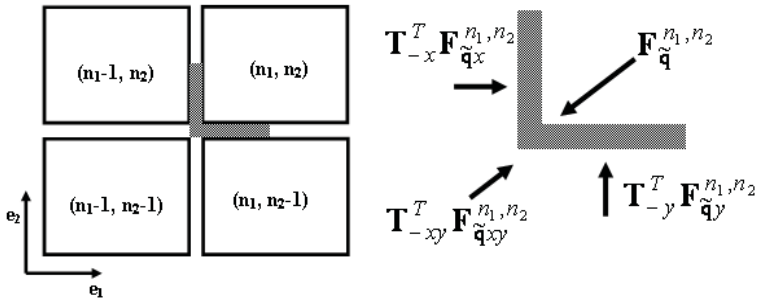

Figure 6: The force exerted on the shaded region by the neighboring cells in depicted on the right picture. The sum of all forces on this imaginary region should be zero.

The left hand side matrix in (13) consists of negative translation operators. We denote this matrix by $\overline{\mathbf{T}}^T$**.** By multiplying Eq. (2) with $\overline{\mathbf{T}}^T$ and using the result of Eq. (13) we have:

$$\overline{\mathbf{T}}^T(-\omega^2\mathbf{M}+\mathbf{K})\mathbf{q}=\mathbf{0}=(-\boldsymbol{\omega}^2\overline{\mathbf{T}}^T\mathbf{M}+\overline{\mathbf{T}}^T\mathbf{K})\mathbf{q}. \tag{14}$$

Note that up until now, $\overline{\mathbf{T}}^T$ is made up of pull-back operators, which are in unknown forms. However as we will see later, in the absence of energy dissipation in the system $\overline{\mathbf{T}}^T=\mathbf{T}^H$, in which $\mathbf{T}^H$ is the conjugate transpose of $\mathbf{T}$.

Next we enforce the periodicity of the structure. Treating the unit cell at (n_1,n_2) as a control volume, the input to the volume is $\mathbf{F}_{\tilde{\mathbf{q}}}^{n_1,n_2}$ and the outputs are $\mathbf{F}_{\tilde{\mathbf{q}}x}^{n_1,n_2}$,$\mathbf{F}_{\tilde{\mathbf{q}}y}^{n_1,n_2}$and $\mathbf{F}_{\tilde{\mathbf{q}}xy}^{n_1,n_2}$. Due to the periodicity of the structure, for the solutions sought, the operator $\overline{\mathbf{T}}^T$ must be the same for all unit cells in the lattice structure; *i.e.,* the relations between the input-output forces are the same throughout the lattice.

In the following, we adopt the strategy used to prove Bloch's theorem in quantum mechanics [56],[57] and apply it in our problem. Given that Eq. (14) holds for any cell in a periodic structure, we can apply $\mathbf{T_V}$ on its right hand side:

$$\mathbf{T_V}((-\boldsymbol{\omega}^2\overline{\mathbf{T}}^T\mathbf{MT} + \overline{\mathbf{T}}^T\mathbf{KT})\widehat{\mathbf{q}}) = \mathbf{0}, \tag{15}$$

in which all $\mathbf{M}$, $\mathbf{K}$, $\overline{\mathbf{T}}^T$, $\mathbf{T}$ and $\mathbf{q}$ are translated along a lattice vector $\mathbf{V}$. Note that $\mathbf{T_V}(\overline{\mathbf{T}}^T\mathbf{MT}) = \overline{\mathbf{T}}^T\mathbf{MT}$ and $\mathbf{T_V}(\overline{\mathbf{T}}^T\mathbf{KT}) = \overline{\mathbf{T}}^T\mathbf{KT}$, since $\mathbf{M}$, $\mathbf{K}$, $\mathbf{T}$ and $\overline{\mathbf{T}}^T$ are invariant under the translation operator. Consequently,

$$(-\boldsymbol{\omega}^2\overline{\mathbf{T}}^T\mathbf{MT} + \overline{\mathbf{T}}^T\mathbf{KT})\mathbf{T_V}(\widehat{\mathbf{q}}) = \mathbf{0}, \tag{16}$$

which implies that $\mathbf{T_V}(\widehat{\mathbf{q}})$ and $\widehat{\mathbf{q}}$ are both eigenvectors for the same general eigenvalue problem (14). In order to simplify the demonstration we assume that the geometric multiplicity of the eigenvalue $\boldsymbol{\omega}^2$ is one. In cases of higher multiplicity, we can use the same method, however with more care for eigenfunctions (see Appendix B). As a result, $\mathbf{T_V}(\widehat{\mathbf{q}})$ and $\widehat{\mathbf{q}}$ should be along the same eigenvector direction; *i.e.,* one should be a multiple of the other,

$$\mathbf{T_V}(\mathbf{q}) = \lambda(\mathbf{V})\mathbf{q}\ , \tag{17}$$

where the coefficient λ is a function of $\mathbf{V}$. If we set $\mathbf{V}' = n_3\mathbf{a}_1 + n_4\mathbf{a}_2$, then

$$\mathbf{T_{V'}}(\mathbf{T_V}(\mathbf{q})) = \mathbf{T_{V'}}(\lambda(\mathbf{V})\mathbf{q}), \tag{18}$$

or,

$$\mathbf{T_V}(\mathbf{q}) = \lambda(\mathbf{V})\mathbf{q}. \tag{19}$$

If we denote the displacement vector of a unit cell by $\mathbf{q}$, then $\mathbf{T_V}(\mathbf{q})$ is the displacement vector of another unit cell obtained by translating the original unit cell by the vector $\mathbf{V}$. Renaming $\lambda(\mathbf{V})\mathbf{q}$ by $\mathbf{q}'$, then by the same argument as Eq. (17), we have:

$$\mathbf{T_{V'}}(\mathbf{q}') = \lambda(\mathbf{V}')\lambda(\mathbf{V})\mathbf{q}. \tag{20}$$

We also have (proceeding from left to right),

$$\mathbf{T}_{\mathbf{V}'}(\mathbf{T}_{\mathbf{V}}(\mathbf{q})) = \mathbf{q}((n_1+n_3)\mathbf{a}_1 + (n_2+n_4)\mathbf{a}_2) = \mathbf{T}_{\mathbf{V}+\mathbf{V}'}(\mathbf{q}) = \lambda(\mathbf{V}+\mathbf{V}')\mathbf{q}\ , \tag{21}$$

i.e. $\lambda(\mathbf{V}+\mathbf{V}') = \lambda(\mathbf{V})\lambda(\mathbf{V}')$, so for a general $\mathbf{V}$ we can write λ as a power function of $\mathbf{V}$. For the base lattice vector $\mathbf{a}_i$, we can write $\lambda(\mathbf{a}_i) = e^{2\pi i k_i}$ with proper choice of k_i. Then using the definition of $\mathbf{V} \equiv n_1\mathbf{a}_1 + n_2\mathbf{a}_2$,

$$\lambda(\mathbf{V}) = \lambda(\mathbf{a}_1)^{n_1}\lambda(\mathbf{a}_2)^{n_2} = e^{2\pi i(n_1k_1+n_2k_2)}. \tag{22}$$

Writing the right hand side of (22) as $e^{i\mathbf{k}\cdot\mathbf{V}}$, we recognize it to be a plane wave with wavevector $\mathbf{k} = k_1\mathbf{b}_1 + k_2\mathbf{b}_2$, in which $\mathbf{b}_i$'s are reciprocal lattice vectors satisfying $\mathbf{b}_i \cdot \mathbf{a}_j = 2\pi\delta_{ij}$. Furthermore, $2\pi i(n_1k_1 + n_2k_2)$ is recognized to be the propagation constant. This establishes equation (3), and we are finished with the rigorous demonstration of Bloch formalism for displacements.

In addition to the displacements relation, we can find the translation operator $\mathbf{T}_{\mathbf{V}}$ by application to (2),

$$\mathbf{T}_{\mathbf{V}}((-\omega^2\mathbf{M}+\mathbf{K})\mathbf{q}) = \mathbf{T}_{\mathbf{V}}(\mathbf{F}). \tag{23}$$

However, the left-hand side of Eq.(23) can be simplified as

$$(-\omega^2\mathbf{M}+\mathbf{K})\mathbf{T}_{\mathbf{V}}(\mathbf{q}) = (-\omega^2\mathbf{M}+\mathbf{K})e^{i\mathbf{k}\cdot\mathbf{V}}\mathbf{q}\ . \tag{24}$$

By comparing (23),(24) and (2) one obtains $\mathbf{T}_{\mathbf{V}}(\mathbf{F}) = e^{i\mathbf{k}\cdot\mathbf{V}}\mathbf{F}$. Since $\widetilde{\mathbf{q}}_x$ of the cell (n_1, n_2) is contained by $\widetilde{\mathbf{q}}$ of the cell (n_1+1, n_2), $\mathbf{T}_{\mathbf{x}}$ can be defined for the displacements, and we are guaranteed that the same translation applies to the forces. The same argument is valid for $\mathbf{T}_{\mathbf{y}}$ and $\mathbf{T}_{\mathbf{xy}}$.

In addition, we can show that $i\mathbf{k}$ is an imaginary number for the case in which constant energy flows into and out of the unit cells; *i.e.,* when the average input power to each unit cell over one period of vibration is the same. Dissipative periodic systems have received little attention and should be investigated in future work. For the conservative case we can write:

$$\frac{1}{2}\,\mathrm{Re}\left\{\left\langle \mathbf{F}_{\widetilde{\mathbf{q}}}, \dot{\widetilde{\mathbf{q}}}\right\rangle\right\} \;= \frac{1}{2}\,\mathrm{Re}\left\{\left\langle \mathbf{T}_{\mathbf{V}}(\mathbf{F}_{\widetilde{\mathbf{q}}}), \mathbf{T}_{\mathbf{V}}(\dot{\widetilde{\mathbf{q}}})\right\rangle\right\}\,, \tag{25}$$

in which $\frac{1}{2}\,\mathrm{Re}\left\langle \mathbf{F}_{\mathbf{q}}, \dot{\widetilde{\mathbf{q}}}\right\rangle$ is the time averaged power entering unit cell at $\dot{\widetilde{\mathbf{q}}}$. The right-hand side can be simplified to

$$\frac{1}{2}\,\mathrm{Re}\left\{\left\langle e^{i\mathbf{k}\cdot\mathbf{V}}\mathbf{F}_{\mathbf{q}}, e^{i\mathbf{k}\cdot\mathbf{V}}\dot{\mathbf{q}}\right\rangle\right\} \;= \frac{1}{2}\,\mathrm{Re}\left\{e^{i\mathbf{k}\cdot\mathbf{V}}\overline{e^{i\mathbf{k}\cdot\mathbf{V}}}\left\langle \mathbf{F}_{\mathbf{q}}, \dot{\mathbf{q}}\right\rangle\right\} \;= \frac{1}{2}\left|e^{i\mathbf{k}\cdot\mathbf{V}}\right|^2 \mathrm{Re}\left\{\left\langle \mathbf{F}_{\mathbf{q}}, \dot{\mathbf{q}}\right\rangle\right\}, \tag{26}$$

which results in $\left|e^{i\mathbf{k}\cdot\mathbf{V}}\right|^2 = 1$, or $i\mathbf{k}$ an imaginary number. Further properties of the eigenvalue problem are discussed in the Appendix.

It should be noted that we started from an equation of motion (2) which is characterized by linear differential operators. We then used the linearity of the equations to obtain (16) and to conclude (17). Consequently, the linearity of the differential operator is a sufficient condition for the existence of the propagation constant. This does not rule out the existence of a propagation constant for nonlinear structures. However, in the Appendix, we show by example that the existence of the propagation constant in a nonlinear lattice violates the conservation of energy. Hence, in general, we cannot apply Bloch to nonlinear periodic structures.

2.3 Sufficiency of the Irreducible Brillouin zone

It is well-known that to investigate the band structure of a periodic material, it is sufficient to inspect wavevectors lying in the first Brillouin zone. However, in many

circumstances, we are only interested in uncovering frequency band gaps. In a given band structure, band gaps are bounded by extrema of each band**.** Consequently, the extrema of each band is of special interest. Due to the existing symmetry in most of the crystals and structures, the extrema most-probably occur on the boundary of the irreducible Brillouin zone (IBZ)[60]. Nonetheless, this assumption needs to be made carefully, especially in the case of structures with asymmetries, as shown next.

It is common practice to investigate the boundary of the IBZ when constructing the band structure of lattices [61]-[63]. Some researchers have acknowledged that the boundary may be insufficient [48],[64] and [65]. Others have investigated wavevectors in the interior of the IBZ [66],[67]; however, these studies do not provide a discussion on its importance or necessity. One of the primary reasons that only the IBZ boundary is considered in investigating crystalline structures is that sufficient symmetry exists to warrant the assumption. Adams *et al.* [52] considered a quasi-one-dimensional structure in which the extrema of the dispersion curves occur inside the Brillouin zone. Here, as a complementary result, we show that in a simple engineering lattice the extrema of ω occur on the *interior* of the Irreducible Brillouin zone.

In the general lattice of Fig. 7, we find by construction a set of stiffnesses which place one extremum of ω at an arbitrary point inside the IBZ. The equations governing the propagation of Bloch waves are given as,

$$\left(-\omega^2 \begin{bmatrix} m & 0 & 0 & 0 \\ 0 & m & 0 & 0 \\ 0 & 0 & m & 0 \\ 0 & 0 & 0 & m \end{bmatrix} + \mathbf{K} \right) \begin{bmatrix} \widetilde{\mathbf{q}} \\ \widetilde{\mathbf{q}}_x \\ \widetilde{\mathbf{q}}_y \\ \widetilde{\mathbf{q}}_{xy} \end{bmatrix} = \begin{bmatrix} \mathbf{F}_{\widetilde{\mathbf{q}}} \\ \mathbf{F}_{\widetilde{\mathbf{q}}x} \\ \mathbf{F}_{\widetilde{\mathbf{q}}y} \\ \mathbf{F}_{\widetilde{\mathbf{q}}xy} \end{bmatrix}, \tag{27}$$

in which $\widetilde{\mathbf{q}}$, $\widetilde{\mathbf{q}}_x$, $\widetilde{\mathbf{q}}_y$ and $\widetilde{\mathbf{q}}_{xy}$ represent out of plane coordinates of the left bottom, right bottom, left top and right top masses, respectively. The stiffness matrix $\mathbf{K}$ for the system of interest is given as

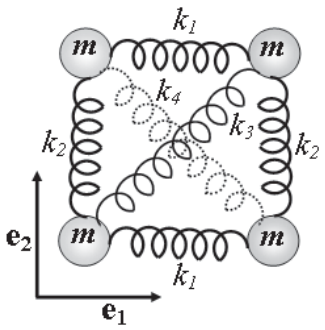

Figure 7: A unit cell of a simple lattice structure with out of plane displacements for the masses.

$$\mathbf{K} = \begin{bmatrix} K_1+K_2+K_3 & -K_1 & -K_2 & -K_3 \\ -K_1 & K_1+K_2+K_4 & -K_4 & -K_2 \\ -K_2 & -K_4 & K_1+K_2+K_4 & -K_1 \\ -K_3 & -K_2 & -K_1 & K_1+K_2+K_3 \end{bmatrix}. \quad (28)$$

By using the Bloch procedure and our previous result,

$$\mathbf{q} = \begin{bmatrix} 1 & e^{i\mu_x} & e^{i\mu_y} & e^{i(\mu_x+\mu_y)} \end{bmatrix}^T \widetilde{\mathbf{q}} \ , \ \begin{bmatrix} 1 & e^{-i\mu_x} & e^{-i\mu_y} & e^{-i(\mu_x+\mu_y)} \end{bmatrix} \mathbf{F} = \mathbf{0}, \quad (29)$$

in which $2\pi x_1$ and $2\pi x_2$ are replaced by μ_x and μ_y for ease of notation. From the resulting eigenvalue problem,

$$\begin{aligned} \omega^2 &= \frac{1}{2m}(-K_3\cos(\mu_x+\mu_y) - K_4\cos(\mu_x-\mu_y) - 2K_2\cos(\mu_y) \\ &\quad -2K_1\cos(\mu_x) + 2K_1 + 2K_2 + K_3 + K_4). \end{aligned} \quad (30)$$

We next find the extrema of ω^2 as a function of μ_x and μ_y:

$$\begin{aligned} \frac{\partial\omega^2}{\partial\mu_x} &= K_3\sin(\mu_x+\mu_y) + K_4\sin(\mu_x-\mu_y) + 2K_1\sin(\mu_x) = 0, \quad (31) \\ \frac{\partial\omega^2}{\partial\mu_y} &= K_3\sin(\mu_x+\mu_y) - K_4\sin(\mu_x-\mu_y) + 2K_2\sin(\mu_y) = 0. \end{aligned}$$

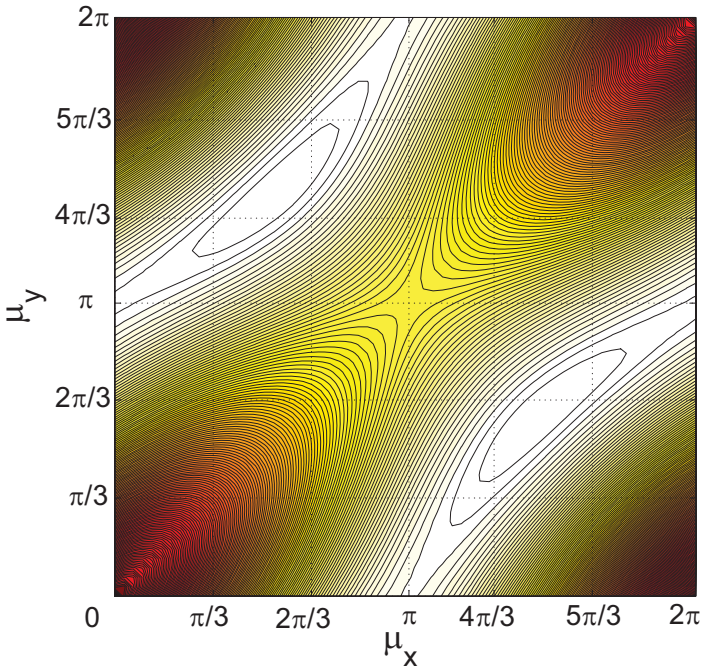

Figure 8: Contour graph of ω as a function of μ_x and μ_y. As can bee seen, the maximum ω occurs inside of the Brillouin zone

In order to have a relative maximum at a point $c(\mu_x, \mu_y)$, the following conditions have to be met:

$$\frac{\partial^2\omega^2}{\partial\mu_x^2} > 0 \quad \text{and} \quad \frac{\partial^2\omega^2}{\partial\mu_x^2}\frac{\partial^2\omega^2}{\partial\mu_y^2} - \left(\frac{\partial^2\omega^2}{\partial\mu_x\partial\mu_y}\right)^2 > 0. \tag{32}$$

Next we can choose arbitrary normalized wavenumbers μ_x and μ_y for the maximum point $c(\mu_x, \mu_y)$ and then find $K_i > 0$ such that (31) and (32) are satisfied. Without loss of generality, we choose to specify c to be located at $\mu_x = 3\pi/2$ and $\mu_y = 2\pi/3$. Note that this point is not on the boundary of the irreducible Brillouin zone. For a straight-forward normalization we also chose $K_4 = 2$ and find the conditions for all other stiffnesses. It can be easily verified that by the choice

$$K_3 < 0.07,\ K_1 = \frac{1+K_3}{2},\ K_2 = \frac{1-K_3}{\sqrt{3}}, \tag{33}$$

all desired conditions are satisfied. The contour graph and the dispersion surface for

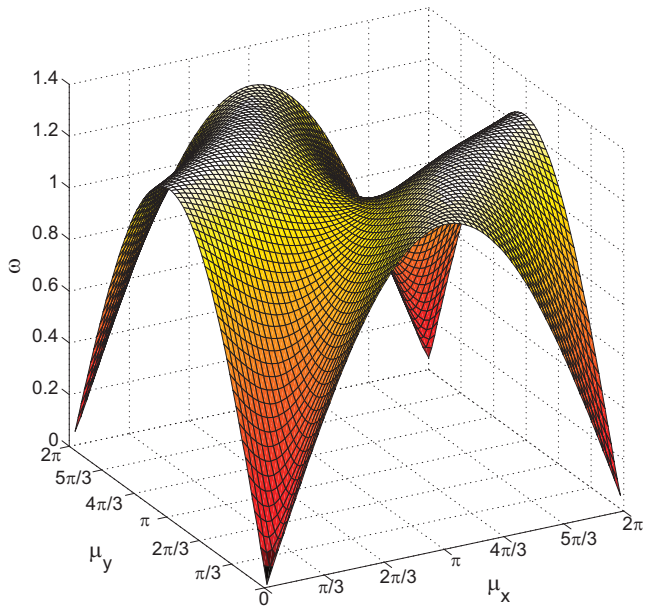

Figure 9: ω as a function of μ_x and μ_y for the example of Fig. 7

$K_3 = .05$ are shown in Fig. 8 and Fig. 9. As evident in the figures, the maximum ω is achieved at the designed-for $\mu_x = 3\pi/2$ and $\mu_y = 2\pi/3$. This constructed example clearly shows that neglecting points inside the irreducible Brillouin zone may result in an erroneous conclusion regarding the band gaps. In other words, inspecting only the boundary of IBZ, one might conclude the existence of a band gap larger in magnitude than the actual band gap in the lattice.

2.4 Bloch Analysis in Nonlinear Periodic Structures

In this section, it is shown that the existence of the propagation constant in a nonlinear system with no dissipation of energy would violate conservation of energy. Consider

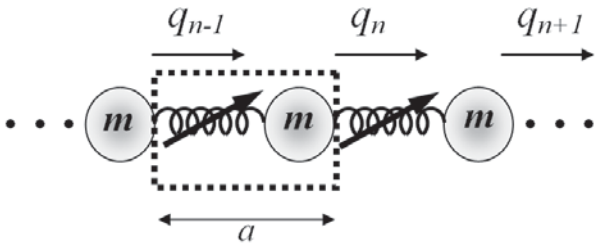

Figure 10: An infinite mass-spring system with nonlinear spring stiffness. The unit cell boundaries are marked by dashed lines.

an infinite periodic mass-spring chain as depicted in Fig. 10. Let's assume that in the mass-spring system of Fig. 10, the following Bloch relation holds:

$$\mathbf{q}_{n-1} = e^{-i\mu_x}\mathbf{q}_n \ , \ \ \mathbf{q}_{n+1} = e^{i\mu_x}\mathbf{q}_n \ . \tag{34}$$

Let the spring force be a nonlinear function of displacement, such that the force exerted on the right boundary of the unit cell (collocated with $\mathbf{q}_n$) takes the form:

$$\mathbf{F}_{\mathbf{q}_n} = K_1(\mathbf{q}_{n+1} - \mathbf{q}_n) + K_2(\mathbf{q}_{n+1} - \mathbf{q}_n)^m. \tag{35}$$

in which $m \neq 1$ defines the nonlinearity in the spring. As a result, the equation of motion for a unit cell is:

$$M\ddot{\mathbf{q}}_n + K_1\mathbf{q}_n(1-e^{i\mu_x}) + K_1\mathbf{q}_n(1-e^{-i\mu_x}) + K_2(\mathbf{q}_n)^m(\mathbf{1}-e^{i\mu_x})^m + K_2(\mathbf{q}_n)^m(\mathbf{1}-e^{-i\mu_x})^m = 0. \tag{36}$$

The first difficulty with this differential equation is its nonlinearity, so in general we cannot presume harmonic motion as a solution, *i.e.* we cannot write $\ddot{\mathbf{q}}_n$as $-\omega^2\mathbf{q}$. Then for m=1.5 and $\mu_x = \pi$, conservation of energy for the specified unit cell, implies that the input energy should equates to the output energy over one period. Let E_{input}

and E_{output} be the input and output energy in a period:

$$E_{input} = \int \mathrm{Re}\left\{\left(K_1(\mathbf{q}_{n-1}-\mathbf{q}_n)+K_2(\mathbf{q}_{n-1}-\mathbf{q}_n)^{1.5}\right)\right\}\mathrm{Re}\left\{\dot{\mathbf{q}}_{n-1}\right\}dt, \quad (37)$$

$$E_{output} = \int \mathrm{Re}\left\{\left(K_1(\mathbf{q}_{n}-\mathbf{q}_{n+1})+K_2(\mathbf{q}_{n}-\mathbf{q}_{n+1})^{1.5}\right)\right\}\mathrm{Re}\left\{\dot{\mathbf{q}}_{n}\right\}dt\ , \quad (38)$$

in which the integral is over one period. We then apply Bloch relation (34) on expressions (37),(38) for $\mu_x = \pi$. The simplified results would take the form:

$$E_{input} = \int \mathrm{Re}\left\{2K_1\mathbf{q}_n\right\}\mathrm{Re}\left\{\dot{\mathbf{q}}_n\right\}dt + \frac{1}{2}\int \mathrm{Re}\left\{-i2\sqrt{2}K_2(\mathbf{q}_n)^{1.5}\right\}\mathrm{Re}\left\{\dot{\mathbf{q}}_n\right\}dt, \quad (39)$$

$$E_{output} = \int \mathrm{Re}\left\{2K_1\mathbf{q}_n\right\}\mathrm{Re}\left\{\dot{\mathbf{q}}_n\right\}dt + \frac{1}{2}\int \mathrm{Re}\left\{2\sqrt{2}K_2(\mathbf{q}_n)^{1.5}\right\}\mathrm{Re}\left\{\dot{\mathbf{q}}_n\right\}dt\ . \quad (40)$$

The first terms of these expressions are the same; *i.e.,* if $K_2 = 0$ the nonlinear part of the spring vanishes and we recover $E_{input} = E_{output}$. Otherwise, in general, the two expressions are not equal. For example, when $K_1 = K_2 = M = |\mathbf{q}_n| = 1$, from (36) we calculate $\omega^2 = 4 + 4\sqrt{2}$. Then the second integral terms in (39),(40) evaluate numerically to 4.52 and 0.00 respectively. This would clearly violate the conservation of energy.

2.5 Further Properties of the Eigenvalues

It was found that the push-forward operator $\mathbf{T}$ acts the same way on the displacements and on the forces. By using the common displacement between two adjacent cells, we can find the form of this operator for a given wavevector $\mathbf{k}$. The relation between the minimum number of displacements $\widehat{\mathbf{q}}$ and all the displacements of a unit cell is written as:

$$\mathbf{q} = \mathbf{T}[\ \mathbf{q}_i \quad \widetilde{\mathbf{q}}\ ]^T = \mathbf{T}\widehat{\mathbf{q}}, \quad (41)$$

which results in the eigenvalue problem

$$\overline{\mathbf{T}}^T(-\omega^2\mathbf{M}+\mathbf{K})\mathbf{T}\widehat{\mathbf{q}}=\mathbf{0}. \tag{42}$$

In the uniform energy flow case, wavevectors are real, hence $e^{-i\mu_x}$ and $e^{i\mu_x}$ are complex conjugates. The same relation holds between $e^{-i\mu_y}$, $e^{i\mu_y}$, $e^{-i(\mu_x+\mu_y)}$ and $e^{i(\mu_x+\mu_y)}$. This would make $\overline{\mathbf{T}}^T$ equals to $\mathbf{T}^H$, which is complex conjugate of $\mathbf{T}$. Consequently (42) takes the form:

$$\mathbf{T}^H(-\omega^2\mathbf{M}+\mathbf{K})\mathbf{T}\widehat{\mathbf{q}}=\mathbf{0}. \tag{43}$$

We prove that in the eigenvalue problem of (43), the eigenvalues (ω^2's) are real and positive; hence they are physically realizable. In Eq. (2) the mass matrix $\mathbf{M}$ and the stiffness matrix $\mathbf{K}$ can be derived by Lagrangian mechanics. In deriving the Lagrangian of a mechanical system, all of the terms in the potential energy contain displacement $\mathbf{q}$'s measured from the equilibrium positions. As a result, the potential energy $\mathbf{V}=1/2\mathbf{q}^T\mathbf{K}\mathbf{q}=1/2\left\langle\mathbf{q},\mathbf{K}\mathbf{q}\right\rangle$ is always positive for non-zero $\mathbf{q}$ [68]. The same is true for the kinetic energy which can be stated as $1/2\dot{\mathbf{q}}^T\mathbf{M}\dot{\mathbf{q}}=1/2\left\langle\dot{\mathbf{q}},\mathbf{M}\dot{\mathbf{q}}\right\rangle$. Consequently $\mathbf{K}$ and $\mathbf{M}$ are positive definite matrices. From Eq. (43):

$$\mathbf{T}^H\mathbf{K}\mathbf{T}\widehat{\mathbf{q}}=\omega^2\mathbf{D}\widehat{\mathbf{q}}, \tag{44}$$

in which $\mathbf{T}^H\mathbf{M}\mathbf{T}$ is replaced by $\mathbf{D}$ for simplicity. We want to next prove that ω^2 in (44) is real and positive. Otherwise, ω becomes a complex number. To prove this, we write:

$$\omega^2\left\langle\mathbf{D}\widehat{\mathbf{q}},\widehat{\mathbf{q}}\right\rangle=\left\langle\omega^2\mathbf{D}\widehat{\mathbf{q}},\widehat{\mathbf{q}}\right\rangle=\left\langle\mathbf{T}^H\mathbf{K}\mathbf{T}\widehat{\mathbf{q}},\widehat{\mathbf{q}}\right\rangle=\left\langle\widehat{\mathbf{q}},(\mathbf{T}^H\mathbf{K}\mathbf{T})^H\widehat{\mathbf{q}}\right\rangle=\left\langle\widehat{\mathbf{q}},\mathbf{T}^H\mathbf{K}^H\mathbf{T}\widehat{\mathbf{q}}\right\rangle=$$
$$\left\langle\widehat{\mathbf{q}},\mathbf{T}^H\mathbf{K}\mathbf{T}\widehat{\mathbf{q}}\right\rangle=\left\langle\widehat{\mathbf{q}},\omega^2\mathbf{D}\widehat{\mathbf{q}}\right\rangle=\overline{\omega^2}\left\langle\widehat{\mathbf{q}},\mathbf{D}\widehat{\mathbf{q}}\right\rangle=\overline{\omega^2}\left\langle\mathbf{D}^H\widehat{\mathbf{q}},\widehat{\mathbf{q}}\right\rangle=\overline{\omega^2}\left\langle\mathbf{D}\widehat{\mathbf{q}},\widehat{\mathbf{q}}\right\rangle.$$

Since $\left\langle\mathbf{D}\widetilde{\mathbf{q}},\widetilde{\mathbf{q}}\right\rangle$ is not always zero, we have $\omega^2=\overline{\omega^2}$, implying ω^2 is real. What remains is to show that ω^2 is positive. It was shown that $\mathbf{K}$ and $\mathbf{M}$ are positive definite operators on $\mathbf{R}^n$. As a result:

$\forall \mathbf{v} \in \mathbf{R}^n$; $0 \leqslant \langle \mathbf{K}\mathbf{v}, \mathbf{v} \rangle$, so $0 \leqslant \langle \mathbf{K}\mathbf{T}\widehat{\mathbf{q}}, \mathbf{T}\widehat{\mathbf{q}} \rangle$ and then $0 \leqslant \left\langle \mathbf{T}^H\mathbf{K}\mathbf{T}\widehat{\mathbf{q}}, \widehat{\mathbf{q}} \right\rangle$. Similarly, $0 < \left\langle \mathbf{T}^H\mathbf{M}\mathbf{T}\widehat{\mathbf{q}}, \widehat{\mathbf{q}} \right\rangle$ *i.e.* $0 < \langle \mathbf{D}\widehat{\mathbf{q}}, \widehat{\mathbf{q}} \rangle$.

Now, $0 \leqslant \left\langle \mathbf{T}^H\mathbf{K}\mathbf{T}\widehat{\mathbf{q}}, \widehat{\mathbf{q}} \right\rangle$, so $0 \leqslant \langle \omega^2\mathbf{D}\widehat{\mathbf{q}}, \widehat{\mathbf{q}} \rangle = \omega^2 \langle \mathbf{D}\widehat{\mathbf{q}}, \widehat{\mathbf{q}} \rangle$. But $0 < \langle \mathbf{D}\widehat{\mathbf{q}}, \widehat{\mathbf{q}} \rangle$, so we have $0 \leqslant \omega^2$.

In this chapter, we rigorously arrived at the Bloch relation for displacements and forces. In the next chapter, we further clarify the relation between the forces when analyzing a reference unit cell. Corner forces are discussed in more detail and a worked-out example is provided to compare correct and incorrect application of the Bloch theorem to the corner forces.

CHAPTER III

TREATMENT OF INTERNAL FORCES IN BLOCH ANALYSIS

In the previous chapter we rigorously arrived at the Bloch transformation $\mathbf{T_V}$. We next use this transformation to clarify internal forces which arise when analyzing a single unit cell. We also provide a worked-out example of Bloch wave propagation in a periodic hexagonal lattice.

3.1 Equations of Motion and the Force Term

After invoking Lagrangian or Newtonian dynamics, the equations of motion for a general unit cell assume the form,

$$\mathbf{M}\ddot{\mathbf{q}}+\mathbf{K}\mathbf{q} = \mathbf{F}, \tag{45}$$

in which matrices $\mathbf{M}$ and $\mathbf{K}$ represents the global mass and stiffness matrix of the unit cell, $\mathbf{q}$ and $\ddot{\mathbf{q}}$ represents the (nodal) displacements and accelerations, and $\mathbf{F}$ denotes the (nodal) forces. For plane harmonic waves, $\ddot{\mathbf{q}}$ can be replaced by $-\omega^2\mathbf{q}$ so that the equations of motion can be rewritten as:

$$(-\omega^2\mathbf{M} + \mathbf{K})\mathbf{q} = \mathbf{F}. \tag{46}$$

For plane waves in a periodic lattice, the Bloch analysis reduces the number of displacements in (46), *i.e.,* we can write

$$\mathbf{q} = \mathbf{T}\widehat{\mathbf{q}}. \tag{47}$$

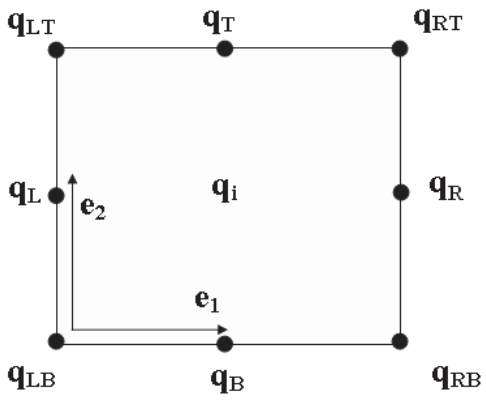

Figure 11: Depiction of the nine displacements in a square honeycomb lattice.

In a planar lattice structure, $\mathbf{T}$ is a linear transformation parametrized by μ_x and μ_y. For example, in the case of a square honeycomb (Fig. 11), if $\mathbf{q}_{sq}$ denotes the displacements of the unit cell, we have $\mathbf{q}_{sq}= \mathbf{T}_{sq}\widehat{\mathbf{q}}_{sq}$ in which:

$$\mathbf{q}_{sq}= \begin{bmatrix} \mathbf{q}_i \\ \mathbf{q}_B \\ \mathbf{q}_T \\ \mathbf{q}_L \\ \mathbf{q}_R \\ \mathbf{q}_{LB} \\ \mathbf{q}_{RB} \\ \mathbf{q}_{LT} \\ \mathbf{q}_{RT} \end{bmatrix}, \quad \mathbf{T}_{sq}= \begin{bmatrix} \mathbf{I} & \mathbf{0} & \mathbf{0} & \mathbf{0} \\ \mathbf{0} & \mathbf{I} & \mathbf{0} & \mathbf{0} \\ \mathbf{0} & \mathbf{I}e^{\mu_y} & \mathbf{0} & \mathbf{0} \\ \mathbf{0} & \mathbf{0} & \mathbf{I} & \mathbf{0} \\ \mathbf{0} & \mathbf{0} & \mathbf{I}e^{\mu_x} & \mathbf{0} \\ \mathbf{0} & \mathbf{0} & \mathbf{0} & \mathbf{I} \\ \mathbf{0} & \mathbf{0} & \mathbf{0} & \mathbf{I}e^{\mu_x} \\ \mathbf{0} & \mathbf{0} & \mathbf{0} & \mathbf{I}e^{\mu_y} \\ \mathbf{0} & \mathbf{0} & \mathbf{0} & \mathbf{I}e^{\mu_x+\mu_y} \end{bmatrix}, \quad \widehat{\mathbf{q}}_{sq} = \begin{bmatrix} \mathbf{q}_i \\ \mathbf{q}_B \\ \mathbf{q}_L \\ \mathbf{q}_{LB} \end{bmatrix}. \tag{48}$$

Note that $\mathbf{q}_{RB} = e^{\mu_x}\mathbf{q}_{LB}$ holds because $\mathbf{q}_{RB}$ is the common point for two adjacent cells: the cells located at $n_1e_1 + n_2e_2$ and $(n_1 + 1)e_1 + n_2e_2$ (see Fig. 12), *i.e.*, $\mathbf{q}_{RB}^{n_1,n_2} = \mathbf{q}_{LB}^{n_1+1,n_2}$. By the Floquet-Bloch theorem, $\mathbf{q}_{LB}^{n_1+1,n_2} = e^{\mu_x}\mathbf{q}_{LB}^{n_1+1,n_2}$. These two equations and similar relations yield (48). In a general case (not square honeycomb),

eq (47) would result in an equation of motion in the form of $(-\omega^2\mathbf{M}+\mathbf{K})\mathbf{T}\widehat{\mathbf{q}}=\mathbf{F}$. If the external force term on the right hand side of this equation could be eliminated, it would establish an eigenvalue problem yielding ω. We have showed that a matrix $\overline{\mathbf{T}}$ obtained from $\mathbf{T}$ by replacing μ_x, μ_y with $-\mu_x$, $-\mu_y$ will have the property that $\overline{\mathbf{T}}^T\mathbf{F}=\mathbf{0}$, where $\overline{\mathbf{T}}^T$ denotes the transpose of $\overline{\mathbf{T}}$. For example, for the special case of the square honeycomb:

$$\overline{\mathbf{T}}_{sq}^T\mathbf{F}_{sq}=\begin{bmatrix} \mathbf{0} \\ \mathbf{F}_B+e^{-\mu_y}\mathbf{F}_T \\ \mathbf{F}_L+e^{-\mu_x}\mathbf{F}_R \\ \mathbf{F}_{LB}+e^{-\mu_x}\mathbf{F}_{RB}+e^{-\mu_y}\mathbf{F}_{LT}+e^{-\mu_y-\mu_y}\mathbf{F}_{RT} \end{bmatrix}, \tag{49}$$

Note that others apply the Bloch approach to the forces in (49), and combine it with the equilibrium condition for the remaining terms in $\overline{\mathbf{T}}_{sq}^T\mathbf{F}_{sq}$, and arrive at the equations,

$$\mathbf{F}_T = -e^{\mu_y}\mathbf{F}_B\ , \qquad \mathbf{F}_R=-e^{\mu_y}\mathbf{F}_L, \tag{50}$$

$$\mathbf{F}_{RB} = -e^{\mu_x}\mathbf{F}_{LB}\ , \quad \mathbf{F}_{LT}=-e^{\mu_y}\mathbf{F}_{LB}\ , \qquad \mathbf{F}_{RT}=e^{\mu_y+\mu_y}\mathbf{F}_{LB}, \tag{51}$$

resulting in the desired outcome $\overline{\mathbf{T}}_{sq}^T\mathbf{F}_{sq}=\mathbf{0}$. This procedure can not be followed, however. While $\mathbf{F}_{LB}^{(n_1+1)e_1+n_2e_2}=e^{\mu_x}\mathbf{F}_{LB}^{n_1e_1+n_2e_2}$ holds, we cannot write $\mathbf{F}_{RB}^{n_1e_1+n_2e_2}=\pm\mathbf{F}_{LB}^{(n_1+1)e_1+n_2e_2}$ in general. In order to investigate this we consider the square honeycomb lattice structure pictured in Fig. 12.

For the top and right location in the lattice we have:

$$\mathbf{F}_T^{n_1e_1+n_2e_2} = -\mathbf{F}_B^{(n_1+1)e_1+n_2e_2} = -e^{\mu_y}\mathbf{F}_B^{n_1e_1+n_2e_2}\ , \tag{52}$$

$$\mathbf{F}_L^{n_1e_1+n_2e_2} = -\mathbf{F}_R^{(n_1+1)e_1+n_2e_2} = -e^{\mu_x}\mathbf{F}_R^{n_1e_1+n_2e_2}, \tag{53}$$

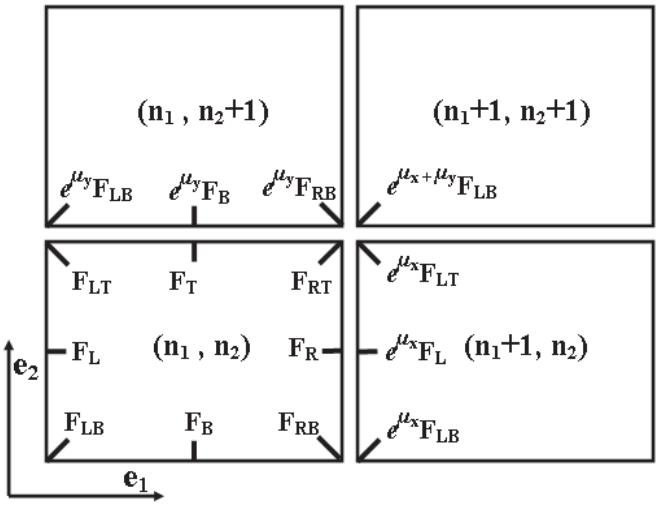

Figure 12: Square honeycomb with e_1, e_2 as the coordinate unit vectors and the cells located at (n_1, n_2) , $(n_1 + 1, n_2)$, $(n_1, n_2 + 1)$ and $(n_1 + 1, n_2 + 1)$.

which makes the second and third row of $\overline{\mathbf{T}}_{sq}^{T}\mathbf{F}_{sq}$ in (49) zero. However, for the right-bottom, left-top and right-top lattice locations similar equations cannot be derived because at these corners, more than two cells meet. On the other hand, the equilibrium condition at these coordinates together with the Bloch analysis yield (see center point of Fig. 12)

$$e^{\mu_x+\mu_y}\mathbf{F}_{LB} + e^{\mu_y}\mathbf{F}_{RB} + e^{\mu_x}\mathbf{F}_{LT} + \mathbf{F}_{RT} = 0. \tag{54}$$

Note that if we multiply both sides of (54) by $e^{-\mu_x-\mu_y}$, it will establish the last row of the $\overline{\mathbf{T}}_{sq}^{T}\mathbf{F}_{sq}$ is zero.

Langley has shown that (51) violates the power flow assumption through the square lattice structure. Here, we show by example that (51) does not hold. However, we did show in Chapter 3 that $\overline{\mathbf{T}}^{T}\mathbf{F} = \mathbf{0}$ holds in general for cases such as triangular honeycomb, hexagonal honeycomb and general 3-D structures.

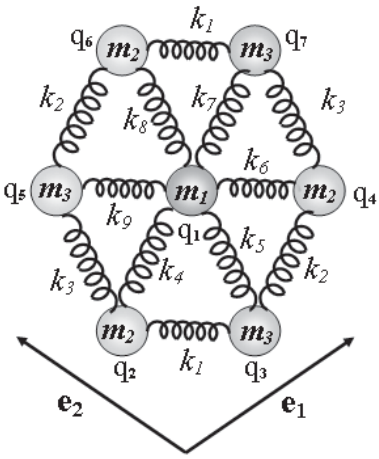

Figure 13: A hexagonal honeycomb lattice with an internal degree of freedom and forces

3.2 Analysis of Free Wave Motion in an example

In this example, we consider a hexagonal honeycomb lattice structure (Fig. 13). Each mass has one degree of freedom; it can vibrate in a direction orthogonal to the plane spanned by e_1, e_2 and the springs exert forces outward or inward to this plane. The internal degree of the freedom and the internal forces are modelled by the internal mass m_3 and springs k_4 to k_9. The arbitrary values for the k's and m's are tabulated in Table 1. For this case:

$$\mathbf{q}_i = [\mathbf{q}_1], \widetilde{\mathbf{q}} = \begin{bmatrix} \mathbf{q}_2 \\ \mathbf{q}_3 \end{bmatrix}, \widetilde{\mathbf{q}}_x = [\mathbf{q}_4], \quad \widetilde{\mathbf{q}}_y = [\mathbf{q}_5], \quad \widetilde{\mathbf{q}}_{xy} = \begin{bmatrix} \mathbf{q}_6 \\ \mathbf{q}_7 \end{bmatrix}$$

$$\mathbf{T}_x = \begin{bmatrix} \mathbf{I}e^{\mu_x} & \mathbf{0} \end{bmatrix}, \quad \mathbf{T}_y = \begin{bmatrix} \mathbf{0} & \mathbf{I}e^{\mu_y} \end{bmatrix}, \quad \mathbf{T}_{xy} = \begin{bmatrix} \mathbf{I}e^{\mu_x+\mu_y} & \mathbf{0} \\ \mathbf{0} & \mathbf{I}e^{\mu_x+\mu_y} \end{bmatrix}$$

As it was proved for the general case, equation (13) holds in this case. Utilizing (43), the dispersion curves for the values of Table 1 for the hexagonal honeycomb were found (Fig. 14).

Table 1: Parameters chosen for the hexagonal honeycomb.

m_1	m_2	m_3	k_1	k_2	k_3	k_4	k_5	k_6	k_7	k_8	k_9
1	2	3	10	20	30	40	50	10	20	30	10

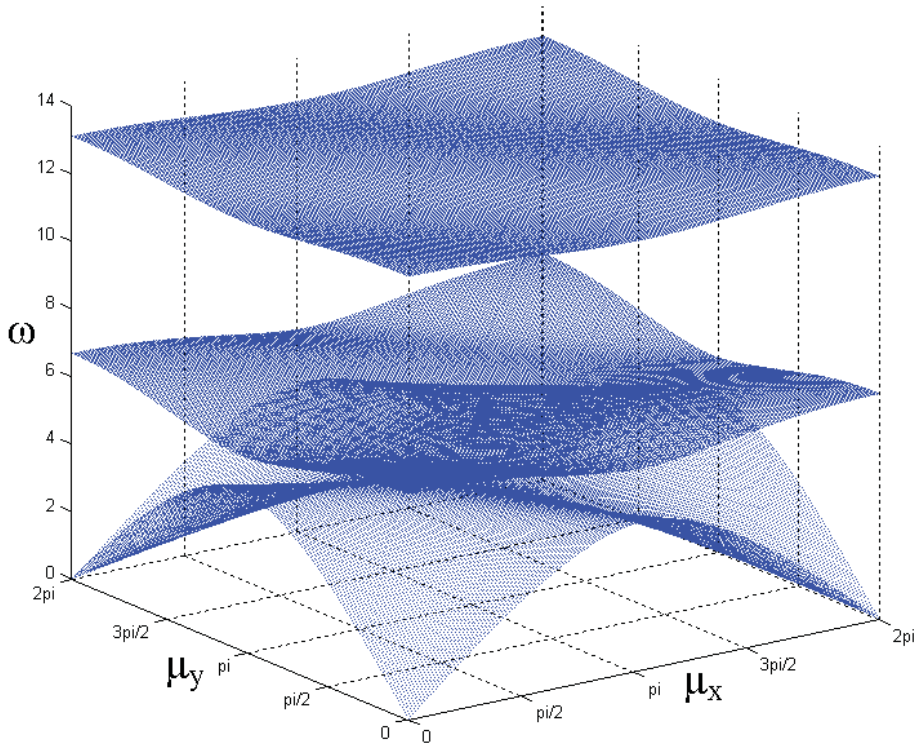

Figure 14: Three ω's versus μ_x and μ_y in the case of the mass-spring hexagonal lattice

Table 2: Comparison between the force $\mathbf{F}_6$; the external force on the cell collocated with $\mathbf{q}_6$, and the force obtained by direct use of Bloch analysis $e^{\mu_x+\mu_y}\mathbf{F}_2$.

F_6	-21	1	-9	17	11	3	10	7	16	14
$e^{\mu_x+\mu_y}F_2$	-31	-13	-33	6	-7	-16	-8	-8	-5	2
Difference	10	14	24	11	18	19	18	15	21	12

Also external forces on the unit cell collocated with $\mathbf{q}_6$ was obtained for ten random values of $\widetilde{\mathbf{q}}$ and $\mathbf{q}_i$ and it is compared with $e^{\mu_x+\mu_y}\mathbf{F}_2$ for $\mu_x = \mu_y = 0.5$. These numbers are tabulated in Table 2. It is apparent from this table that the Bloch analysis is not valid for the forces in this case.

In this chapter, we close the thorough investigation of Bloch relation in systems with no energy dissipation. In the next chapter we start the investigation of the Bloch analysis in structures with energy dissipation. We discuss phenomena arising only in structures with energy dissipation.

CHAPTER IV

ANALYSIS OF BLOCH'S METHOD IN STRUCTURES WITH ENERGY DISSIPATION

4.1 Bloch's Method in Structures with Energy Dissipation

Damping arises in periodic structures via several mechanisms. These include energy loss caused by internal mechanisms such as crystal defects, grain boundaries and thermoelastic couplings, or by means of external mechanisms such as interactions with a surrounding fluid. For several practical applications, the assumption of linear damping agrees well with experimental results. In micromachined structures, the most substantial damping comes from air interaction [86] and can be modeled by a revised mass and an added linear damping term in the equations of motion [87]. The associated damping coefficient depends on the air pressure [88] and can be obtained experimentally [89] (See Fig. 15) For small amplitude excitation of micromachined silicon, it has been shown that the linear damping assumption agrees well with experimental data [90], [91]. Since little work has addressed the effect of damping on wave propagation in periodic structures, and due to close agreement with experiments, only linear damping will be considered herein.

4.1.1 Damped Formulation

In any lattice structure, a unit cell is repeated along three lattice vectors $\mathbf{a}_1, \mathbf{a}_2, \mathbf{a}_3$ [28]. In this chapter, for ease of notation, we investigate planar lattices only; *i.e.*, the

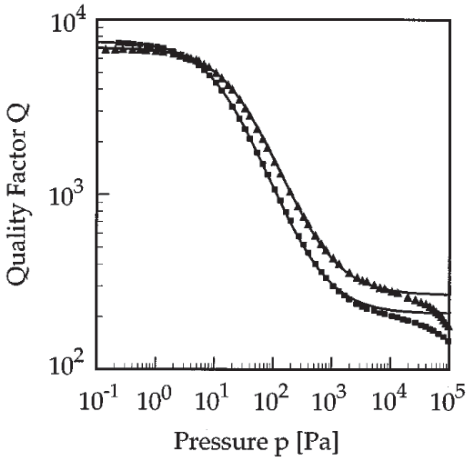

Figure 15: Quality factor of vibrating beam-microresonator vs surrounding gas pressure for beam sizes of $250\times150\mu m$ (marked by triangles) and $300\times200\mu m$ (marked by squares). Solid lines are fit with the linear damping model [92].

unit cell is repeated along $\mathbf{a}_1, \mathbf{a}_2$. Applying a Lagrangian or Newtonian approach, the equations of motion for the unit cell take the form:

$$\mathbf{M}\ddot{\mathbf{q}}+\mathbf{C}\dot{\mathbf{q}} + \mathbf{K}\mathbf{q} = \mathbf{F}, \tag{55}$$

where $\mathbf{M}$, $\mathbf{C}$ and $\mathbf{K}$ represent the global mass, damping and stiffness matrix of the unit cell; $\mathbf{q}$, $\dot{\mathbf{q}}$ and $\ddot{\mathbf{q}}$ represent the (nodal) displacements, velocities and accelerations; and $\mathbf{F}$ denotes the (nodal) forces on the unit cell applied by neighboring cells in the structure. Seeking a harmonic solution for the linear differential equation (55), $\dot{\mathbf{q}}$ and $\ddot{\mathbf{q}}$ can be replaced by $i\omega\mathbf{q}$ and $-\omega^2\mathbf{q}$ respectively, such that (55) takes the form:

$$(-\omega^2\mathbf{M}+i\omega\mathbf{C} + \mathbf{K})\mathbf{q} = \mathbf{F}. \tag{56}$$

Previous work [93], [94] has shown that in an undamped structure, forces can be removed from the formulation by applying an appropriate operator to both sides of the equation. This yields an eigenvalue problem and allows for rigorous determination of the Bloch relation. In (56) however, if $\mathbf{F}$ vanishes, the resultant equation would

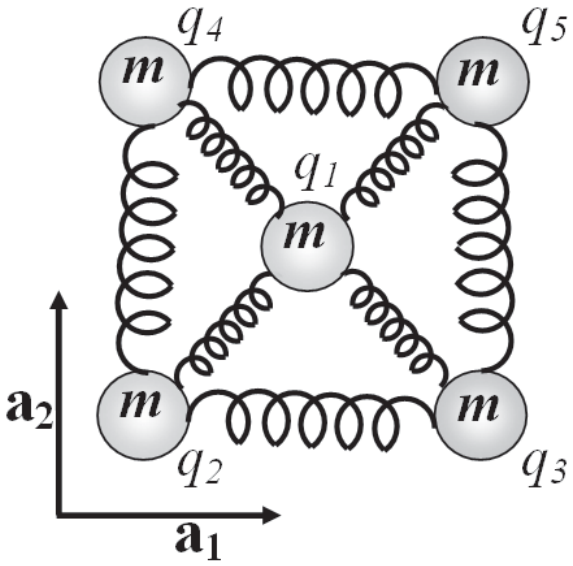

Figure 16: Square honeycomb with out of plane motion. For this geometry, $\mathbf{q}_i = [\mathbf{q}_1]$, $\widetilde{\mathbf{q}} = [\mathbf{q}_2]$, $\widetilde{\mathbf{q}}_x = [\mathbf{q}_3]$, $\widetilde{\mathbf{q}}_y = [\mathbf{q}_4]$, $\widetilde{\mathbf{q}}_{xy} = [\mathbf{q}_5]$.

not take the typical form of a general eigenvalue problem. To obtain a more desired form, we transform equation (55) from the configuration space to the state space [85]. The resulting equation can be expressed as:

$$\mathbf{M}^*\dot{\mathbf{Q}} + \mathbf{K}^*\mathbf{Q} = \mathbf{F}^*, \tag{57}$$

where,

$$\mathbf{M}^* \triangleq \begin{bmatrix} \mathbf{0} & \mathbf{M} \\ \mathbf{K} & \mathbf{0} \end{bmatrix}, \ \mathbf{K}^* \triangleq \begin{bmatrix} \mathbf{K} & \mathbf{C} \\ \mathbf{0} & -\mathbf{K} \end{bmatrix}, \ \mathbf{F}^* \triangleq \begin{bmatrix} \mathbf{F} \\ 0 \end{bmatrix} \text{ and } \mathbf{Q} \triangleq \begin{bmatrix} \mathbf{q} \\ \dot{\mathbf{q}} \end{bmatrix}. \tag{58}$$

By seeking harmonic motions, eq. (57) takes the form:

$$(i\omega\mathbf{M}^* + \mathbf{K}^*)\mathbf{Q} = \mathbf{F}^* \tag{59}$$

We now follow an established procedure [94] to formulate a generally-damped Bloch analysis. First, for each lattice vector $\mathbf{V} = n_1\mathbf{a}_1 + n_2\mathbf{a}_2$, we define a translational

operator $\mathbf{T_V}$ which upon operating on any function $f(\mathbf{r})$, shifts the argument by $\mathbf{V}$ **:**

$$\mathbf{T_V} : f(\mathbf{r}) \longmapsto f(\mathbf{r} + \mathbf{V}). \tag{60}$$

Then with the use of symmetry in the structure, we find the mathematical expression required for this mapping. As in previous work, x and y represent generally nonorthogonal axes oriented along the $\mathbf{a}_1$ and $\mathbf{a}_2$ directions, and $\mathbf{T_V}$ is represented by $\mathbf{T}_x$, $\mathbf{T}_y$ or $\mathbf{T}_{xy}$ when $\mathbf{V}$ is equal to $\mathbf{a}_1$, $\mathbf{a}_2$, or $\mathbf{a}_1 + \mathbf{a}_2$, respectively. In each unit cell, we define a minimal set of displacements denoted by $\mathbf{q}_i$ and $\widetilde{\mathbf{q}}$ representing internal and essential boundary displacements, respectively. The remaining nodal displacements can be derived by applying push-forward $\mathbf{T}_x$, $\mathbf{T}_y$ and $\mathbf{T}_{xy}$ on $\widetilde{\mathbf{q}}$; see Fig. 16 for an example geometry. This establishes a relation between the minimum set of displacements $\mathbf{q}_i$, $\widetilde{\mathbf{q}}$ and the totality of unit cell displacements $\mathbf{q}$ [93]:

$$\mathbf{q} = \mathbf{T} \begin{bmatrix} \mathbf{q}_i \\ \widetilde{\mathbf{q}} \end{bmatrix}, \tag{61}$$

in which

$$\mathbf{T} = \begin{bmatrix} \mathbf{I} & \mathbf{0} \\ \mathbf{0} & \mathbf{I} \\ \mathbf{0} & \mathbf{T}_x \\ \mathbf{0} & \mathbf{T}_y \\ \mathbf{0} & \mathbf{T}_{xy} \end{bmatrix}. \tag{62}$$

I.e., we can write $\mathbf{q}$ as:

$$\mathbf{q} = \begin{bmatrix} \mathbf{q}_i \\ \widetilde{\mathbf{q}} \\ \widetilde{\mathbf{q}}_x \\ \widetilde{\mathbf{q}}_y \\ \widetilde{\mathbf{q}}_{xy} \end{bmatrix}, \tag{63}$$

where

$$\widetilde{\mathbf{q}}_x = \mathbf{T}_x\widetilde{\mathbf{q}},\ \ \widetilde{\mathbf{q}}_y = \mathbf{T}_y\widetilde{\mathbf{q}}\ \text{ and }\ \widetilde{\mathbf{q}}_{xy} = \mathbf{T}_{xy}\widetilde{\mathbf{q}}_{xy}. \tag{64}$$

In the same way that we defined push-forward operator $\mathbf{T}$, we can define a pull-back operator $\overline{\mathbf{T}}^T$:

$$\overline{\mathbf{T}}^T = \begin{bmatrix} \mathbf{I} & \mathbf{0} & \mathbf{0} & \mathbf{0} & \mathbf{0} \\ \mathbf{0} & \mathbf{I} & \mathbf{T}_{-x}^T & \mathbf{T}_{-y}^T & \mathbf{T}_{-xy}^T \end{bmatrix}, \tag{65}$$

which consists of pull-back operations in the x, y and xy directions denoted by $\mathbf{T}_{-x}^T$, $\mathbf{T}_{-y}^T$ and $\mathbf{T}_{-xy}^T$ respectively. *I.e.*, $\mathbf{T}_{-x}^T$, $\mathbf{T}_{-y}^T$ and $\mathbf{T}_{-xy}^T$ are special cases of $\mathbf{T}_{\mathbf{V}}$ when $\mathbf{V}$ is equal to $-\mathbf{a}_1$, $-\mathbf{a}_2$, and $-\mathbf{a}_1 - \mathbf{a}_2$, respectively. We have shown previously [94] that:

$$\overline{\mathbf{T}}^T\mathbf{F} = \mathbf{0}. \tag{66}$$

We next define two new operators $\mathbf{T}_S$ and $\overline{\mathbf{T}}_S^T$ as:

$$\mathbf{T}_S = \begin{bmatrix} \mathbf{T} & \mathbf{0} \\ \mathbf{0} & \mathbf{T} \end{bmatrix} \text{ and } \overline{\mathbf{T}}_S^T = \begin{bmatrix} \overline{\mathbf{T}}^T & \mathbf{0} \\ \mathbf{0} & \overline{\mathbf{T}}^T \end{bmatrix}. \tag{67}$$

In the same manner that we wrote $\mathbf{q}$ in terms of a minimal set of coordinates, we write $\mathbf{Q}$ as:

$$\mathbf{Q} = \mathbf{T}_S \begin{bmatrix} \mathbf{q}_i \\ \widetilde{\mathbf{q}} \\ \dot{\mathbf{q}}_i \\ \dot{\widetilde{\mathbf{q}}} \end{bmatrix}. \tag{68}$$

From eqs. (58) and (66), it is easily verified that:

$$\overline{\mathbf{T}}_S^T\mathbf{F}^* = \mathbf{0}. \tag{69}$$

Consequently,

$$(i\omega\overline{\mathbf{T}}_S^T\mathbf{M}^*+\overline{\mathbf{T}}_S^T\mathbf{K}^*)\mathbf{Q}=\mathbf{0}. \tag{70}$$

We next borrow the same argument used for the undamped case [94]. Equation (70) holds for any unit cell in the structure, thus it is invariant with respect to any shift,

$$\mathbf{T_V}((i\omega\overline{\mathbf{T}}_S^T\mathbf{M}^*+\overline{\mathbf{T}}_S^T\mathbf{K}^*)\mathbf{Q})=\mathbf{0}. \tag{71}$$

Due to translational symmetry of the lattice structure,

$$\mathbf{T_V}(\overline{\mathbf{T}}_S^T\mathbf{M}^*)=\overline{\mathbf{T}}_S^T\mathbf{M}^*\ ,\ \mathbf{T_V}(\overline{\mathbf{T}}_S^T\mathbf{K}^*)=\overline{\mathbf{T}}_S^T\mathbf{K}^*. \tag{72}$$

As a result, eq. (71) is written in the form:

$$(i\omega\overline{\mathbf{T}}_S^T\mathbf{M}^*+\overline{\mathbf{T}}_S^T\mathbf{K}^*)\mathbf{T_V}(\mathbf{Q})=\mathbf{0}. \tag{73}$$

Since both $\mathbf{Q}$ and $\mathbf{T_V}(\mathbf{Q})$ are eigenvectors of the same eigenvalue problem (70), we conclude that:

$$\mathbf{T_V}(\mathbf{Q})=\lambda(\mathbf{V})\mathbf{Q}, \tag{74}$$

where $\lambda(\mathbf{V})$ is a coefficient to be determined.

We now examine the properties of the operator $\mathbf{T_V}$. First we can easily verify that for two lattice vectors $\mathbf{V}=n_1\mathbf{a}_1+n_2\mathbf{a}_2$ and $\mathbf{V'}=n_3\mathbf{a}_1+n_4\mathbf{a}_2$:

$$\mathbf{T_{V'}}(\mathbf{T_V}(\mathbf{Q}))=\mathbf{T_{V'}}(\lambda(\mathbf{V})\mathbf{Q})=\lambda(\mathbf{V'})\lambda(\mathbf{V})\mathbf{Q}. \tag{75}$$

We can then use the definition of $\mathbf{T_V}$ to write:

$$\mathbf{T_{V'}}(\mathbf{T_V}(\mathbf{Q}))=\mathbf{Q}((n_1+n_3)\mathbf{a}_1+(n_2+n_4)\mathbf{a}_2)=\mathbf{T_{V+V'}}(\mathbf{Q})=\lambda(\mathbf{V}+\mathbf{V'})\mathbf{Q}. \tag{76}$$

Comparing eq. (75) and eq. (76), we conclude that for a general lattice vector $\mathbf{V} = n_1\mathbf{a}_1 + n_2\mathbf{a}_2$, $\lambda(\mathbf{V})$ is a power function of $\mathbf{V}$, *i.e.,* eq. (74) is rephrased as:

$$\mathbf{T}_{\mathbf{V}}(\mathbf{Q}) = e^{2\pi i(n_1k_1+n_2k_2)}\mathbf{Q}. \tag{77}$$

The right-hand side of (77) is written in the short form of $e^{i\mathbf{k}\cdot\mathbf{V}}$ by introducing the wavevector $\mathbf{k} = k_1\mathbf{b}_1 + k_2\mathbf{b}_2$, in which $\mathbf{b}_i$'s are reciprocal lattice vectors satisfying $\mathbf{b}_i \cdot \mathbf{a}_j = 2\pi\delta_{ij}$. Applying $\mathbf{T}_{\mathbf{V}}$ on both sides of eq. (59) and using eq. (77), we can extract the following relation for neighbor forces:

$$\mathbf{T}_{\mathbf{V}}(\mathbf{F}^*) = e^{2\pi i(n_1k_1+n_2k_2)}\mathbf{F}^*. \tag{78}$$

Having established the Bloch relation, we can express $\mathbf{T}_x$, $\mathbf{T}^T_{-x}$, $\mathbf{T}_y$, $\mathbf{T}^T_{-y}$, $\mathbf{T}_{xy}$ and $\mathbf{T}^T_{-xy}$ in functional form. For the example geometry depicted in Fig. 16, these forms are given as:

$$\mathbf{T}_x = \left[\mathbf{I}e^{2\pi ik_1}\right],\ \mathbf{T}_y = \left[\mathbf{I}e^{2\pi ik_2}\right],\ \mathbf{T}_{xy} = \left[\mathbf{I}e^{2\pi i(k_1+k_2)}\right], \tag{79}$$

$$\mathbf{T}^T_{-x} = \left[\mathbf{I}e^{-2\pi ik_1}\right],\ \mathbf{T}^T_{-y} = \left[\mathbf{I}e^{-2\pi ik_2}\right],\ \mathbf{T}^T_{-xy} = \left[\mathbf{I}e^{-2\pi i(k_1+k_2)}\right]. \tag{80}$$

Note that in the presence of damping the wavevector components k_1 and k_2 are complex numbers:

$$k_1 = k_1^R + ik_1^I,\ k_2 = k_2^R + ik_2^I. \tag{81}$$

The final equation of motion is:

$$\overline{\mathbf{T}}^T_S(i\omega\mathbf{M}^* + \mathbf{K}^*)\mathbf{T}_S\widehat{\mathbf{q}}_S = \mathbf{0}, \tag{82}$$

where

$$\widehat{\mathbf{q}}_S = \begin{bmatrix} \mathbf{q}_i \\ \widetilde{\mathbf{q}} \\ \dot{\mathbf{q}}_i \\ \dot{\widetilde{\mathbf{q}}} \end{bmatrix}. \tag{83}$$

Rearranging eq. (82), we get the desired general eigenvalue problem:

$$\overline{\mathbf{T}}_S^T \mathbf{K}^* \mathbf{T}_S \widehat{\mathbf{q}}_S = i\omega \overline{\mathbf{T}}_S^T \mathbf{M}^* \mathbf{T}_S \widehat{\mathbf{q}}_S. \tag{84}$$

4.1.2 Qualitative Discussion

In eq. (84), $\overline{\mathbf{T}}_S^T$ and $\mathbf{T}_S$ are functions of k_1 and k_2. We are interested in the steady-state condition for which ω is a real number. In the absence of energy dissipation, wavevectors are real. In this case, k_1 and k_2 are chosen without constraint and we are guaranteed to get a real ω [94]. Also due to the power functional form of the Bloch relation in an undamped case, $\overline{\mathbf{T}}_S^T$ and $\mathbf{T}_S$ are periodic functions of k_1 and k_2 with period 1. As a result, one can first pick any number of (k_1, k_2) in $[0,1] \times [0,1]$, then establish $\overline{\mathbf{T}}_S^T$ and $\mathbf{T}_S$, and finally solve the general eigenvalue problem for ω. In this manner, the dispersion curves are plotted. However, as we shall demonstrate in the next section, in the case with energy dissipation, the choices for k_1 and k_2 are restricted; *i.e.,* only a subset of k_1^R, k_1^I, k_2^R and k_2^I result in real ω. It should also be noted that $\overline{\mathbf{T}}_S^T$ and $\mathbf{T}_S$ are periodic functions of k_1^R and k_2^R; however, we are not guaranteed that all the k_1^R and k_2^R in the interval $[0,1]$ result in a real ω. Therefore, previous algorithms designed to obtain dispersion curves cannot be borrowed in whole since they freely choose (k_1, k_2) and find ω. One must instead design an algorithm which take as input real ω and finds complex wavevectors k_1 and k_2.

4.2 Investigating Dispersion Curves

4.2.1 One-Dimensional Structures

In this section, for ease of notation and explanation, we start our investigation with one-dimensional lattices, then we explore lattices with two dimensions. In a one-dimensional lattice, the wave and lattice vectors simplify to scalars k and a, respectively. Analyzing equations of motion in state space allowed us to established the Bloch relation in structures with damping, and to ultimately find the functional form $\mathbf{T_V}$. With $\mathbf{T_V}$ obtained, we can return to configuration space. As is noted in the last section, we specify real values for ω and seek complex values for k in the following equation:

$$\overline{\mathbf{T}}^T(-\omega^2\mathbf{M}+i\omega\mathbf{C}+\mathbf{K})\mathbf{T}\widehat{\mathbf{q}}=\mathbf{0}, \tag{85}$$

where $\widehat{\mathbf{q}}$ denotes $\begin{bmatrix} \mathbf{q}_i & \widetilde{\mathbf{q}} \end{bmatrix}^T$. Note that $\overline{\mathbf{T}}^T$ and $\mathbf{T}$ are functions of real and imaginary components of k which are denoted by k_R and k_I. In order for eq. (85) to be satisfied, the following condition should hold:

$$\det(\overline{\mathbf{T}}^T(-\omega^2\mathbf{M}+i\omega\mathbf{C}+\mathbf{K})\mathbf{T}) = 0. \tag{86}$$

For each ω, the left-hand side of eq. (86) results in a complex expression, and thus two real equations must be satisfied. For the example structure depicted in Fig. 17, after simplification these equations are given by:

$$-\omega^2 m + 2K - K\cos 2\pi k_R\,(e^{2\pi k_I}+e^{-2\pi k_I}) - c\omega\sin 2\pi k_R\,(e^{2\pi k_I}-e^{-2\pi k_I}) = 0 \tag{87}$$

$$2\omega C - K\sin 2\pi k_R\,(e^{-2\pi k_I}-e^{2\pi k_I}) - c\omega\cos 2\pi k_R\,(e^{2\pi k_I}+e^{-2\pi k_I}) = 0 \tag{88}$$

Eliminating ω from the two equations yields:

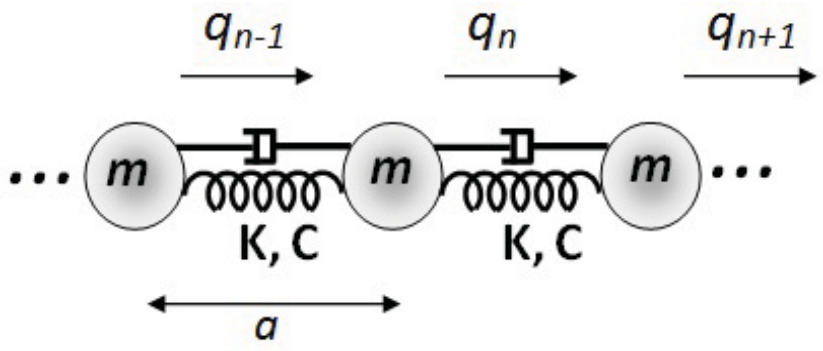

Figure 17: A simple mass-spring-damper structure, a is the lattice constant,and K, C are stiffness and damping coefficient respectively.

$$mK^2 \sin^2 2\pi k_R \ (y^2-1)+2C^2K(y\cos 2\pi k_R-1)(\sin^2 2\pi k_R \ (y^2-1)+(y\cos 2\pi k_R-1)^2) = 0, \tag{89}$$

where $y \equiv \cosh 2\pi k_I$. For a fixed k_R, the left-hand side of eq. (89) is a function of y which we term $z(y)$. Since the hyperbolic cosine is always greater than or equal to one, any solution y of eq. (89) should be greater than or equal to one. As is evident in Fig. 18 for an example k_R, as damping increases, this condition is ultimately not satisfied; *i.e.*, propagation with wave number k_R is not possible. This is due to the graph of $z(y)$ shifting downwards with increased damping.

Much like the frequency band gap notion well-established in undamped structures, the behavior described above indicates a wave number gap. In Figs. In Figs. 19 and 20 dispersion curves of the repeating mass-spring-damper structure of Fig. 17 are depicted. It is evident that unlike the undamped structure, k_R does not occupy every value in the range $[-0.5, 0.5]$. In fact, as the damping increases, the occupation interval of k_R decreases. A second feature observed in the damped dispersion curves is that for each k_R there may exist more than one ω belonging to the same branch. This results from the dispersion curves bending back towards the origin as k_R approaches 0.5. Note that in an undamped structure, the number of frequencies for a single k_R

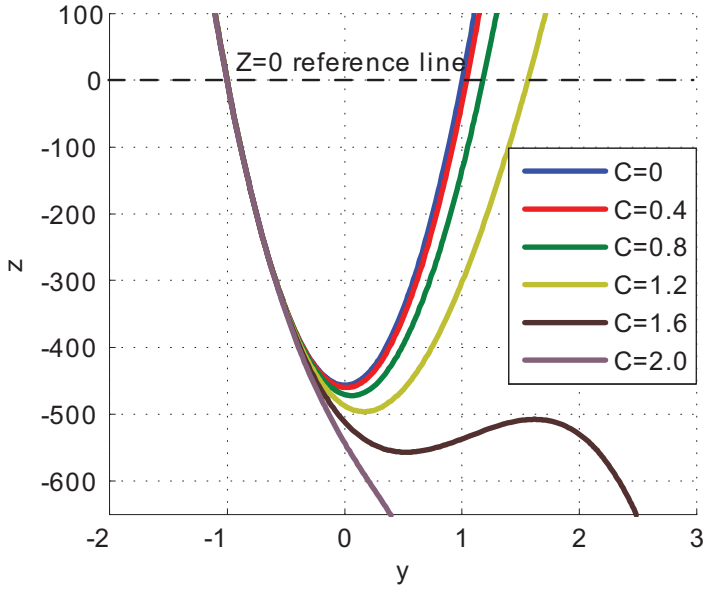

Figure 18: Plot of $z(y)$ for varying values of C using a fixed $2\pi k_R = 2.4$, mass $m = 10$ and stiffness $K = 5$.

is determined by the degrees of freedom in a unit cell. This qualitative feature no longer holds in the damped case.

Another notable feature observed in Fig. 20 is that for frequencies higher than a certain frequency -in this case approximately 2.3 Hz- the imaginary wavevector of the higher damping cases becomes smaller than the ones with lower damping ratios. In other words, increasing damping helps the propagation of the wave. These dispersion curves were verified by numerical simulation of the equations of motion for a finite chain. In the simulation, similar to that described in [95], a mass-spring-damper chain with over one hundred cells was excited by a sinusoidal force at one end. Snap shots of the mass displacements were taken at a time such that the initiated wave has not reached the other end. In order to obtain the spatial wavevector, the best function with least squares error passing through the mass displacements with the form of $e^{-2\pi k_i} \sin(2\pi k_R x - \varphi)$ was found. Simulations were run for several input frequencies and five different damping constants. The simulation results are marked in Figs. 19

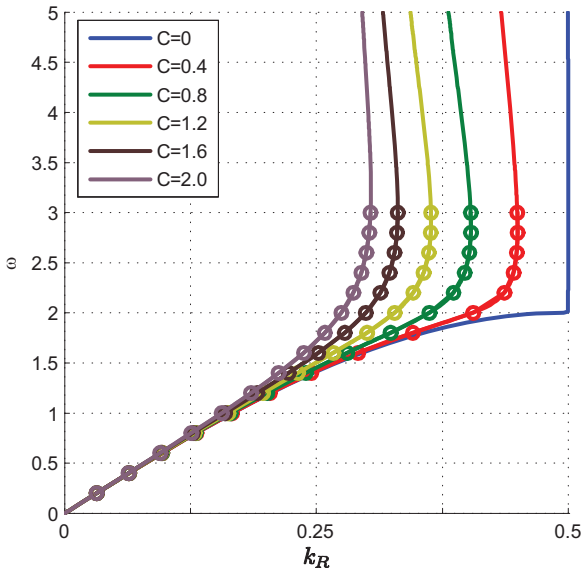

Figure 19: Dispersion curves for the mass-spring-damper structure of Fig. 17 for various damping coefficients C and stiffness $K = 5$, lattice vector $a = 0.1$, and mass $m = 5$. The real part of the wavevector is depicted here with the simulation results marked by open circles. As is evident, the real part of the wavevector does not cover the interval $[0, 0.5]$. Due to symmetry, only the positive part of the graph is depicted.

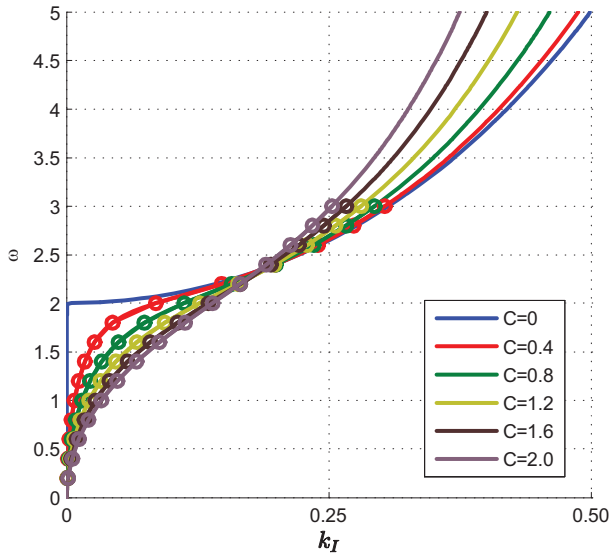

Figure 20: Dispersion curves for the mass-spring-damper structure of Fig. 17 for various damping coefficients C and stiffness of $K = 5$, lattice vector $a = 0.1$, and mass $m = 5$. The imaginary part of the wavevector is depicted here with the simulation results marked by open circles. Due to symmetry, only the positive part of the graph is depicted.

and 20 by open circles. As can be noted, the simulation results agree very well with the calculated dispersion curves. The simulations also verify the existence of multiple frequencies at a given real wavenumber.

In the case of undamped structure, we have $C = 0$ in eq. (89). Therefore we should have either $\{y = 1, k_R \in [-0.5, 0.5]\}$ (implying no decay in the wave amplitude), or $\{y \in [1, \infty], k_R = 0, 0.5]\}$ (implying an evanescent wave). The frequency range for which $k_R = 0.5$ is termed the stop band(s). However, in the presence of damping, $y \neq 1$ implies $k_I \neq 0$ for all frequencies.

For structures with more than one mass per unit cell, the set of equations analogous to (87), (88) contain polynomials of ω with degrees higher than two. Therefore, elimination of ω becomes intractable. Instead, an alternative solution strategy is pursued.

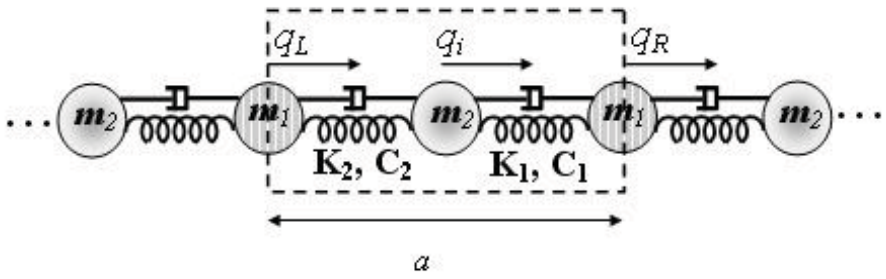

Figure 21: A model of diatomic chain which includes linear damping.

Note that in eq. (86), only $\mathbf{T}$ and $\overline{\mathbf{T}}^T$ are functions of k_I and k_R. These are push-forward and pull-back operators in which k_I, k_R dependence appear as $e^{2\pi i(k_R+ik_I)}$ and $e^{-2\pi i(k_R+ik_I)}$. We denote these by x and x^{-1}. As a result, eq. (86) is transformed to a polynomial of x with coefficients which are functions of ω and M, K and C matrix elements. After solution of this polynomial expression for x, we have:

$$k_I = -\frac{\ln(|x|)}{2\pi}, \tag{90}$$

$$k_R = \frac{\arctan(\frac{\mathrm{Im}\{x\}}{\mathrm{Re}\{x\}})}{2\pi}. \tag{91}$$

in which $|x|$, $\mathrm{Im}\{x\}$, $\mathrm{Re}\{x\}$ are the absolute value of x, imaginary and real parts of x, respectively. This procedure is illustrated for the case of a two-mass structure depicted in Fig. 21.

The necessary matrices for the system shown in Fig. 21 are:

$$\begin{aligned}
\mathbf{M} &= \begin{bmatrix} m_2 & 0 & 0 \\ 0 & \frac{m_1}{2} & 0 \\ 0 & 0 & \frac{m_1}{2} \end{bmatrix}, \mathbf{C} = \begin{bmatrix} C_1+C_2 & -C_2 & -C_1 \\ -C_2 & C_2 & 0 \\ -C_1 & 0 & C_1 \end{bmatrix}, \\
\mathbf{K} &= \begin{bmatrix} K_1+K_2 & -K_2 & -K_1 \\ -K_2 & K_2 & 0 \\ -K_1 & 0 & K_1 \end{bmatrix}, \mathbf{q} = \begin{bmatrix} q_i \\ q_L \\ q_R \end{bmatrix}, \mathbf{F} = \begin{bmatrix} 0 \\ F_L \\ F_R \end{bmatrix}.
\end{aligned} \tag{92}$$

Push-forward and pull-back operators are defined as:

$$\mathbf{T} = \begin{bmatrix} 1 & 0 \\ 0 & 1 \\ 0 & x \end{bmatrix}, \overline{\mathbf{T}}^T = \begin{bmatrix} 1 & 0 & 0 \\ 0 & 1 & \frac{1}{x} \end{bmatrix}, \tag{93}$$

in which $x = e^{2\pi i(k_R + ik_I)}$. Using these operators we can determine further that:

$$\begin{aligned}
\overline{\mathbf{T}}^T\mathbf{M}\mathbf{T} &= \begin{bmatrix} m_2 & 0 \\ 0 & m_1 \end{bmatrix}, \overline{\mathbf{T}}^T\mathbf{C}\mathbf{T} = \begin{bmatrix} C_1+C_2 & -C_1x - C_2 \\ -C_1x^{-1} - C_2 & C_1+C_2 \end{bmatrix}, \\
\overline{\mathbf{T}}^T\mathbf{K}\mathbf{T} &= \begin{bmatrix} K_1+K_2 & -K_1x - K_2 \\ -K_1x^{-1} - K_2 & K_1+K_2 \end{bmatrix}, \widehat{\mathbf{q}} = \begin{bmatrix} q_i \\ q_L \end{bmatrix}.
\end{aligned} \tag{94}$$

Substituting these expressions into the determinant of eq. (86) we find:

$$Ax + B + Ax^{-1} = 0, \tag{95}$$

where:

$$A = i\omega C_1K_2 - \omega^2C_1C_2 + K_1K_2 + i\omega C_2K_1 \tag{96}$$

$$\begin{aligned}
B &= -\omega^4m_1m_2 + i\omega^3m_2C_1 + i\omega^3m_1C_2 + i\omega^3m_1C_1 + i\omega^3m_2C_2 + \omega^2m_1K_2 + \omega^2m_2K_1... \\
&\quad +\omega^2m_2K_2 + \omega^2m_1K_1 + 2\omega^2C_1C_2 - 2i\omega K_1C_2 - 2i\omega K_2C_1 - 2K_1K_2.
\end{aligned}$$

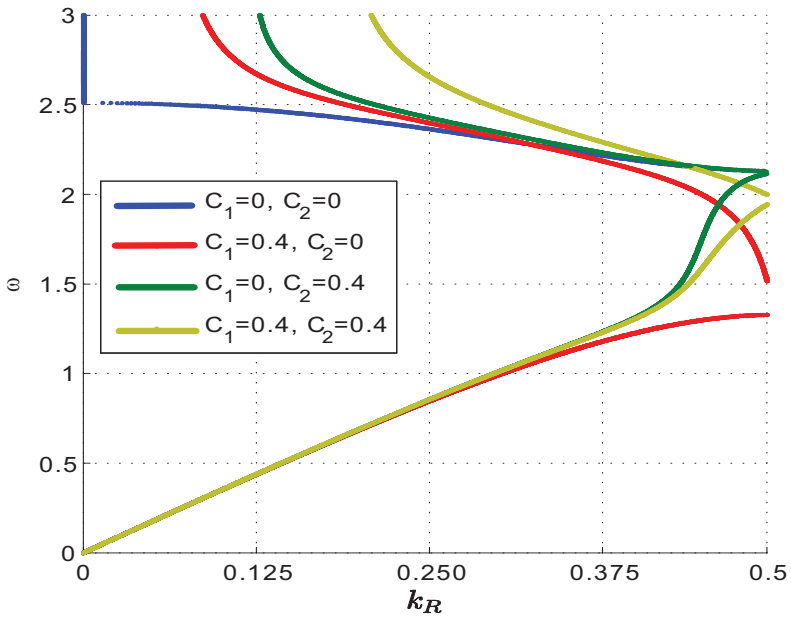

Figure 22: Real part of the wave vector for the diatomic chain. Damping in the structure, has changed dispersion curves.

Equation (95) can be stated as a quadratic equation which can be solved readily for $x(\omega)$. Due to the symmetric form of eq. (95), if x is the solution, so is x^{-1}. This is to be expected since one solution results in a right-ward moving wave and the other a left-ward moving wave. Note that as we increase the number of masses, the order of ω would increase in eq. (96). However, eq. (95) remains unchanged and thus the procedure described changes little.

Dispersion curves for the example problem of Fig. 21 are investigated in Figs. 22 and 23 for various damping coefficients. These curves demonstrate that damping can drastically change the character of the branches, the upper branch (optical) shifts upward at low wavenumbers while it shifts downward at high wavenumbers. As evident in Fig. 22, the distance between acoustic and optical branches decreases at high wavenumbers, implying that the evanescent wave has changed into a traveling wave.

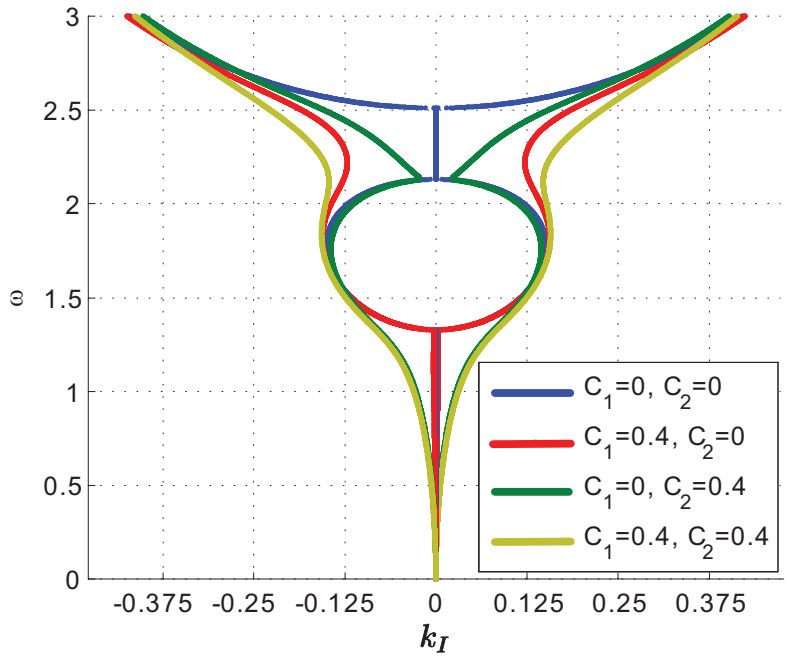

Figure 23: Imaginary part of the wave vector for the diatomic chain with damping.

4.2.2 Two-Dimensional Structures

For two-dimensional lattice structures, the wavevector has two components along the directions of the reciprocal lattice vectors. These two components are defined by two complex numbers k_1 and k_2 as in eq. (81). Dispersive relation between frequency ω and the wave numbers k_1^R, k_1^I, k_2^R and k_2^I is defined by (86). In this case, $\overline{\mathbf{T}}^T$ and $\mathbf{T}$ are functions of $e^{2\pi i k_1}$, $e^{2\pi i k_2}$, $e^{2\pi i(k_1+k_2)}$, $e^{-2\pi i k_1}$, $e^{-2\pi i k_2}$ and $e^{-2\pi i(k_1+k_2)}$. By adopting the same method we used for one-dimensional lattices, we denote these exponential terms by x, y, xy, x^{-1}, y^{-1} and $x^{-1}y^{-1}$, respectively. Equation (86) is then transformed to a polynomial of x and y with coefficients which are functions of the variable ω and M, K and C matrix elements.

For two-dimensional lattice depicted in Fig. 24, the aforementioned polynomial is stated as:

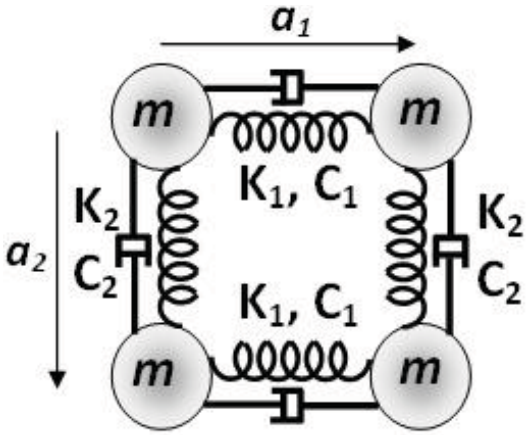

Figure 24: Unit cell of a simple two-dimensional lattice with out of plane motion.

$$\frac{1}{xy}(-2\,y^2xK_2 - 2\,x^2yK_1 + 4\,xyK_1 - 2\,ix^2y\omega\,C_1 - 2\,iy^2x\omega\,C_2 - 2\,xK_2 + \ldots \quad (97)$$
$$4\,ixy\omega\,C_2 - 2\,yK_1 + 4\,xyK_2 + 4\,ixy\omega\,C_1 - 2\,ix\omega\,C_2 - 2\,iy\omega\,C_1 - 4\,xy\omega^2m) = 0.$$

Equation (97) identifies the dispersive relation between ω and the complex numbers x and y. To obtain dispersion surfaces from eq. (97) we pick a real number ω and a complex number y, then we solve the resultant quadratic equation for x. Finally, The wave numbers k_1^R, k_1^I are computed by (90). Similar equation relates y and k_2^R, k_2^I. Since there are five variables k_1^R, k_1^I, k_2^R, k_2^I and ω involved in the dispersion relation, they are plotted in separate graphs. For illustration, we pick two different values for k_2^I; zero and $3/2\pi$. Then x was calculated for several values of k_2^R and ω. We then calculate k_1^R and k_1^I from x and plot them in different graphs. k_1^R and k_1^I vs. (ω, k_2^R) for $k_2^I = 0$ are demonstrated in Fig. 25a and Fig. 25b, respectively, while in Fig. 25c and Fig. 25d the same variables are plotted for $k_2^I = 3/2\pi$. As it is evident from these dispersion surfaces, k_1^R and k_2^R do not occupy every value in the range $[-0.5, 0.5]$. This was expected as we observed the same phenomenon in the one-dimensional lattice. Therefore, as it can bee seen in Fig. 26 the cross-section

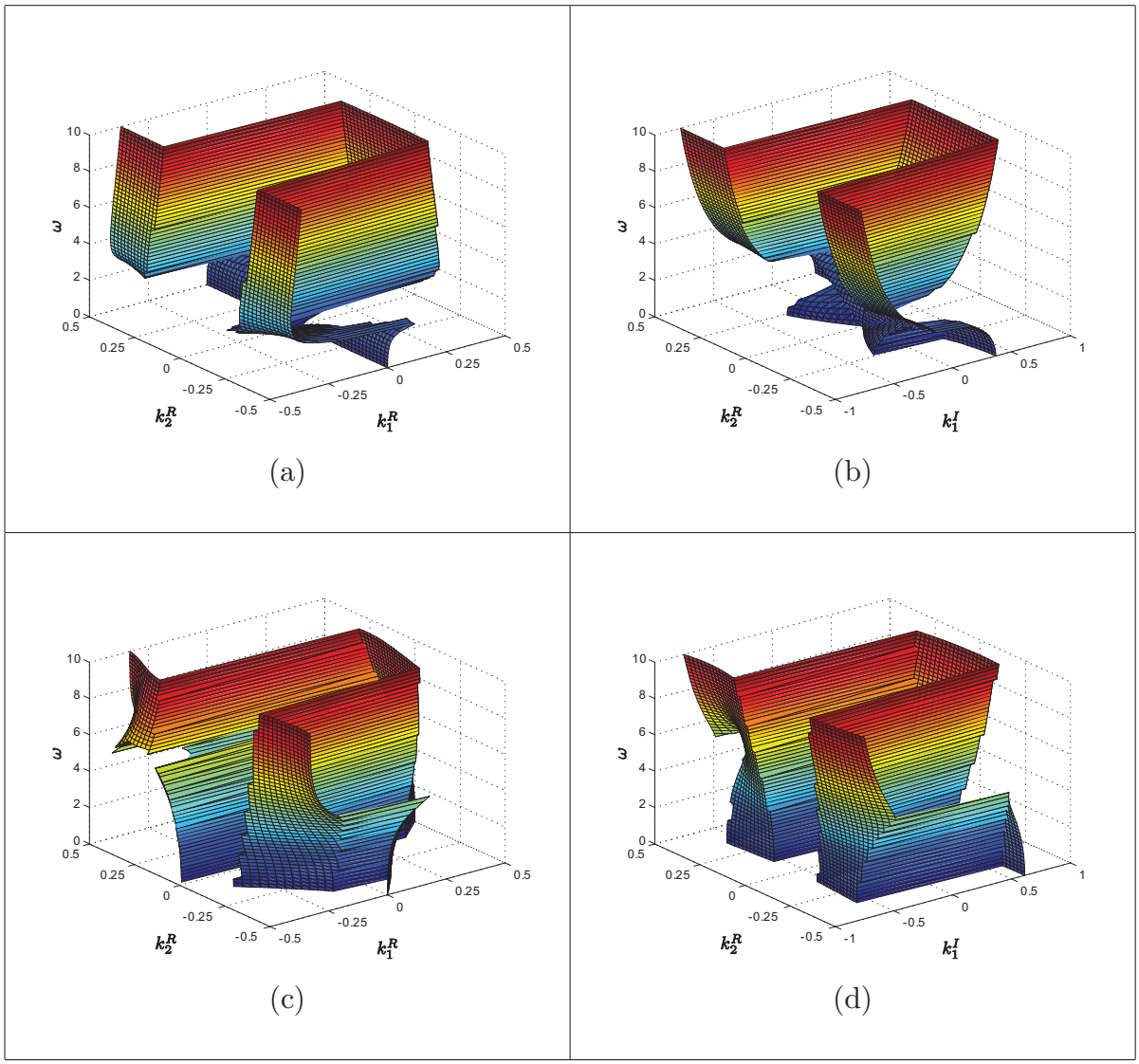

Figure 25: Dispersion surfaces for the structure depicted in Fig. 16 with $K_1 = 1$, $K_2 = 2$, $C_1 = 0.1$, $C_2 = 0.2$ and $m = 1$. For $k_2^I = 0$, (k_1^R, k_2^R, ω) and (k_1^I, k_2^R, ω) are plotted in (a) and (b) while (c) and (d) are the dispersion surfaces for $k_2^I = 3/2\pi$.

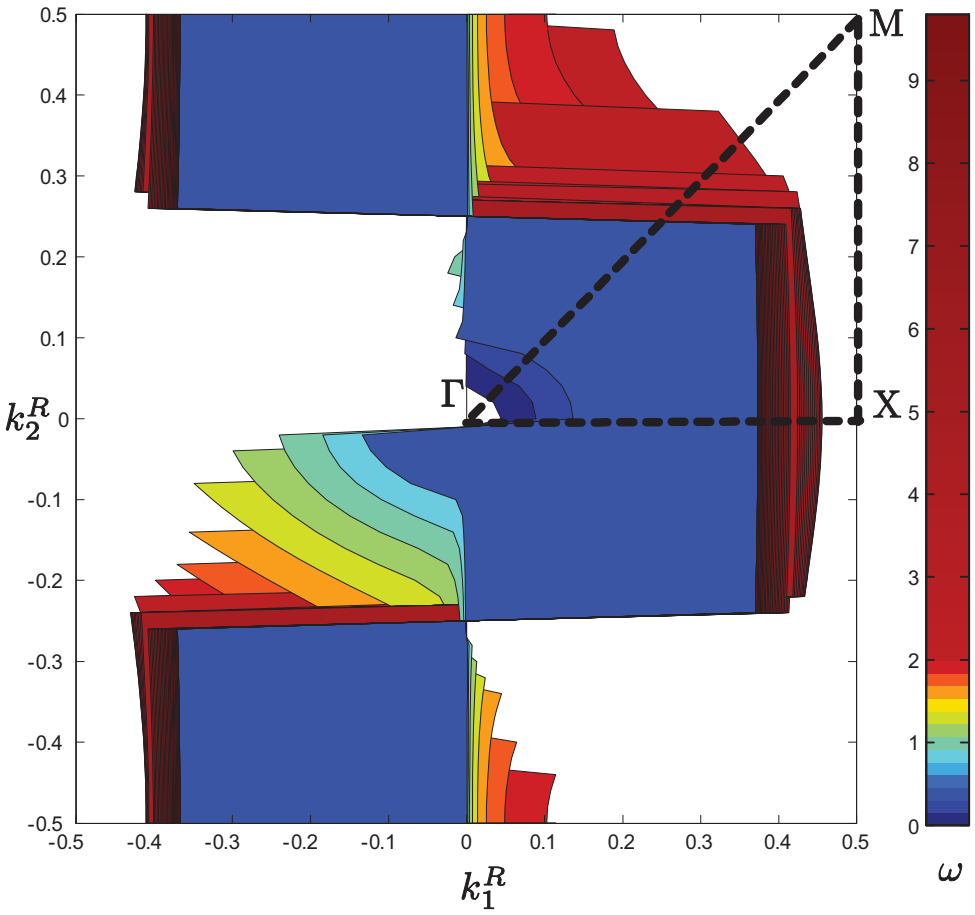

Figure 26: Symmetry lines Γ-X, X-M and M-Γ and contour graph of the dispersion surface depicted in Fig. 25a. It is evident that these symmetry lines do not capture the extrema values of ω.

of the dispersion surface along the symmetry lines Γ-X, X-M and M-Γ do not capture the extrema values of ω. This requires us to depart from the standard way of representing dispersion curves only along the high symmetry lines.

For a unit cell with two different masses and diagonal lattice vectors, such as the one depicted in Fig. 27, the dispersion polynomial relating x, y and ω has more terms compared to the eq. (97). However, it has the same degree for x and y. Thus the same procedure is followed to calculate the dispersion relation. For this case,

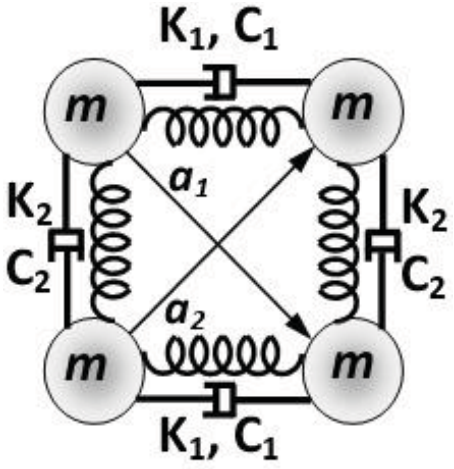

Figure 27: Unit cell of a two-dimensional lattices with diagonal lattice vectors and out of plane motion.

k_1^R and k_1^I vs. (ω, k_2^R) are depicted for two values of k_2^I in Figs. 28. Similar to the one-dimensional structure, in these surfaces we observe that for each pair of (k_1^R, k_2^R) there may exist more than one ω belonging to the same surface.

This chapter was the last part of our investigation of the Bloch analysis concerned with periodic structures. In the next chapter, we first demonstrate that eq. (45) can also model phonon dispersion in crystals. Then we use the framework we developed in the previous chapters to derive a method to calculate the maximum number of wavevectors for each frequency in a dispersion relation.

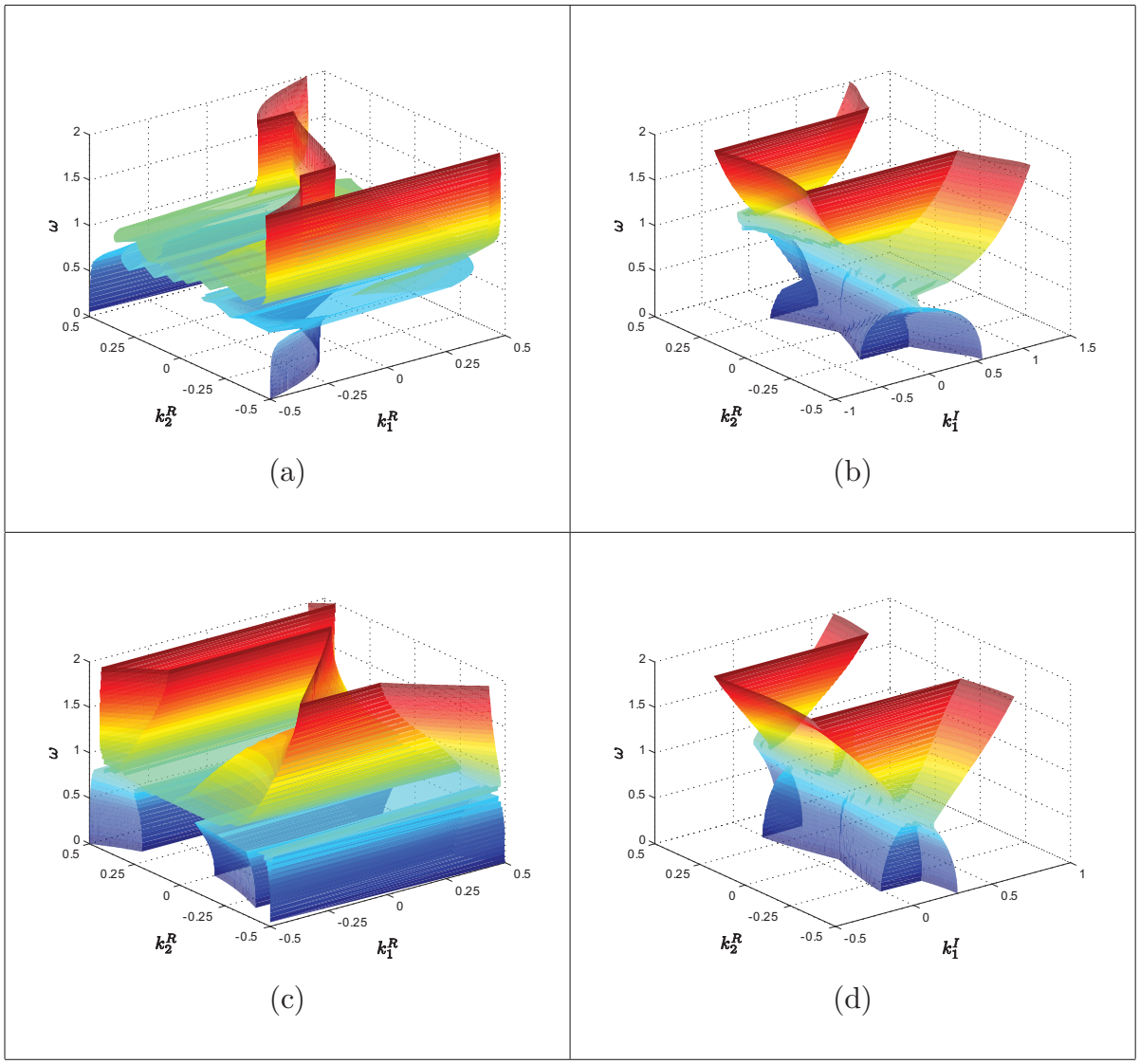

Figure 28: Dispersion surfaces for the structure depicted in Fig. 19 with $K_1 = 1$, $K_2 = 2$, $C_1 = 0.1$, $C_2 = 0.2$, $m_1 = 5$ and $m_1 = 4$. In (a) and (b), (k_1^R, k_2^R, ω) and (k_1^I, k_2^R, ω) are plotted when $k_2^I = 0$, while (c) and (d) shows the dispersion surfaces for $k_2^I = 3/2\pi$.

CHAPTER V

FORCE-CONSTANT MODEL AND NUMBER OF WAVEVECTORS FOR EACH ω

5.1 Introduction

Throughout the previous chapters, we discussed Bloch analysis as applied to wave propagation analysis of discrete periodic structures. Any unit cell of a periodic structure can be modelled by a discrete system of equations after invoking finite element analysis. What's more, there are structures which are inherently modeled as discrete, such as crystals. In this chapter we first discuss the force constant model as applied to the study of phonon dispersion analysis. Later, we investigate the number of wave vectors for each ω in a dispersion relation.

5.2 Force-Constant Model as a Tool to Calculate Phonon Dispersion Curves

In this section, we first overview phonon dispersion curves of crystalline materials, and then a mass-spring model is presented as a tool with which we can reproduce experimental results.

In the investigation of phonon dispersion curves of crystals, there have been different approaches; semiempirical, and *ab initio,* or first-principle, calculation. In some semiempirical approaches, the model relies to some extent on experimental characterization of force field parameters. Phonon dispersion curves are experimentally

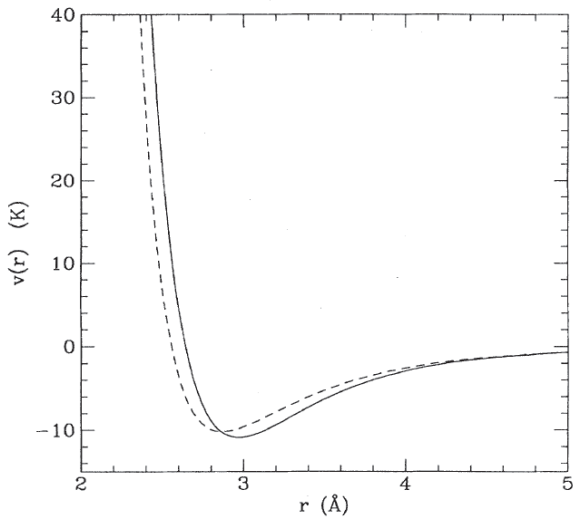

Figure 29: Semiempirical potential between two helium atoms; solid line by Aziz *et. al.* [17] and Lennard-Jones with $\epsilon = 10.22$ K and $\sigma = 2.556$ Å (dashed line) [18]

obtained by means of neutron scattering [14],[15] or Raman spectroscopy [16]. Interaction potentials and forces are then assumed in functional form, for example by a power function. The constants of these functions are found by fitting the experimental results with the theoretical calculation. The Lennard-Jones (LJ) potential and the Morse potential are two commonly used potential models. The Lennard-Jones potential is stated as:

$$V(r) = 4\epsilon \left[\left(\frac{\sigma}{r}\right)^{12} - \left(\frac{\sigma}{r}\right)^{6} \right], \tag{98}$$

where r is the distance between particles, σ is the distance at which the potential is zero and ϵ is the depth of the potential well. These parameters are found to fit the experimental data. Two such attempts for helium are depicted in Fig.29.

The Morse potential is stated as

$$V(r) = D_e(1 - e^{-a(r-r_e)})^2, \tag{99}$$

in which a controls the width of the potential, and D_e, r, r_e denote the well depth

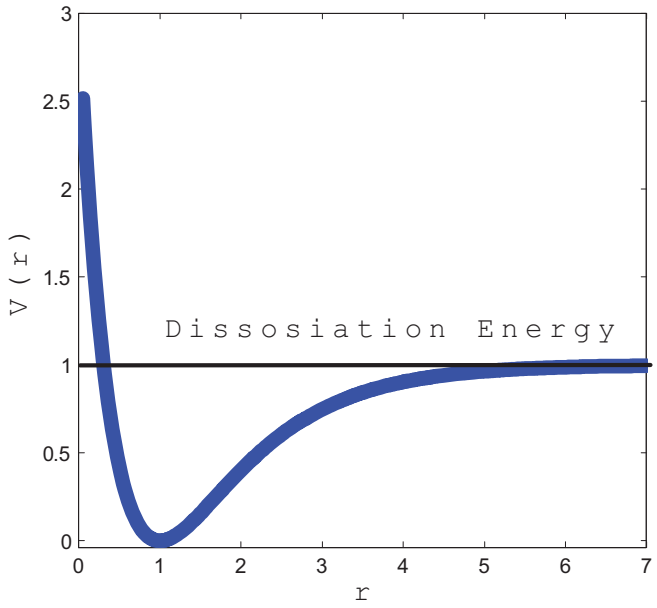

Figure 30: Morse potential function when D_e, r_e and a are equal to one.

and the distance between particles in the nonequilibrium and equilibrium situations, respectively. An example of this potential is depicted in Fig.30.

Since in the semiempirical approach we rely on experiments to determine the coefficients of fitting functions, they are inherently *ad hoc,* and experiments have to be performed for each material. In contrast, when we use the *ab initio* method, all the calculations are based on the laws of physics, such as quantum mechanics and density functional theory [19]. Although this method is more general, it is a computationally costly method, and in most cases it is overly complicated.

As is evident in Figs. 29 and 30, the potential energy function resembles a quadratic function when the particles are close to the equilibrium position. Hence, in the semiempirical calculation of phonon dispersion curves, the potential energy between the particles is assumed to be quadratic. In this kind of model - called force constant model - forces are represented by linear springs and then the spring constants are found by fitting the theoretical phonon dispersion curves with the experimental

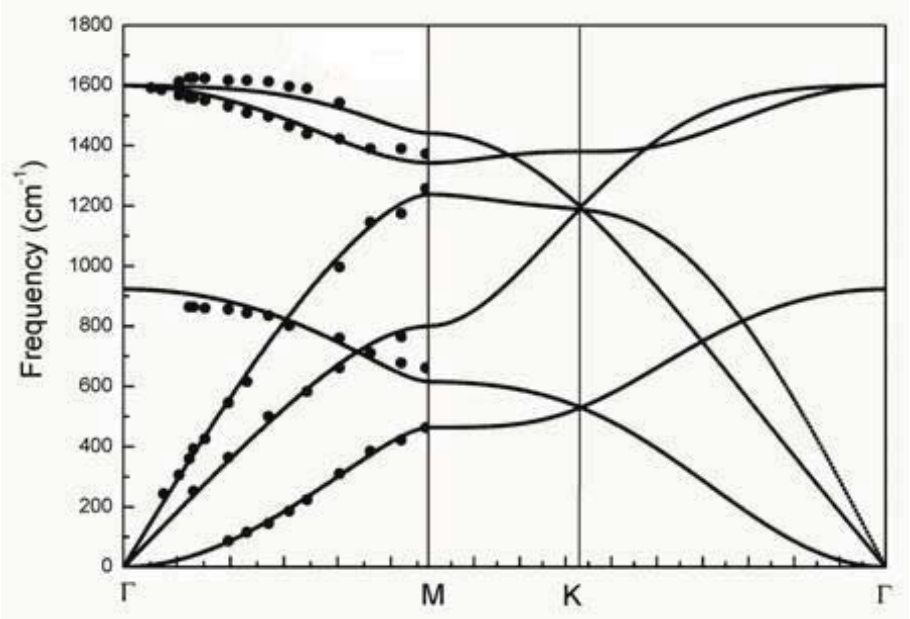

Figure 31: Phonon dispersion curves of graphene claculated by the force constant model, taking into account up to the fourth nearest neighbor interaction [22]. Experimental results marked by circles, obtained by energy loss spectroscopy [23],[24].

dispersion curves.

Generally speaking, in a semiempirical method, it is assumed that particles separated beyond certain cut-off distances, have negligible force effect, and hence it is safe to omit them in the calculation. It is however, the matter of best fitting that dictates the cut-off distance. Jishi et al. [20] showed that to calculate phonon dispersion curves for graphite, it suffices to consider the interaction of atoms up to the fourth nearest neighbor, both interplane and intraplane. A model with less than a fourth nearest neighbor cannot reproduce the experimental results. The same fourth nearest neighbor model has been shown [21]-[22] to agree well with the experimental results for graphene, C-60 and nanotubules. Fig. 31 shows the experimental results and dispersion curves of graphene obtained by the force constant model which includes up to the fourth nearest neighbor. Fig. 32 shows similar results obtained by the Matlab code in the appendix. As can bee seen in this figure, the force constant

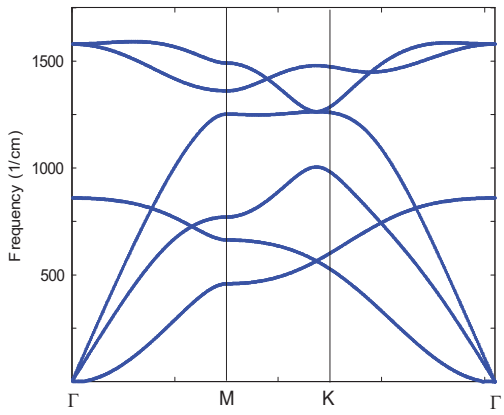

Figure 32: Phonon dispersion curves of graphene claculated by the Matlab code in the appendix which utilizes force constant model

model, although simple in principle, can produce complicated dispersion curves which characterize phonon dispersion curves of nanostructures.

5.3 Number of Wavevectors for each ω in a Dispersion Relation

5.3.1 Introduction

In the previous chapter we considered simple (*i.e.*, nearest neighbor interaction) one and two-dimensional structures which eq. (86) expressed as polynomials of degree two. In this section we investigate the degree of polynomial in general cases. In a bimaterial chain (or diatomic crystal chain), if we consider the nearest neighbor interaction only, the optical and acoustic branches are monotonic; meaning that for each ω there would be only one corresponding positive wavevector in the first Brillouin zone [26] as is evident in the dispersion curve for an example diatomic chain in Fig. 33. If we increase the number of interactions or consider two-dimensional lattices, there might be more than one wavevector corresponding to each ω. This fact was first investigated in a rigorous way by Brillouin [28] for a simple monatomic chain.

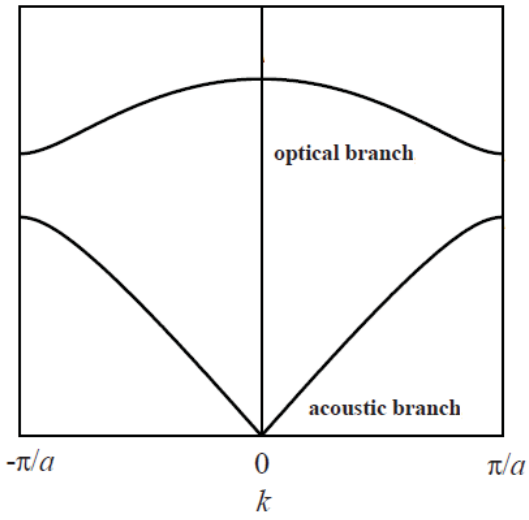

Figure 33: Optical and acoustic branches in the dispersion relation [27]. It is evident that the dispersion curves are monotonic.

We reinvestigate this fact for structures with damping; also we would extend our investigation to structures with two or three dimensions.

5.3.2 Number of wavevectors for each ω

Recall from the previous chapter that the displacements of a unit cell can be stated as:

$$\mathbf{q} = \begin{bmatrix} \mathbf{q}_i \\ \widetilde{\mathbf{q}} \\ \widetilde{\mathbf{q}}_x \\ \widetilde{\mathbf{q}}_y \\ \widetilde{\mathbf{q}}_{xy} \end{bmatrix}, \tag{100}$$

where

$$\widetilde{\mathbf{q}}_x = \mathbf{T}_x\widetilde{\mathbf{q}},\ \ \widetilde{\mathbf{q}}_y = \mathbf{T}_y\widetilde{\mathbf{q}} \ \text{ and } \ \widetilde{\mathbf{q}}_{xy} = \mathbf{T}_{xy}\widetilde{\mathbf{q}}_{xy}. \tag{101}$$

In this section, we partition mass, stiffness and damping matrices accordingly, *i.e.*, the mass matrix is expressed as:

$$\mathbf{M} = \begin{bmatrix} \mathbf{M}_i & \mathbf{0} & \mathbf{0} & \mathbf{0} & \mathbf{0} \\ \mathbf{0} & \mathbf{M}_m & \mathbf{0} & \mathbf{0} & \mathbf{0} \\ \mathbf{0} & \mathbf{0} & \mathbf{M}_x & \mathbf{0} & \mathbf{0} \\ \mathbf{0} & \mathbf{0} & \mathbf{0} & \mathbf{M}_y & \mathbf{0} \\ \mathbf{0} & \mathbf{0} & \mathbf{0} & \mathbf{0} & \mathbf{M}_{xy} \end{bmatrix}, \tag{102}$$

and stiffness and damping matrices are in the form:

$$\mathbf{K} = \begin{bmatrix} \mathbf{K}_i & \mathbf{K}_{im} & \mathbf{K}_{ix} & \mathbf{K}_{iy} & \mathbf{K}_{ixy} \\ \mathbf{K}_{im}^T & \mathbf{K}_m & \mathbf{K}_{mx} & \mathbf{K}_{my} & \mathbf{K}_{mxy} \\ \mathbf{K}_{ix}^T & \mathbf{K}_{mx}^T & \mathbf{K}_x & \mathbf{K}_{xy} & \mathbf{K}_{xxy} \\ \mathbf{K}_{iy}^T & \mathbf{K}_{my}^T & \mathbf{K}_{xy}^T & \mathbf{K}_y & \mathbf{K}_{yxy} \\ \mathbf{K}_{ixy}^T & \mathbf{K}_{mxy}^T & \mathbf{K}_{xxy}^T & \mathbf{K}_{yxy}^T & \mathbf{K}_{xy} \end{bmatrix}, \tag{103}$$

and

$$\mathbf{C} = \begin{bmatrix} \mathbf{C}_i & \mathbf{C}_{im} & \mathbf{C}_{ix} & \mathbf{C}_{iy} & \mathbf{C}_{ixy} \\ \mathbf{C}_{im}^T & \mathbf{C}_m & \mathbf{C}_{mx} & \mathbf{C}_{my} & \mathbf{C}_{mxy} \\ \mathbf{C}_{ix}^T & \mathbf{C}_{mx}^T & \mathbf{C}_x & \mathbf{C}_{xy} & \mathbf{C}_{xxy} \\ \mathbf{C}_{iy}^T & \mathbf{C}_{my}^T & \mathbf{C}_{xy}^T & \mathbf{C}_y & \mathbf{C}_{yxy} \\ \mathbf{C}_{ixy}^T & \mathbf{C}_{mxy}^T & \mathbf{C}_{xxy}^T & \mathbf{C}_{yxy}^T & \mathbf{C}_{xy} \end{bmatrix}. \tag{104}$$

Note that the elements of the mass, stiffness and damping matrices are matrices themselves properly dimensioned. For example, if $\mathbf{q}_i$ and $\widetilde{\mathbf{q}}_x$ are $n \times 1$ and $r \times 1$, respectively, then $\mathbf{K}_{ix}$ is $n \times r$. Similar to the previous chapter, the dispersion relation is expressed as:

$$\det(\overline{\mathbf{T}}^T(-\omega^2\mathbf{M}+i\omega\mathbf{C}+\mathbf{K})\mathbf{T}) = 0, \tag{105}$$

in which $\mathbf{T}$ is a function of x and y, and $\overline{\mathbf{T}}^T$ is a function of x^{-1} and y^{-1}. It should be pointed out that x and y stand for $e^{2\pi i k_1}$and $e^{2\pi i k_2}$ in which k_1 and k_2 are the complex wavevectors. In structures with no energy dissipation, the number of temporal frequencies ω for each wavevector depends on the degree of freedom of a unit cell. In other words, the number of dispersion branches equates to the degree of freedom of the unit cell. For example, as we saw in the first chapter, the phonon dispersion curve of graphene has six branches since a unit cell of graphene consists of two atoms of carbon, and each atom has three degrees of freedom. However, in experimentally-obtained graphene dispersion curves, unlike Fig. 33, there is more than one wavevector corresponding to each ω. This is because graphene is a two-dimensional lattice, and also each atom interacts with not only its closest neighbor, but also up to the fourth nearest neighbors. Consequently, in the proposed force-constant method, the stiffness matrix $\mathbf{K}$ is a banded matrix with more than three non-zero elements. In this section we investigate the relation between the maximum number of wavevectors for each frequency, and the dimension of mass and stiffness matrices.

The key to this relation is the degree of x and y in the polynomial of eq. (105). In order to investigate the degree of x and y in the polynomial, we first decompose $\mathbf{T}$ and $\overline{\mathbf{T}}^T$ into terms which include x and y and terms which are not functions of x and y. Matrices $\mathbf{T}$ and $\overline{\mathbf{T}}^T$ are in the form of:

$$\mathbf{T} = \begin{bmatrix} \mathbf{I} & \mathbf{0} \\ \mathbf{0} & \mathbf{I} \\ \mathbf{0} & \mathbf{T}_x \\ \mathbf{0} & \mathbf{T}_y \\ \mathbf{0} & \mathbf{T}_{xy} \end{bmatrix}, \tag{106}$$

and:

$$\overline{\mathbf{T}}^T = \begin{bmatrix} \mathbf{I} & \mathbf{0} & \mathbf{0} & \mathbf{0} & \mathbf{0} \\ \mathbf{0} & \mathbf{I} & \mathbf{T}_{-x}^T & \mathbf{T}_{-y}^T & \mathbf{T}_{-xy}^T \end{bmatrix}, \tag{107}$$

in which $\mathbf{T}_x$, $\mathbf{T}_y$, $\mathbf{T}_{xy}$, $\mathbf{T}_{-x}^T$, $\mathbf{T}_{-y}^T$ and $\mathbf{T}_{-xy}^T$ are push-forward/pull-back operators. Note that all the elements in $\mathbf{T}_x$ have the term $e^{2\pi i k_1}$, which we call x. There is no term in $\mathbf{T}_x$ without x; also there is no term with higher powers of x. As a result, we can factor out x from $\mathbf{T}_x$. By the same argument, we can factor out y, xy, x^{-1}, y^{-1} and $x^{-1}y^{-1}$ from $\mathbf{T}_y$, $\mathbf{T}_{xy}$, $\mathbf{T}_{-x}^T$, $\mathbf{T}_{-y}^T$ and $\mathbf{T}_{-xy}^T$, respectively. We then rephrase these matrices as:

$$\mathbf{T}_x = x\widehat{\mathbf{T}}_x, \quad \mathbf{T}_{-x}^T = x^{-1}\widehat{\mathbf{T}}_{-x}^T, \tag{108}$$

$$\mathbf{T}_y = y\widehat{\mathbf{T}}_y, \quad \mathbf{T}_{-y}^T = y^{-1}\widehat{\mathbf{T}}_{-y}^T, \tag{109}$$

$$\mathbf{T}_{xy} = xy\widehat{\mathbf{T}}_{xy}, \quad \mathbf{T}_{-xy}^T = x^{-1}y^{-1}\widehat{\mathbf{T}}_{-xy}^T. \tag{110}$$

In the example of a honeycomb lattice depicted in Fig.34 we have

$$\mathbf{T}_x = \begin{bmatrix} \mathbf{I}e^{2\pi i k_1} & \mathbf{0} \end{bmatrix} = x \begin{bmatrix} \mathbf{I} & \mathbf{0} \end{bmatrix}, \tag{111}$$

$$\mathbf{T}_{-x}^T = \begin{bmatrix} \mathbf{I}e^{-2\pi i k_1} \\ \mathbf{0} \end{bmatrix} = x^{-1} \begin{bmatrix} \mathbf{I} \\ \mathbf{0} \end{bmatrix}, \tag{112}$$

$$\mathbf{T}_y = \begin{bmatrix} \mathbf{0} & \mathbf{I}e^{2\pi i k_2} \end{bmatrix} = y \begin{bmatrix} \mathbf{I} & \mathbf{0} \end{bmatrix}, \tag{113}$$

$$\mathbf{T}_{-y}^T = \begin{bmatrix} \mathbf{I}e^{-2\pi i k_2} \\ \mathbf{0} \end{bmatrix} = y^{-1} \begin{bmatrix} \mathbf{I} \\ \mathbf{0} \end{bmatrix}, \tag{114}$$

$$\mathbf{T}_{xy} = \begin{bmatrix} \mathbf{I}e^{2\pi i(k_1+k_2)} & \mathbf{0} \\ \mathbf{0} & \mathbf{I}e^{2\pi i(k_1+k_2)} \end{bmatrix} = xy \begin{bmatrix} \mathbf{I} & \mathbf{0} \\ \mathbf{0} & \mathbf{I} \end{bmatrix}, \tag{115}$$

$$\mathbf{T}_{-xy}^T = \begin{bmatrix} \mathbf{I}e^{2\pi i(k_1+k_2)} & \mathbf{0} \\ \mathbf{0} & \mathbf{I}e^{2\pi i(k_1+k_2)} \end{bmatrix} = x^{-1}y^{-1} \begin{bmatrix} \mathbf{I} & \mathbf{0} \\ \mathbf{0} & \mathbf{I} \end{bmatrix}. \tag{116}$$

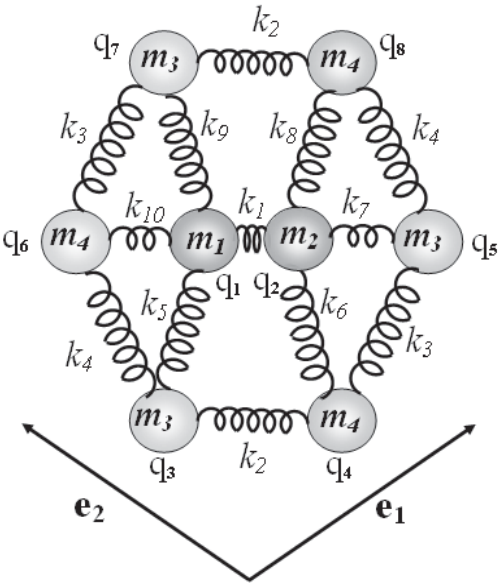

Figure 34: A hexagonal honeycomb lattice in which $\mathbf{q}_i = \begin{bmatrix} \mathbf{q}_1 & \mathbf{q}_2 \end{bmatrix}^T$, $\widetilde{\mathbf{q}} = \begin{bmatrix} \mathbf{q}_3 & \mathbf{q}_4 \end{bmatrix}^T$, $\widetilde{\mathbf{q}}_x = [\mathbf{q}_5]$, $\widetilde{\mathbf{q}}_y = [\mathbf{q}_6]$, $\widetilde{\mathbf{q}}_{xy} = \begin{bmatrix} \mathbf{q}_7 & \mathbf{q}_8 \end{bmatrix}^T$.

Since the pulling-back and pushing-forward operations in the e_1 direction are embedded in x and x^{-1}, it can be easily verified that:

$$\widehat{\mathbf{T}}_x^T = \widehat{\mathbf{T}}_{-x}^T, \tag{117}$$

the same relations hold for the other operators:

$$\widehat{\mathbf{T}}_y^T = \widehat{\mathbf{T}}_{-y}^T \text{ and } \widehat{\mathbf{T}}_{xy}^T = \widehat{\mathbf{T}}_{-xy}^T. \tag{118}$$

Let $\mathbf{D} = \overline{\mathbf{T}}^T(-\omega^2\mathbf{M} + i\omega\mathbf{C} + \mathbf{K})\mathbf{T}$, then by substituting $\mathbf{M}$, $\mathbf{C}$, $\mathbf{K}$, $\mathbf{T}$ and $\overline{\mathbf{T}}^T$ with (102)-(104) and (108)-(110), we get:

$$\mathbf{D} = \begin{bmatrix} \mathbf{D}_{11} & \mathbf{D}_{12} \\ \mathbf{D}_{21} & \mathbf{D}_{22} \end{bmatrix}, \tag{119}$$

in which:

$$\mathbf{D}_{11} = -\omega^2\mathbf{M}_i + i\omega\ \mathbf{C}_i + \mathbf{K}_i, \tag{120}$$

$$\mathbf{D}_{12} = i\omega\,\mathbf{C}_{im} + \mathbf{K}_{im} + (i\omega\,\mathbf{C}_{ix} + \mathbf{K}_{ix})\,x\widehat{\mathbf{T}}_x + (i\omega\,\mathbf{C}_{iy} + \mathbf{K}_{iy})\,y\widehat{\mathbf{T}}_y + (i\omega\,\mathbf{C}_{ixy} + \mathbf{K}_{ixy})\,xy\widehat{\mathbf{T}}_{xy}, \tag{121}$$

$$\mathbf{D}_{21} = i\omega\,\mathbf{C}_{im}^T + \mathbf{K}_{im}^T + \frac{\widehat{\mathbf{T}}_x^T\left(i\omega\,\mathbf{C}_{ix}^T + \mathbf{K}_{ix}^T\right)}{x} + \frac{\widehat{\mathbf{T}}_y^T\left(i\omega\,\mathbf{C}_{iy}^T + \mathbf{K}_{iy}^T\right)}{y} + \frac{\widehat{\mathbf{T}}_{xy}^T\left(i\omega\ \mathbf{C}_{ixy}^T + \mathbf{K}_{ixy}^T\right)}{xy}, \tag{122}$$

$$\begin{aligned}\mathbf{D}_{22} = {} & -\omega^2\mathbf{M}_m + i\omega\ \mathbf{C}_m + \mathbf{K}_m + (i\omega\,\mathbf{C}_{mx} + \mathbf{K}_{mx})\,x\widehat{\mathbf{T}}_x \\ & + (i\omega\,\mathbf{C}_{my} + \mathbf{K}_{my})\,y\widehat{\mathbf{T}}_y + (i\omega\,\mathbf{C}_{mxy} + \mathbf{K}_{mxy})\,xy\widehat{\mathbf{T}}_{xy} \\ & + \widehat{\mathbf{T}}_x^T(-\omega^2\mathbf{M}_x + i\omega\ \mathbf{C}_x + \mathbf{K}_x)\widehat{\mathbf{T}}_x + \widehat{\mathbf{T}}_x^T\,(i\omega\,\mathbf{C}_{xxy} + \mathbf{K}_{xxy})\,y\widehat{\mathbf{T}}_{xy} \\ & + \frac{\widehat{\mathbf{T}}_x^T\left(i\omega\,\mathbf{C}_{mx}^T + \mathbf{K}_{mx}^T\right)}{x} + \frac{\widehat{\mathbf{T}}_x^T\,(i\omega\,\mathbf{C}_{xy} + \mathbf{K}_{xy})\,y\widehat{\mathbf{T}}_y}{x} \\ & + \widehat{\mathbf{T}}_y^T(-\omega^2\mathbf{M}_y + i\omega\ \mathbf{C}_y + \mathbf{K}_y)\widehat{\mathbf{T}}_y + \widehat{\mathbf{T}}_y^T\,(i\omega\,\mathbf{C}_{yxy} + \mathbf{K}_{yxy})\,x\widehat{\mathbf{T}}_{xy} \\ & + \frac{\widehat{\mathbf{T}}_y^T\left(i\omega\,\mathbf{C}_{my}^T + \mathbf{K}_{my}^T\right)}{y} + \frac{\widehat{\mathbf{T}}_y^T\left(i\omega\mathbf{C}_{xy}^T + \mathbf{K}_{xy}^T\right)x\widehat{\mathbf{T}}_x}{y} \\ & + \frac{\widehat{\mathbf{T}}_{xy}^T\left(i\omega\,\mathbf{C}_{mxy}^T + \mathbf{K}_{mxy}^T\right)}{xy} + \widehat{\mathbf{T}}_{xy}^T(-\omega^2\mathbf{M}_{xy} + i\omega\ \mathbf{C}_{xy} + \mathbf{K}_{xy})\widehat{\mathbf{T}}_{xy} \\ & + \frac{\widehat{\mathbf{T}}_{xy}^T\left(i\omega\mathbf{C}_{xxy}^T + \mathbf{K}_{xxy}^T\right)x\widehat{\mathbf{T}}_x}{y} + \frac{\widehat{\mathbf{T}}_{xy}^T\left(i\omega\mathbf{C}_{yxy}^T + \mathbf{K}_{yxy}^T\right)y\widehat{\mathbf{T}}_y}{x}.\end{aligned} \tag{123}$$

$\mathbf{D}_{11}$ and $\mathbf{D}_{12}$ have the same row dimensions; also $\mathbf{D}_{12}$ and $\mathbf{D}_{22}$ have the same number of columns. Our goal is to determine the highest degree of x and y in the determinant of $\mathbf{D}$. Using the Leibniz formula to calculate the determinant (see appendix), each term in the polynomial of $\det(\mathbf{D})$ consists of exactly one element from each row and column. Thus, in order to get the highest power of x and y, in each row/column, we pick the term with the highest power of x and y. Now it is noted that $\mathbf{D}_{11}$ and $\mathbf{D}_{21}$ do not contain any term with positive powers of x or y.

In general, dispersion analysis is performed in the following Brillouin zone cases:

$$\left\{ \begin{array}{c} x \text{ varies while } y \text{ is a constant number} \\ y \text{ varies while } x \text{ is a constant number} \\ y = x^a \end{array} \right\},$$

in which a can assume any real number. However, in most of the dispersion curve analysis, only the boundary of irreducible Brillouin zone is considered, meaning that the ω is calculated for the the first two lines and third line with one value of a. In the example of a square lattice, these lines are noted by Γ-X, X-M and M-Γ, in which the line M-Γ corresponds to the third line with $a = 1$. In our representation, we can cover more of the Brillouin zone by picking more values for a. We investigate the degree of x or y on each of these lines separately.

5.3.2.1 First line: x varies while y is a constant number

On the first line in which y is constant, we will show that the x degree in the $\det(\mathbf{D})$ is bounded above by:

$$Rank\left(\widehat{\mathbf{D}}_x\right), \tag{124}$$

in which,

$$\widehat{\mathbf{D}}_x = \left[\begin{array}{c} \mathbf{D}_{1x} \\ \mathbf{D}_{2x} \end{array} \right], \tag{125}$$

and

$$\mathbf{D}_{1x} = \left(i\omega\,\mathbf{C}_{ix} + \mathbf{K}_{ix}\right)\widehat{\mathbf{T}}_x + \left(i\omega\,\mathbf{C}_{ixy} + \mathbf{K}_{ixy}\right)\widehat{\mathbf{T}}_{xy}, \tag{126}$$

$$\begin{aligned} \mathbf{D}_{2x} = {} & \left(i\omega\,\mathbf{C}_{mx} + \mathbf{K}_{mx}\right)\widehat{\mathbf{T}}_x + \left(i\omega\,\mathbf{C}_{mxy} + \mathbf{K}_{mxy}\right)\widehat{\mathbf{T}}_{xy} \\ & + \widehat{\mathbf{T}}_y^T\left(i\omega\,\mathbf{C}_{yxy} + \mathbf{K}_{yxy}\right)\widehat{\mathbf{T}}_{xy} + \widehat{\mathbf{T}}_y^T\left(i\omega\,\mathbf{C}_{xy}^T + \mathbf{K}_{xy}^T\right)\widehat{\mathbf{T}}_x. \end{aligned} \tag{127}$$

Note that $\mathbf{D}_{1x}$ and $\mathbf{D}_{2x}$ consist of those terms in $\mathbf{D}_{12}$ and $\mathbf{D}_{22}$ with dependence on x. On the line Γ-X the variable y assumes a constant value, hence the only remaining variable is x. Assuming damping is zero whenever stiffness is zero, we can replace $\mathbf{D}_{1x}$ and $\mathbf{D}_{2x}$ by:

$$\begin{aligned} \mathbf{D}'_{1x} &= \mathbf{K}_{ix}\widehat{\mathbf{T}}_x + \mathbf{K}_{ixy}\widehat{\mathbf{T}}_{xy}, \\ \mathbf{D}'_{2x} &= \mathbf{K}_{mx}\widehat{\mathbf{T}}_x + \mathbf{K}_{mxy}\widehat{\mathbf{T}}_{xy} + \widehat{\mathbf{T}}_y^T\mathbf{K}_{yxy}\widehat{\mathbf{T}}_{xy} + \widehat{\mathbf{T}}_y^T\mathbf{K}_{xy}^T\widehat{\mathbf{T}}_x, \end{aligned} \tag{128}$$

without changing the rank of $\widehat{\mathbf{D}}_x$.

In order to show that on the line Γ-X the determinant of the matrix $\mathbf{D}$ is a function of x with highest power defined by (124), we use the Leibniz formula. First we make an augmented matrix by matrix $\mathbf{D}$ next to $\widehat{\mathbf{D}}_x$:

$$\mathbf{D}_{aug} = \left[\begin{array}{cc|c} \mathbf{D}_{11} & \mathbf{D}_{12} & \mathbf{D}_{1x} \\ \mathbf{D}_{21} & \mathbf{D}_{22} & \mathbf{D}_{2x} \end{array}\right]. \tag{129}$$

The determinant of $\mathbf{D}$ in (119) remains constant by any sequence of row operations. We can apply a sequence of row operations on $\mathbf{D}_{aug}$ to make $\widehat{\mathbf{D}}_x$ a row echelon matrix. Note that due to the relation between $\widehat{\mathbf{D}}_x$ and $\mathbf{D}_{12}, \mathbf{D}_{22}$, by making $\widehat{\mathbf{D}}_x$ a row echelon matrix, the second column of $\mathbf{D}$ becomes a row echelon matrix in terms of x, meaning that any row or column has at most one entry with x. This is clarified by an example later in this section. According to the Leibniz formula, any term in the determinant of $\mathbf{D}$ has exactly one element from each row and column. Since $\mathbf{D}_{11}$ and $\mathbf{D}_{21}$ do not contain any positive power of x, the highest power of x in $\det(\mathbf{D})$ is achieved by choosing from each row the leading entry of $\left[\begin{array}{cc} \mathbf{D}_{12} & \mathbf{D}_{22} \end{array}\right]^T$ with x. It can be shown [96] that the rank of a matrix equals the number of non-zero pivots of a row echelon form of that matrix. Consequently, the highest power of x in $\det(\mathbf{D})$ equals to $Rank(\widehat{\mathbf{D}}_x)$. It should be noted that due to symmetry, both x and x^{-1} are roots

of equation $\det(\mathbf{D}) = 0$. As a result, in $\det(\mathbf{D}) = 0$, we can multiply both sides by x to the power of $Rank(\widehat{\mathbf{D}}_x)$ to obtain an equation in which the left hand side is a polynomial of x with power of $2Rank(\widehat{\mathbf{D}}_x)$.

To illustrate the proof, first we consider a simple matrix and then an example structure. In the following matrix,

$$\begin{bmatrix} 1 & 2 & x & 2x+2 & 2 \\ 4 & 5 & 2 & 0 & 3 \\ 2 & 2 & x+1 & x+3 & 1 \\ 2+\frac{1}{x} & 5+\frac{2}{x} & 3x+1+\frac{2}{x} & 3x+\frac{1}{x} & 5 \\ 1 & 2+\frac{3}{x} & 4 & 1 & 2+\frac{6}{x} \end{bmatrix}, \tag{130}$$

we have

$$\begin{aligned} \mathbf{D}_{11} &= \begin{bmatrix} 1 & 2 \\ 4 & 5 \\ 2 & 2 \end{bmatrix}, \ \mathbf{D}_{12} = \begin{bmatrix} x & 2x+2 & 2 \\ 2 & 0 & 3 \\ x+1 & x+3 & 1 \end{bmatrix}, \\ \mathbf{D}_{21} &= \begin{bmatrix} 2+\frac{1}{x} & 5+\frac{2}{x} \\ 1 & 2+\frac{1}{2x} \end{bmatrix}, \ \mathbf{D}_{22} = \begin{bmatrix} 3x+1+\frac{2}{x} & 3x+\frac{1}{x} & 5 \\ 4 & 1 & 2+\frac{6}{x} \end{bmatrix}. \end{aligned} \tag{131}$$

Then $\mathbf{D}_{1x}$ and $\mathbf{D}_{2x}$ are:

$$\mathbf{D}_{12} = \begin{bmatrix} 1 & 2 & 0 \\ 0 & 0 & 0 \\ 1 & 1 & 0 \end{bmatrix}, \ \mathbf{D}_{22} = \begin{bmatrix} 3 & 3 & 0 \\ 0 & 0 & 0 \end{bmatrix}, \tag{132}$$

which makes $\mathbf{D}_{aug}$ in the form of

$$\mathbf{D}_{aug} = \left[\begin{array}{ccccc|ccc} 1 & 2 & x & 2x+2 & 2 & 1 & 2 & 0 \\ 4 & 5 & 2 & 0 & 3 & 0 & 0 & 0 \\ 2 & 2 & x+1 & x+3 & 1 & 1 & 1 & 0 \\ 2+\frac{1}{x} & 5+\frac{2}{x} & 3x+1 & 3x & 5 & 3 & 3 & 0 \\ 1 & 2+\frac{3}{x} & 4 & 1 & 2 & 0 & 0 & 0 \end{array}\right]. \tag{133}$$

After making the right matrix a row echelon matrix by row operations, we get the matrix:

$$\left[\begin{array}{ccccc|ccc} 3 & 2 & x+2 & 4 & 0 & 1 & 0 & 0 \\ -1 & 0 & -1 & x-1 & 1 & 0 & 1 & 0 \\ 4 & 5 & 2 & 0 & 3 & 0 & 0 & 0 \\ -4+\frac{1}{x} & -1+\frac{2}{x} & -2+\frac{2}{x} & -9+\frac{1}{x} & 2 & 0 & 0 & 0 \\ 1 & 2+\frac{3}{x} & 4 & 1 & 2+\frac{6}{x} & 0 & 0 & 0 \end{array}\right]. \tag{134}$$

Evidently, in (134) the rank of the right block matrix is two. It can also be verified easily that $Rank(\left[\begin{array}{cc} \mathbf{D}_{12} & \mathbf{D}_{22} \end{array}\right]^T)$ is also two. There are two nonzero columns on the right block matrix which correspond to two columns (third and fourth) on the left block matrix containing x. The determinant of matrix $\mathbf{D}$ is:

$$\det(\mathbf{D}) = \frac{5\,x^4 + 49\,x^3 + 131x^2 + 127x + 75}{x^2}. \tag{135}$$

Multiplying both sides by x^2 we obtain an equation with x to the power of four which agrees well with that expected.

This relation between the rank of $\widehat{\mathbf{D}}_x$ and the x power can also be investigated in the structure depicted in Fig. 35 with out of plane motion. Damping terms have been omitted for simplicity of notation. For this structure we have:

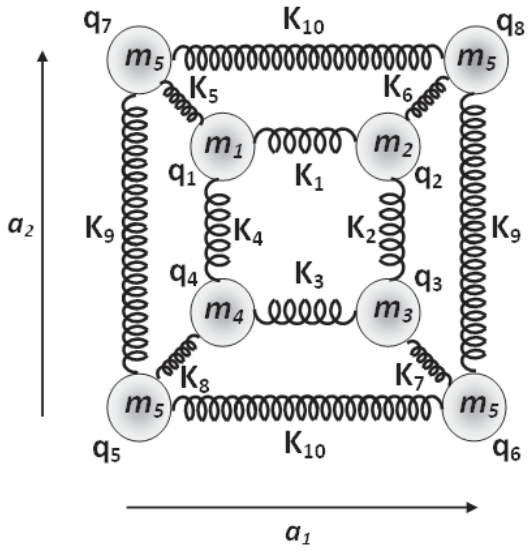

Figure 35: Unit cell of a periodic system with four internal masses

$$\begin{aligned}
\mathbf{q}_i &= \begin{bmatrix} q_1 \\ q_2 \\ q_3 \\ q_4 \end{bmatrix}, \widetilde{\mathbf{q}} = \begin{bmatrix} q_5 \end{bmatrix}, \widetilde{\mathbf{q}}_x = \begin{bmatrix} q_6 \end{bmatrix}, \\
\widetilde{\mathbf{q}}_y &= \begin{bmatrix} q_7 \end{bmatrix}, \widetilde{\mathbf{q}}_{xy} = \begin{bmatrix} q_8 \end{bmatrix},
\end{aligned}$$

and

$$\mathbf{T} = \begin{bmatrix} \mathbf{I} & \mathbf{0} \\ \mathbf{0} & 1 \\ \mathbf{0} & x \\ \mathbf{0} & y \\ \mathbf{0} & xy \end{bmatrix},$$

in which $\mathbf{I}$ is a 4×4 matrix. Mass and stiffness matrices are as follows:

$$\mathbf{K}_i = \begin{bmatrix} \text{K}_1+\text{K}_4+\text{K}_5 & \text{-K}_1 & 0 & \text{-K}_4 \\ \text{-K}_1 & \text{K}_1+\text{K}_2+\text{K}_6 & \text{-K}_2 & 0 \\ 0 & \text{-K}_2 & \text{K}_2+\text{K}_3+\text{K}_7 & \text{-K}_3 \\ \text{-K}_4 & 0 & \text{-K}_3 & \text{K}_3+\text{K}_4+\text{K}_8 \end{bmatrix}, \tag{136}$$

$$\mathbf{K}_{im} = \begin{bmatrix} 0 \\ 0 \\ 0 \\ \text{-K}_8 \end{bmatrix}, \ \mathbf{K}_{ix} = \begin{bmatrix} 0 \\ 0 \\ \text{-K}_7 \\ 0 \end{bmatrix}, \ \mathbf{K}_{iy} = \begin{bmatrix} \text{-K}_5 \\ 0 \\ 0 \\ 0 \end{bmatrix}, \ \mathbf{K}_{ixy} = \begin{bmatrix} 0 \\ \text{-K}_6 \\ 0 \\ 0 \end{bmatrix},$$

$$\mathbf{K}_{mx} = \text{-K}_{10}, \quad \mathbf{K}_{mxy} = 0, \quad \mathbf{K}_{yxy} = \text{-K}_{10},$$

$$\mathbf{K}_{xy} = 0, \quad \mathbf{K}_{xxy} = \text{-K}_9,$$

and

$$\mathbf{M} = \begin{bmatrix} m_1 & 0 & 0 & 0 & 0 & 0 & 0 & 0 \\ 0 & m_2 & 0 & 0 & 0 & 0 & 0 & 0 \\ 0 & 0 & m_3 & 0 & 0 & 0 & 0 & 0 \\ 0 & 0 & 0 & m_4 & 0 & 0 & 0 & 0 \\ 0 & 0 & 0 & 0 & m_5 & 0 & 0 & 0 \\ 0 & 0 & 0 & 0 & 0 & m_5 & 0 & 0 \\ 0 & 0 & 0 & 0 & 0 & 0 & m_5 & 0 \\ 0 & 0 & 0 & 0 & 0 & 0 & 0 & m_5 \end{bmatrix}. \tag{137}$$

Using eq. 128,

$$\mathbf{D}_{1x} = \begin{bmatrix} 0 \\ 0 \\ \text{-K}_7 \\ 0 \end{bmatrix} \times 1 + \begin{bmatrix} 0 \\ \text{-K}_6 \\ 0 \\ 0 \end{bmatrix} \times 1 = \begin{bmatrix} 0 \\ \text{-K}_6 \\ \text{-K}_7 \\ 0 \end{bmatrix}, \quad \mathbf{D}_{2x} = \text{-2K}_{10}\text{-K}_9. \tag{138}$$

Then:

$$\widehat{\mathbf{D}}_x = \begin{bmatrix} 0 \\ \text{-}\mathrm{K}_6 \\ \text{-}\mathrm{K}_7 \\ 0 \\ \text{-}2\mathrm{K}_{10}\text{-}\mathrm{K}_9 \end{bmatrix}. \tag{139}$$

Since $\widehat{\mathbf{D}}_x$ is a column matrix, its rank is obviously 1. Then the final polynomial in terms of x should be of power two. Matrix $\mathbf{D}$ takes the form of:

$$\mathbf{D} = \begin{bmatrix} \mathbf{D}_{11} & \mathbf{D}_{12} \\ \mathbf{D}_{21} & \mathbf{D}_{22} \end{bmatrix}, \tag{140}$$

in which:

$$\begin{aligned}
\mathbf{D}_{11} &= \begin{bmatrix} \mathrm{K}_1\text{+}\mathrm{K}_4\text{+}\mathrm{K}_5 & \text{-}\mathrm{K}_1 & 0 & \text{-}\mathrm{K}_4 \\ \text{-}\mathrm{K}_1 & \mathrm{K}_1\text{+}\mathrm{K}_2\text{+}\mathrm{K}_6 & \text{-}\mathrm{K}_2 & 0 \\ 0 & \text{-}\mathrm{K}_2 & \mathrm{K}_2\text{+}\mathrm{K}_3\text{+}\mathrm{K}_7 & \text{-}\mathrm{K}_3 \\ \text{-}\mathrm{K}_4 & 0 & \text{-}\mathrm{K}_3 & \mathrm{K}_3\text{+}\mathrm{K}_4\text{+}\mathrm{K}_8 \end{bmatrix}, \\
\mathbf{D}_{21} &= \begin{bmatrix} \frac{\text{-}\mathrm{K}_5}{y} & \frac{\text{-}\mathrm{K}_6}{xy} & \frac{\text{-}\mathrm{K}_7}{x} & \text{-}\mathrm{K}_8 \end{bmatrix}, \\
\mathbf{D}_{12} &= \begin{bmatrix} 0 \\ \text{-}\mathrm{K}_6 xy \\ \text{-}\mathrm{K}_7 x \\ \text{-}\mathrm{K}_8 \end{bmatrix}, \\
\mathbf{D}_{22} &= \left[\mathrm{K}_5\text{+}\mathrm{K}_6\text{+}\mathrm{K}_7\text{+}\mathrm{K}_8\text{+}4\mathrm{K}_9\text{+}4\mathrm{K}_{10}\text{-}2\mathrm{K}_{10}x\text{-}2\mathrm{K}_9 y\text{+}\frac{\text{-}2\mathrm{K}_{10}}{x}\text{+}\frac{\text{-}2\mathrm{K}_9}{y} \right].
\end{aligned} \tag{141}$$

Determinant of $\mathbf{D}$ takes the form:

$$\det(\mathbf{D}) = \frac{[x^2(A+By) + y^2(C+Dx) + Exy + Fx + Gy]}{xy}, \tag{142}$$

in which A, B, C, D, E, F and G are constants. For example (obtained using a symbolic manipulator),

B= -2K$_1$K$_6$K$_3$K$_8$K$_{10}$-2K$_1$K$_5$K$_3$K$_4$K$_{10}$-2K$_1$K$_6$K$_3$K$_4$K$_{10}$-2K$_5$K$_6$K$_3$K$_4$K$_{10}$-K$_1$K$_5$K$_7$K$_3$K$_8$-2K$_1$K$_2$K$_7$K$_4$K$_{10}$
-2K$_2$K$_5$K$_3$K$_4$K$_{10}$-K$_4$K$_6$K$_7$K$_3$K$_8$-K$_1$K$_4$K$_7$K$_3$K$_8$-2K$_4$K$_6$K$_3$K$_8$K$_{10}$-2K$_4$K$_6$K$_7$K$_8$K$_{10}$-2K$_4$K$_6$K$_7$K$_3$K$_{10}$
-2K$_5$K$_2$K$_3$K$_8$K$_{10}$-2K$_4$K$_1$K$_3$K$_8$K$_{10}$-2K$_4$K$_1$K$_7$K$_8$K$_{10}$-2K$_4$K$_1$K$_7$K$_3$K$_{10}$-2K$_5$K$_2$K$_7$K$_8$K$_{10}$-K$_5$K$_6$K$_7$K$_3$K$_8$
-2K$_4$K$_6$K$_2$K$_8$K$_{10}$-K$_1$K$_2$K$_7$K$_3$K$_8$-K$_1$K$_6$K$_7$K$_3$K$_8$-2K$_4$K$_1$K$_2$K$_8$K$_{10}$-K$_1$K$_6$K$_7$K$_4$K$_5$-2K$_5$K$_1$K$_2$K$_8$K$_{10}$
-2K$_5$K$_1$K$_2$K$_4$K$_{10}$-2K$_5$K$_2$K$_7$K$_3$K$_{10}$-K$_5$K$_2$K$_7$K$_3$K$_8$-2K$_5$K$_6$K$_2$K$_3$K$_{10}$-2K$_1$K$_6$K$_2$K$_3$K$_{10}$-K$_1$K$_2$K$_4$K$_7$K$_8$
-2K$_5$K$_6$K$_3$K$_8$K$_{10}$-2K$_5$K$_6$K$_7$K$_4$K$_{10}$-2K$_5$K$_6$K$_7$K$_8$K$_{10}$-2K$_5$K$_6$K$_7$K$_3$K$_{10}$-2K$_5$K$_6$K$_2$K$_8$K$_{10}$-2K$_5$K$_6$K$_2$K$_4$K$_{10}$
-2K$_5$K$_1$K$_2$K$_3$K$_{10}$-2K$_5$K$_1$K$_3$K$_8$K$_{10}$-2K$_5$K$_1$K$_7$K$_4$K$_{10}$-2K$_5$K$_1$K$_7$K$_8$K$_{10}$-2K$_5$K$_1$K$_7$K$_3$K$_{10}$-K$_1$K$_6$K$_7$K$_3$K$_5$
-K$_1$K$_6$K$_3$K$_8$K$_5$-K$_1$K$_6$K$_3$K$_4$K$_5$-K$_4$K$_6$K$_2$K$_3$K$_5$-2K$_1$K$_6$K$_7$K$_4$K$_{10}$-2K$_1$K$_6$K$_7$K$_8$K$_{10}$-2K$_1$K$_6$K$_7$K$_3$K$_{10}$
-2K$_1$K$_6$K$_2$K$_8$K$_{10}$-2K$_1$K$_6$K$_2$K$_4$K$_{10}$-2K$_1$K$_2$K$_3$K$_8$K$_{10}$-2K$_1$K$_2$K$_7$K$_8$K$_{10}$-2K$_1$K$_2$K$_7$K$_3$K$_{10}$-2K$_1$K$_6$K$_7$K$_8$K$_5$
-2K$_1$K$_6$K$_2$K$_3$K$_5$-2K$_1$K$_6$K$_2$K$_8$K$_5$-2K$_1$K$_6$K$_2$K$_4$K$_5$-2K$_4$K$_2$K$_3$K$_8$K$_{10}$-2K$_4$K$_2$K$_7$K$_8$K$_{10}$-2K$_4$K$_2$K$_7$K$_3$K$_{10}$
-K$_4$K$_2$K$_7$K$_3$K$_8$-2K$_4$K$_6$K$_2$K$_3$K$_{10}$-2K$_5$K$_2$K$_7$K$_4$K$_{10}$

For varying x and constant y, eq.(142) can be multiplied by x to obtain a quadratic equation in terms of x. This verifies the result we obtained by calculating $Rank(\widehat{\mathbf{D}}_x)$. As is evident from the constant B, eq. (142) has many terms which make it computationally costly to calculate. On the other hand, the procedure of calculating $Rank(\widehat{\mathbf{D}}_x)$ is simple and does not require the handling of constants with many terms.

5.3.2.2 Second line: y varies while x is a constant number

For the second line, we borrow the same argument we used in the previous section. It can be verified that the y degree in the $\det(\mathbf{D})$ is bounded above by:

$$Rank\left(\widehat{\mathbf{D}}_y\right), \tag{143}$$

in which,

$$\widehat{\mathbf{D}}_y = \begin{bmatrix} \mathbf{D}_{1y} \\ \mathbf{D}_{2y} \end{bmatrix}, \tag{144}$$

and

$$\begin{aligned} \mathbf{D}_{1y} &= (i\omega\,\mathbf{C}_{iy} + \mathbf{K}_{iy})\,\widehat{\mathbf{T}}_y + (i\omega\,\mathbf{C}_{ixy} + \mathbf{K}_{ixy})\,\widehat{\mathbf{T}}_{xy}, & (145)\\ \mathbf{D}_{2y} &= (i\omega\,\mathbf{C}_{my} + \mathbf{K}_{my})\,\widehat{\mathbf{T}}_y + (i\omega\,\mathbf{C}_{mxy} + \mathbf{K}_{mxy})\,\widehat{\mathbf{T}}_{xy} & (146)\\ &\quad + \widehat{\mathbf{T}}_x^T\,(i\omega\,\mathbf{C}_{xxy} + \mathbf{K}_{xxy})\,\widehat{\mathbf{T}}_{xy} + \widehat{\mathbf{T}}_y^T\left(i\omega\,\mathbf{C}_{xy}^T + \mathbf{K}_{xy}^T\right)\widehat{\mathbf{T}}_y. \end{aligned}$$

As before, assuming zero damping whenever stiffness is zero, we can replace $\mathbf{D}_{1y}$ and $\mathbf{D}_{2y}$ by:

$$\begin{aligned} \mathbf{D}_{1y}^{'} &= \mathbf{K}_{iy}\widehat{\mathbf{T}}_y + \mathbf{K}_{ixy}\widehat{\mathbf{T}}_{xy}, & (147)\\ \mathbf{D}_{2y}^{'} &= \mathbf{K}_{my}\widehat{\mathbf{T}}_y + \mathbf{K}_{mxy}\widehat{\mathbf{T}}_{xy} + \widehat{\mathbf{T}}_x^T\mathbf{K}_{xxy}\widehat{\mathbf{T}}_{xy} + \widehat{\mathbf{T}}_y^T\mathbf{K}_{xy}^T\widehat{\mathbf{T}}_y, \end{aligned}$$

without changing the rank of $\widehat{\mathbf{D}}_y$.

5.3.2.3 Third line: $y = x^a$

On the third line, $y = x^a$. Here, for the ease of explanation, we first consider $y = x$ before moving on to the more general case. The relation $y = x$ makes all the xy terms in matrix $\mathbf{D}$ into power two terms of x; namely x^2. As a result, in estimating the highest power of x in the det($\mathbf{D}$), we count the number of xy, and x or y, in a different fashion. This subtle process needs much attention. On the line $y = x$, the variable y is represented by x. We define:

$$\widehat{\mathbf{D}}_{ax} = \begin{bmatrix} \mathbf{D}_{1ax} \\ \mathbf{D}_{2ax} \end{bmatrix}, \tag{148}$$

in which

$$\mathbf{D}_{1ax} = (i\omega\,\mathbf{C}_{ix} + \mathbf{K}_{ix})\,\widehat{\mathbf{T}}_x + (i\omega\,\mathbf{C}_{iy} + \mathbf{K}_{iy})\,\widehat{\mathbf{T}}_y, \tag{149}$$

$$\begin{aligned}\mathbf{D}_{2ax} &= (i\omega\,\mathbf{C}_{mx} + \mathbf{K}_{mx})\,\widehat{\mathbf{T}}_x + (i\omega\,\mathbf{C}_{my} + \mathbf{K}_{my})\,\widehat{\mathbf{T}}_y \\ &\quad + \widehat{\mathbf{T}}_x^T\,(i\omega\,\mathbf{C}_{xxy} + \mathbf{K}_{xxy})\,\widehat{\mathbf{T}}_{xy} + \widehat{\mathbf{T}}_y^T\,(i\omega\,\mathbf{C}_{yxy} + \mathbf{K}_{yxy})\,\widehat{\mathbf{T}}_{xy}.\end{aligned} \tag{150}$$

Note that $\widehat{\mathbf{D}}_{ax}$ includes those terms with power one of x. Then we define:

$$\widehat{\mathbf{D}}_{xy} = \begin{bmatrix} \mathbf{D}_{1xy} \\ \mathbf{D}_{2xy} \end{bmatrix}, \tag{151}$$

in which

$$\mathbf{D}_{1xy} = (i\omega\,\mathbf{C}_{ixy} + \mathbf{K}_{ixy})\,\widehat{\mathbf{T}}_{xy}, \tag{152}$$

$$\mathbf{D}_{2xy} = (i\omega\,\mathbf{C}_{mxy} + \mathbf{K}_{mxy})\,\widehat{\mathbf{T}}_{xy}. \tag{153}$$

Then we show that the power of x in the $\det(\mathbf{D})$ is bounded above by:

$$2 \times Rank\left(\widehat{\mathbf{D}}_{xy}\right) + \left(Rank\left(\widehat{\mathbf{D}}_{xy} + \widehat{\mathbf{D}}_{ax}\right) - Rank\left(\widehat{\mathbf{D}}_{xy}\right)\right), \tag{154}$$

which can be simplified to:

$$Rank\left(\widehat{\mathbf{D}}_{xy}\right) + Rank\left(\widehat{\mathbf{D}}_{xy} + \widehat{\mathbf{D}}_{ax}\right). \tag{155}$$

The rationale behind (155) is explained through an example. Consider Matrix $\mathbf{A}$ as follows:

$$\mathbf{A} = \begin{bmatrix} x^2+x & 0 & 0 & 0 & 0 \\ x^2 & 1 & 0 & x^2 & 0 \\ x^2 & 0 & x & 0 & 0 \\ x^2 & 0 & x & x^2 & x^2 \\ x & 0 & 0 & x^2 & x \end{bmatrix}. \tag{156}$$

Considering only the variables x and x^2, matrix $\mathbf{A}$ has rank four. Matrices $\mathbf{A}_x$ and $\mathbf{A}_{xy}$ consist of those elements with x and x^2, respectively. They are:

$$\mathbf{A}_x = \begin{bmatrix} 1 & 0 & 0 & 0 & 0 \\ 0 & 0 & 0 & 0 & 0 \\ 0 & 0 & 1 & 0 & 0 \\ 0 & 0 & 1 & 0 & 0 \\ 1 & 0 & 0 & 0 & 1 \end{bmatrix}, \ \mathbf{A}_{xy} = \begin{bmatrix} 1 & 0 & 0 & 0 & 0 \\ 1 & 0 & 0 & 1 & 0 \\ 1 & 0 & 0 & 0 & 0 \\ 1 & 0 & 0 & 1 & 1 \\ 0 & 0 & 0 & 1 & 0 \end{bmatrix}, \tag{157}$$

in which we have:

$$Rank\,(\mathbf{A}_x) = 3,\ Rank\,(\mathbf{A}_{xy}) = 3,\ Rank\,(\mathbf{A}_x + \mathbf{A}_{xy}) = Rank\,(\mathbf{A}) = 4. \tag{158}$$

The determinant of $\mathbf{A}$ can be verified to be:

$$\det(A) = (x^2+x)x^4(1-x),$$

which is a polynomial of degree 7. Also,

$$Rank\,(\mathbf{A}_{xy}) + Rank\,(\mathbf{A}_x + \mathbf{A}_{xy}) = Rank\,(\mathbf{A}_{xy}) + Rank\,(\mathbf{A}) = 3 + 4 = 7. \tag{159}$$

To illustrate the reason for (155), we first make the matrix $\mathbf{A}$ into a row echelon matrix in terms of x^2. This process uses row operations and hence does not alter the $\det(\mathbf{A})$. After these row operations matrix $\mathbf{A}$ takes the form:

$$\begin{bmatrix} x^2+x & 0 & 0 & 0 & 0 \\ -x & 1 & 0 & x^2 & 0 \\ 0 & -1 & x & 0 & x^2 \\ -x & 0 & x & 0 & 0 \\ 2x & -1 & 0 & 0 & x \end{bmatrix}. \tag{160}$$

Column operations do not alter the determinant. We perform column operations such that the columns containing pivots are arranged next to each other, *i.e.*,

$$\begin{bmatrix} x^2+x & 0 & 0 & 0 & 0 \\ -x & x^2 & 0 & 1 & 0 \\ 0 & 0 & x & -1 & x^2 \\ -x & 0 & x & 0 & 0 \\ 2x & 0 & 0 & -1 & x \end{bmatrix}, \tag{161}$$

and,

$$\begin{bmatrix} x^2+x & 0 & 0 & 0 & 0 \\ -x & x^2 & 0 & 1 & 0 \\ 0 & 0 & x^2 & -1 & x \\ -x & 0 & 0 & 0 & x \\ 2x & 0 & x & -1 & 0 \end{bmatrix}. \tag{162}$$

In calculating the determinant of (162) by the Leibniz formula, the highest degree of x is achieved by picking x^2 from the first three columns and rows. We perform row operations further to make the corner 2×2 matrix

$$\begin{bmatrix} 0 & x \\ -1 & 0 \end{bmatrix}, \tag{163}$$

a row echelon matrix in x. This is already a row echelon matrix. Note that the number of linearly independent rows in this 2×2 matrix equals to:

$$Rank\left(\mathbf{A}_x + \mathbf{A}_{xy}\right) - Rank\left(\mathbf{A}_x\right) = 4 - 3 = 1. \tag{164}$$

This procedure can be followed for $\mathbf{A}$ with any size.

Following the same procedure, it can be shown that for the case of $y = x^a$, the power of x in the $\det(\mathbf{D})$ is bounded above by:

$$(a+1) \times Rank\left(\widehat{\mathbf{D}}_{xy}\right) + \left(Rank\left(\widehat{\mathbf{D}}_{xy} + \widehat{\mathbf{D}}_{ax}\right) - Rank\left(\widehat{\mathbf{D}}_{xy}\right)\right). \tag{165}$$

5.3.3 Investigating Phonon Dispersion Curves in Boron Nitride

Boron Nitride is a chemical compound which cannot be found in nature and hence is produced synthetically from boron acid or trioxide. It consists of equal numbers of boron and nitrogen atoms and exists in different crystalline structures. Very similar to carbon compounds, it has a hexagonal form (h-BN) like graphite, and a cubic form (c-BN) like diamond. Among other applications, the hexagonal form is used as lubricant. Unlike graphite, h-BN can perform as a lubricant without molecules of air or water trapped between its layers. Compared to diamond, c-BN has superior thermal and chemical stability. Similar to carbon nanotubes, there exists BN nanotubes. They have been theoretically predicted [97] and experimentally verified to exist [3].

In this section we use formulas developed in the previous section to show that phonon dispersion curves of h-BN cannot be reproduced by considering only the nearest neighbor interactions. The theoretical phonon dispersion curves of h-BN are obtained by *ab initio* calculation. Each unit cell of h-BN consists of 18 atoms in three parallel hexagons, three nitrogen and three boron atoms in each hexagons. Each atom

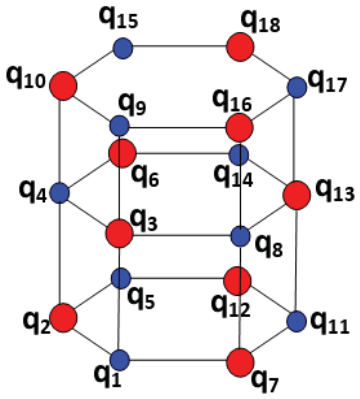

Figure 36: Boron nitride in its hexagonal crystalline form (h-BN), and the unit cell displacements.

can move in three directions, so in our formalism we have:

$$\widetilde{\mathbf{q}} = \begin{bmatrix} \mathbf{q}_1 \\ \mathbf{q}_2 \\ \mathbf{q}_3 \\ \mathbf{q}_4 \end{bmatrix}, \ \mathbf{q}_x = \begin{bmatrix} \mathbf{q}_5 \\ \mathbf{q}_6 \end{bmatrix}, \ \mathbf{q}_y = \begin{bmatrix} \mathbf{q}_7 \\ \mathbf{q}_8 \end{bmatrix}, \ \mathbf{q}_z = \begin{bmatrix} \mathbf{q}_9 \\ \mathbf{q}_{10} \end{bmatrix}, \qquad (166)$$

$$\mathbf{q}_{xy} = \begin{bmatrix} \mathbf{q}_{11} \\ \mathbf{q}_{12} \\ \mathbf{q}_{13} \\ \mathbf{q}_{14} \end{bmatrix}, \ \mathbf{q}_{xz} = [\mathbf{q}_{15}], \ \mathbf{q}_{yz} = [\mathbf{q}_{16}], \ \mathbf{q}_{xyz} = \begin{bmatrix} \mathbf{q}_{17} \\ \mathbf{q}_{18} \end{bmatrix},$$

in which $\mathbf{q}_j$, $j = 1..9$ are vectors of length 3. There is no internal masses, so we

eliminated $\mathbf{q}_i$. For the transformation matrices, we have:

$$\begin{aligned}
\mathbf{T}_x &= x\begin{bmatrix} \mathbf{I} & \mathbf{0} & \mathbf{0} & \mathbf{0} \\ \mathbf{0} & \mathbf{0} & \mathbf{I} & \mathbf{0} \end{bmatrix},\ \mathbf{T}_y = y\begin{bmatrix} \mathbf{0} & \mathbf{I} & \mathbf{0} & \mathbf{0} \\ \mathbf{0} & \mathbf{0} & \mathbf{0} & \mathbf{I} \end{bmatrix}, \\
\mathbf{T}_z &= z\begin{bmatrix} \mathbf{I} & \mathbf{0} & \mathbf{0} & \mathbf{0} \\ \mathbf{0} & \mathbf{I} & \mathbf{0} & \mathbf{0} \end{bmatrix},\ \mathbf{T}_{xy} = xy\begin{bmatrix} \mathbf{I} & \mathbf{0} & \mathbf{0} & \mathbf{0} \\ \mathbf{0} & \mathbf{I} & \mathbf{0} & \mathbf{0} \\ \mathbf{0} & \mathbf{0} & \mathbf{I} & \mathbf{0} \\ \mathbf{0} & \mathbf{0} & \mathbf{0} & \mathbf{I} \end{bmatrix}, \\
\mathbf{T}_{xz} &= xz\begin{bmatrix} \mathbf{I} & \mathbf{0} & \mathbf{0} & \mathbf{0} \end{bmatrix},\ \mathbf{T}_{yz} = y\begin{bmatrix} \mathbf{0} & \mathbf{I} & \mathbf{0} & \mathbf{0} \end{bmatrix}, \\
\mathbf{T}_{xyz} &= xyz\begin{bmatrix} \mathbf{I} & \mathbf{0} & \mathbf{0} & \mathbf{0} \\ \mathbf{0} & \mathbf{I} & \mathbf{0} & \mathbf{0} \end{bmatrix}.
\end{aligned} \tag{167}$$

There is no internal mass, hence there is no $\mathbf{K}_i$, $\mathbf{K}_{im}$, $\mathbf{K}_{ix}$, $\mathbf{K}_{iy}$, $\mathbf{K}_{ixy}$. On the other hand, the crystal is three dimensional and direction z is orthogonal to the hexagonal plane and must be considered. As a result, $\mathbf{D}'_{2x}$ takes the form:

$$\begin{aligned}
\mathbf{D}'_{2x} &= \mathbf{K}_{mx}\widehat{\mathbf{T}}_x + \mathbf{K}_{mxy}\widehat{\mathbf{T}}_{xy} + \mathbf{K}_{mxz}\widehat{\mathbf{T}}_{xz} + \mathbf{K}_{mxyz}\widehat{\mathbf{T}}_{xyz} + \widehat{\mathbf{T}}_y^T(\mathbf{K}_{xy}^T\widehat{\mathbf{T}}_x + \mathbf{K}_{yxy}\widehat{\mathbf{T}}_{xy} \\
&\quad + \mathbf{K}_{yxz}\widehat{\mathbf{T}}_{xz} + \mathbf{K}_{yxyz}\widehat{\mathbf{T}}_{xyz}) + \widehat{\mathbf{T}}_z^T(\mathbf{K}_{xz}^T\widehat{\mathbf{T}}_x + \mathbf{K}_{zxy}\widehat{\mathbf{T}}_{xy} + \mathbf{K}_{zxz}\widehat{\mathbf{T}}_{xz} + \mathbf{K}_{zxyz}\widehat{\mathbf{T}}_{xyz}) \\
&\quad + \widehat{\mathbf{T}}_{yz}^T(\mathbf{K}_{xyz}^T\widehat{\mathbf{T}}_x + \mathbf{K}_{xyyz}^T\widehat{\mathbf{T}}_{xy} + \mathbf{K}_{xzyz}^T\widehat{\mathbf{T}}_{xz} + \mathbf{K}_{yzxyz}\widehat{\mathbf{T}}_{xyz})
\end{aligned} \tag{168}$$

Considering only the nearest neighbor interaction, most of the terms in (168) would be zero. After manipulation, (168) takes the form:

$$\mathbf{D}'_{2x} = \begin{bmatrix} \mathbf{0} & \mathbf{0} & \mathbf{0} & \mathbf{0} \\ \mathbf{K}_A & \mathbf{0} & \mathbf{0} & \mathbf{0} \\ \mathbf{0} & \mathbf{0} & \mathbf{0} & \mathbf{0} \\ \mathbf{0} & \mathbf{0} & \mathbf{K}_B & \mathbf{0} \end{bmatrix} \tag{169}$$

in which $\mathbf{K}_A$ and $\mathbf{K}_B$ are some 3×3 matrices. Consequently

$$Rank\left(\widehat{\mathbf{D}}_x\right) = Rank\left(\mathbf{D}_x\right) = 6. \tag{170}$$

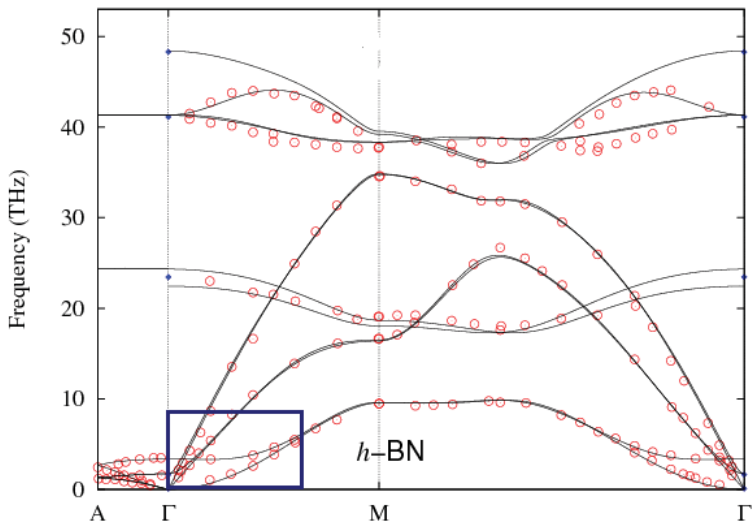

Figure 37: Phonon dispersion curves of h-BN calculated by Wang *et. al.* [100] (solid lines) and X-Ray scattering (circles) by Serrano *et. al.* [101]. The close-up of the blue box is depicted in Fig. 38.

This means for each ω there would be no more than 6 wavevectors when we consider only the nearest neighbor interaction. However, as it can be seen in Fig. 38, there is a range of ω's for which there corresponds more than six wavevectors.

This last result indicates nearest neighbor interactions beyond the first neighbors are important for characterizing dispersion in crystalline structures. In future work, we intend on applying the insight gained to explore the number of nearest neighbor interactions necessary to accurately characterize dispersion in commonly studied crystalline structures.

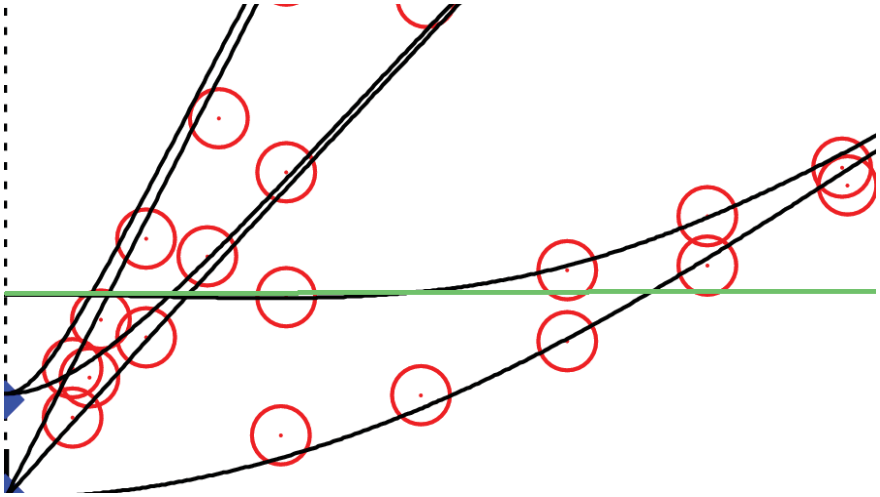

Figure 38: A close-up of the h-BN phonon dispersion curves depicted in 37. Evidently, the green line intersects the dispersion curves seven times.

CHAPTER VI

CONCLUDING REMARKS

6.1 Conclusions

In periodic lattice structures,wave propagation on the infinite domain can be greatly simplified by invoking the Floquet–Bloch theorem. This theorem allows a system's degrees of freedom to be reduced to a small subset contained in a repeating unit cell.

This dissertation contributes several new insights into the development and use of Bloch analysis in structural wave propagation.

- We demonstrated that for any two- or three-dimensional periodic lattice, the internal forces vanish when acted upon by the linear transformation engendered by the degree of freedom reduction, and this transformation results in an eigenvalue problem.
- We demonstrated the existence of a "propagation constant" in the resulting eigenvalue problem. This procedure links the Bloch theorem and the previously used "propagation constant" technique in the elastic wave propagation analysis of discrete structural systems.
- We showed that the translational invariance of the structure is not a sufficient condition for applying Bloch's theorem. In nonlinear systems, one needs to be cautious in applying Bloch's theorem.

- By constructing a simple asymmetrical counter-example, we added to growing evidence that considering only the boundary of the IBZ may lead to erroneous predictions concerning the magnitude of band gaps.
- We investigated the Bloch analysis in structures with linear damping and rigorously found the Bloch relations for structures with energy dissipation.
- Using Bloch analysis in structures with linear damping,
  - We demonstrated that damping may introduce wavenumber band gaps.
  - The existence of two or more temporal frequencies for each dispersion curve and wavenumber was documented.
- A general framework for calculating dispersion curves in structures with damping has been proposed and investigated in example one and two-dimensional lattice structures.
- A framework was developed to predict the maximum number of wavevectors for each ω in the characterization of dispersion.

6.2 Future Work

There are numerous opportunities and unanswered problems in the area of band structure calculation. Overcoming these theoretical obstacles can greatly enhance our understanding of wave propagation in periodic structures for use in new filters for acoustic or ultrasonic waves. Here we summarize just a few of them which are reasonable continuations of the thesis work.

We use finite elements to come up with the mass and stiffness matrices. As we decrease the mesh size, we increase the size of the mass and stiffness matrices, and hence we have more branches. It is not difficult to see that the new branches populate the higher temporal frequencies. In other words, as we add to the size of the mass and stiffness matrices, the structure can accommodate higher frequencies. However, we are also aware that the lower branches will change slightly as well, leading to changes in the width of the band gaps. Note that a band gap width is not necessarily the gap between two branches at the same wavevector. Recall that ω^2 is the eigenvalue of the equation of motion for a fixed wavevector. As a result the band gap width is not the difference between two eigenvalues of a matrix; it is in fact the difference between the eigenvalues of two different matrices. This makes it difficult to see that as we decrease the mesh size, we are guaranteed to not change the band gap drastically. This is of great importance in the optimum designing of the band gap in a continuous periodic structure.

In recent publications, there are numerous methods to optimally find the maximum band gap. In an optimization problem, we want to find - at the very least - the local minimum of a function, say $f(x, y)$. If we can calculate the gradient of f , we can start from any point (x_0, y_0), then take steps in $(\Delta x, \Delta y)$ proportional to the negative of the gradient of f. The issue with band gap optimization, is that the band gap is in fact the difference between eigenvalues of two different matrices. In other words, we have

$$\mathbf{T}^H\mathbf{K}\mathbf{T}(\overrightarrow{\mathbf{k}})\widehat{\mathbf{q}} = -\omega^2\mathbf{T}^H\mathbf{M}\mathbf{T}(\overrightarrow{\mathbf{k}})\widehat{\mathbf{q}} \tag{171}$$

in which $\overrightarrow{\mathbf{k}}$ is the wavevector. Then the band gap is the difference between the $\omega's$ when $\overrightarrow{\mathbf{k}}$ equals to two different wavevectors, say $\overrightarrow{\mathbf{k}_1}$ and $\overrightarrow{\mathbf{k}_2}$. The problem is, when we change mass and stiffness matrices, everything would change, including $\overrightarrow{\mathbf{k}_1}$ and $\overrightarrow{\mathbf{k}_2}$. This makes the steepest descent method extremely difficult to implement. There have been efforts to solve similar problems [102]; however, this problem for the dispersion

band gap has not been addressed fully.

APPENDIX A

GRAPHENE DISPERSION CURVE: MATLAB CODE

This code generates graphene dispersion curves by considering interaction up to the fourth nearest neighbor. Stiffness coefficients are obtained from [25], page 169. Each unit cell consists of tow atoms which are called A and B. In the case of atom A, only the second nearest neighbors are type A; first, third and fourth nearest neighbors are type B. Stiffness values are for principal directions. For other directions, stiffness matrices can be obtained by transforming the original stiffness matrix into the new coordinate system.

```
function f = FFphonon
clc; clear all; warning off all
CarbonCarbon=1.44;
a=CarbonCarbon*sqrt(3);
cc=[CarbonCarbon 0 0]';
a1=[sqrt(3)*a/2,a/2,0]';
a2=[sqrt(3)*a/2,-a/2,0]';
b1=[2*pi/(sqrt(3)*a),2*pi/a,0]';
b2=[2*pi/(sqrt(3)*a),-2*pi/a,0]';
M=1.9926e-026;
c = 299792458; % speed of light in m/s
% the Brillouin zone boundary vectors
GM=(b1+b2)/2;
```

```
MK=(b1-b2)/6;
KG=-(GM+MK);
%%
% force constants parameters for 2D graphite in units of 10^4 dyn/cm
% (from Saito_Dresselhaus book page 169)
phi_r1 = 36.5; phi_1ti= 24.5; phi_1to= 9.82;
phi_r2 = 8.8; phi_2ti = -3.23; phi_2to = -0.4;
phi_r3 = 3.0; phi_3ti = -5.25; phi_3to = 0.15;
phi_r4 = -1.92; phi_ti4 = 2.29; phi_4to = -0.58;
K1 =[phi_r1 0 0
 0 phi_1ti 0
 0 0 phi_1to];
K2 =[phi_r2,0,0;0,phi_2ti,0;0,0,phi_2to];
K3 =[phi_r3,0,0;0,phi_3ti,0;0,0,phi_3to];
K4 =[phi_r4,0,0;0,phi_ti4,0;0,0,phi_4to];
%%
% Vectors from the atom A to its neigbours
RA1=(rotationv([a 0 0]',1*pi/6)); RA2=(rotationv([a 0 0]',3*pi/6));
RA3=(rotationv([a 0 0]',5*pi/6)); RA4=(rotationv([a 0 0]',7*pi/6));
RA5=(rotationv([a 0 0]',9*pi/6));RA6=(rotationv([a 0 0]',11*pi/6));
RB11=(rotationv([CarbonCarbon 0 0]',0*pi/3));
RB12=(rotationv([CarbonCarbon 0 0]',2*pi/3));
RB13=(rotationv([CarbonCarbon 0 0]',4*pi/3));
RB31=(rotationv([2*CarbonCarbon 0 0]',2*pi/6));
RB32=(rotationv([2*CarbonCarbon 0 0]',6*pi/6));
RB33=(rotationv([2*CarbonCarbon 0 0]',10*pi/6));
% distance from atom A to the fourth neigbour B is: norm([CarbonCarbon 0 0]+a1)
```

```
fou=norm([CarbonCarbon 0 0]'+a1);
fourn=[fou 0 0]';
% The angle between the fourth neigbour B and the x axis is calculated
% as a=CarbonCarbon*sqrt(3); a1=[3*a/(sqrt(3)*2),a/2,0];
% theta = atan((a/2)/(CarbonCarbon+3*a/(sqrt(3)*2))=atan(sqrt(3)/5)
teta = atan(sqrt(3)/5);
RB41=rotationv(fourn,teta); RB42=rotationv(fourn,2*pi/3-teta);
RB43=rotationv(fourn,2*pi/3+teta); RB44=rotationv(fourn,4*pi/3-teta);
RB45=rotationv(fourn,4*pi/3+teta); RB46=rotationv(fourn,2*pi-teta);
%%
% Vectors from the atom B to its neigbours, we use the corresponding
% vectors w.r.t the atom A
RB1=RA1; RB2=RA2; RB3=RA3; RB4=RA4; RB5=RA5; RB6=RA6;
RA11=rotationv(RB11,pi/3); RA12=rotationv(RB12,pi/3);
RA13=rotationv(RB13,pi/3); RA31=rotationv(RB31,-2*pi/6);
RA32=rotationv(RB32,-2*pi/6);RA33=rotationv(RB33,-2*pi/6);
RA42=rotationv(RB41,pi/3); RA43=rotationv(RB42,pi/3);RA44=rotationv(RB43,pi/3);
RA45=rotationv(RB44,pi/3); RA46=rotationv(RB45,pi/3);RA41=rotationv(RB46,pi/3);
% number of points in gamma branch GM is GMnbrpnt, the
% rest are adjusted by the reletive length of the branch
GMnbrpnt=150; MKnbrpnt=round(GMnbrpnt*norm(MK)/norm(GM));
KGnbrpnt=round(GMnbrpnt*norm(KG)/norm(GM));
branchnum=0;
for branch=1:3
 branchnum=branchnum+1;
 if branchnum==1, nbrpnts=GMnbrpnt; end
 if branchnum==2, nbrpnts=MKnbrpnt; end
```

```
 if branchnum==3, nbrpnts=KGnbrpnt; end
 for k=1:nbrpnts
 if branchnum==1, kvec=(1/nbrpnts)*k*GM; end
 if branchnum==2, kvec=GM+(1/nbrpnts)*k*(MK); end
 if branchnum==3, kvec=GM+MK+(1/nbrpnts)*k*(KG); end
%%
% D matrices for atom A up to the forth neighbour - - - - - - - - - -
DAA1=rotation(K1,0)+rotation(K1,2*pi/3)+rotation(K1,4*pi/3);
DAA2=rotation(K2,pi/6)+rotation(K2,pi/3+pi/6)+...
rotation(K2,2*pi/3+pi/6)+rotation(K2,3*pi/3+pi/6)+...
rotation(K2,4*pi/3+pi/6)+rotation(K2,5*pi/3+pi/6);
DAA3=rotation(K3,pi/3)+rotation(K3,pi)+rotation(K3,5*pi/3);
DAA4=rotation(K4,teta)+rotation(K4,2*pi/3-teta)+rotation(K4,2*pi/3+teta)+...
rotation(K4,4*pi/3-teta)+rotation(K4,4*pi/3+teta)+rotation(K4,2*pi-teta);
DA=rotation(K2,pi/6)*exp(i*dot(kvec,RA1))+rotation(K2,pi/3+pi/6)*...
exp(i*dot(kvec,RA2))+rotation(K2,2*pi/3+pi/6)*exp(i*dot(kvec,RA3))+...
rotation(K2,3*pi/3+pi/6)*exp(i*dot(kvec,RA4))+rotation(K2,4*pi/3+pi/6)*...
exp(i*dot(kvec,RA5))+rotation(K2,5*pi/3+pi/6)*exp(i*dot(kvec,RA6));
DAA=DAA1+DAA2+DAA3+DAA4-DA;
DAB1=rotation(K1,0)*exp(i*dot(kvec,RB11-cc))+rotation(K1,2*pi/3)*...
exp(i*dot(kvec,RB12-cc))+rotation(K1,4*pi/3)*exp(i*dot(kvec,RB13-cc));
DAB3=rotation(K3,pi/3)*exp(i*dot(kvec,RB31-cc))+rotation(K3,pi)*...
exp(i*dot(kvec,RB32-cc))+rotation(K3,5*pi/3)*exp(i*dot(kvec,RB33-cc));
DAB4=rotation(K4,teta)*exp(i*dot(kvec,RB41-cc))+rotation(K4,2*pi/3-teta)*...
exp(i*dot(kvec,RB42-cc))+rotation(K4,2*pi/3+teta)*exp(i*dot(kvec,RB43-cc))+...
rotation(K4,4*pi/3-teta)*exp(i*dot(kvec,RB44-cc))+rotation(K4,4*pi/3+teta)*...
exp(i*dot(kvec,RB45-cc))+rotation(K4,2*pi-teta)*exp(i*dot(kvec,RB46-cc));
```

```
DAB=-(DAB1+DAB3+DAB4);
% D matrices for atom B up to the forth neighbour - - - - - - - - - -
DBB1=rotation(K1,2*pi/6)+rotation(K1,pi)+rotation(K1,5*pi/3);
DBB2=rotation(K2,pi/6)+rotation(K2,pi/3+pi/6)+rotation(K2,2*pi/3+pi/6)+...
rotation(K2,3*pi/3+pi/6)+rotation(K2,4*pi/3+pi/6)+rotation(K2,5*pi/3+pi/6);
DBB3=rotation(K3,0)+rotation(K3,2*pi/3)+rotation(K3,4*pi/3);
DBB4=rotation(K4,pi/3-teta)+rotation(K4,pi/3+teta)+rotation(K4,pi-teta)+...
rotation(K4,pi+teta)+rotation(K4,5*pi/3-teta)+rotation(K4,5*pi/3+teta);
DB=rotation(K2,pi/6)*exp(i*dot(kvec,RB1))+rotation(K2,pi/3+pi/6)*...
exp(i*dot(kvec,RB2))+rotation(K2,2*pi/3+pi/6)*exp(i*dot(kvec,RB3))+...
rotation(K2,3*pi/3+pi/6)*exp(i*dot(kvec,RB4))+rotation(K2,4*pi/3+pi/6)*...
exp(i*dot(kvec,RB5))+rotation(K2,5*pi/3+pi/6)*exp(i*dot(kvec,RB6));
DBB=DBB1+DBB2+DBB3+DBB4-DB;
DBA1=rotation(K1,2*pi/6)*exp(i*dot(kvec,RA11+cc))+rotation(K1,pi)*...
exp(i*dot(kvec,RA12+cc))+rotation(K1,5*pi/3)*exp(i*dot(kvec,RA13+cc));
DBA3=rotation(K3,0)*exp(i*dot(kvec,RA31+cc))+rotation(K3,2*pi/3)*...
exp(i*dot(kvec,RA32+cc))+rotation(K3,4*pi/3)*exp(i*dot(kvec,RA33+cc));
DBA4=rotation(K4,pi/3-teta)*exp(i*dot(kvec,RA41+cc))+...
rotation(K4,pi/3+teta)*exp(i*dot(kvec,RA42+cc))+rotation(K4,pi-teta)*...
exp(i*dot(kvec,RA43+cc))+rotation(K4,pi+teta)*exp(i*dot(kvec,RA44+cc))...
 +rotation(K4,5*pi/3-teta)*exp(i*dot(kvec,RA45+cc))+...
rotation(K4,5*pi/3+teta)*exp(i*dot(kvec,RA46+cc));
DBA=-(DBA1+DBA3+DBA4);
D=[DAA DAB; DBA DBB];
w=sqrt(eig(D)/(M))/(c*100);
if branchnum==1,plot(k,w,'.b');hold on; end
 if branchnum==2, plot(k+GMnbrpnt,w,'.b');hold on; end
```

```
 if branchnum==3, plot(k+GMnbrpnt+MKnbrpnt,w,'.b');hold on; end ;
 end
end
function rotatedK = rotation(K,theta); % this rotates matrices
Utheta = [cos(theta),sin(theta),0; -sin(theta),cos(theta),0; 0,0,1];
rotatedK = inv(Utheta)*K*Utheta;
function f = rotationv(v,theta); % this rotates vectors
f = [[cos(theta),-sin(theta),0];[sin(theta),cos(theta),0];[0,0,1]]*v;
```

APPENDIX B

THE CASE OF REPEATED EIGENVALUES

Let $\mathbf{D}$ be an operator which can be diagonalized; *i.e.*, its eigenvectors form a complete set. And let operators $\mathbf{A}$, $\mathbf{B}$ in the general eigenvalue problem:

$$\mathbf{A}\mathbf{q}_a = a\mathbf{B}\mathbf{q}_a, \tag{172}$$

be such that the eigenvectors form a complete set. Now consider operator $\mathbf{D}$ which commutes with $\mathbf{A}$ and $\mathbf{B}$:

$$\mathbf{D}\mathbf{A}(\mathbf{q}) = \mathbf{A}\mathbf{D}(\mathbf{q}) \ , \ \mathbf{D}\mathbf{B}(\mathbf{q}) = \mathbf{B}\mathbf{D}(\mathbf{q}). \tag{173}$$

We shall prove that there exists eigenvectors $\mathbf{q}_a^i, i = 1, 2, ...,$ of (172) that are also eigenvectors of $\mathbf{D}$: $\mathbf{D}\mathbf{q}_a^i = \lambda_i \mathbf{q}_a^i$. To this end let $\mathbf{Q}_a$ denote the subspace containing all the eigenvectors of (172) with eigenvalue a. That is:

$$\mathbf{q} \in \mathbf{Q}_a \iff \mathbf{A}\mathbf{q} = a\mathbf{B}\mathbf{q}. \tag{174}$$

First we show that $\mathbf{D}$ is $\mathbf{Q}_a$-invariant, that is:

$$\mathbf{q} \in \mathbf{Q}_a \Rightarrow \mathbf{D}\mathbf{q} \in \mathbf{Q}_a. \tag{175}$$

We have:

$$\begin{aligned} \mathbf{q} \quad &\in \quad \mathbf{Q}_a \Rightarrow \mathbf{A}\mathbf{q} = \mathbf{a}\mathbf{B}\mathbf{q} \Rightarrow \mathbf{D}\mathbf{A}\mathbf{q} = \mathbf{a}\mathbf{D}\mathbf{B}\mathbf{q} \Rightarrow \\ \mathbf{A}\mathbf{D}\mathbf{q} = \mathbf{a}\mathbf{B}\mathbf{D}\mathbf{q} \quad &\Rightarrow \quad \mathbf{D}\mathbf{q} \in \mathbf{Q}_a. \end{aligned} \tag{176}$$

Let $\mathbf{D}_a$ denote the restriction of $\mathbf{D}$ to the subspace $\mathbf{Q}_a$:

$$\mathbf{D}_a = \mathbf{D}\,|_{\mathbf{Q}_a} \ . \tag{177}$$

Then

$$\mathbf{D}_a : \mathbf{Q}_a \mapsto \mathbf{Q}_a, \tag{178}$$

and $\mathbf{D}_a$ has a complete set of eigenvectors in $\mathbf{Q}_a$ since it is a restriction of $\mathbf{D}$. Thus there exists $\mathbf{q}_a^1$, $\mathbf{q}_a^2$, $\mathbf{q}_a^3$, ..., $\mathbf{q}_a^n$, ...$\in \mathbf{Q}_a$ such that

$$\mathbf{D}\mathbf{q}_a^i = \lambda_i \mathbf{q}_a^i \ , \ i = 1, 2, ... \tag{179}$$

These $\mathbf{q}_a^i \in \mathbf{Q}_a$ are also eigenvectors of (172) corresponding to a. Replacing the original eigenvectors of (172) by $\mathbf{q}_a^i$ $i = 1, 2, ...$ completes the proof.

Return to the problem of Chapter II, $\mathbf{T_V}$, $\overline{\mathbf{T}}^T\mathbf{K}\mathbf{T}$ and $\overline{\mathbf{T}}^T\mathbf{M}\mathbf{T}$ take the place of $\mathbf{D}$, $\mathbf{A}$ and $\mathbf{B}$, respectively. The translation operator $\mathbf{T_V}$ is the same operator used in quantum mechanics, and its eigenvectors form a complete set. Also it commutes with matrices $\overline{\mathbf{T}}^T\mathbf{M}\mathbf{T}$ and $\overline{\mathbf{T}}^T\mathbf{K}\mathbf{T}$. So in case that ω is a repeated eigenvalue, we showed that we can find eigenvectors in the eigenspace of ω which are also eigenvectors of $\mathbf{T_V}$. As a result, similar to [57] pp. 224-225, if $\overline{\mathbf{T}}^T\mathbf{K}\mathbf{T}\widehat{\mathbf{q}} = -\boldsymbol{\omega}^2\overline{\mathbf{T}}^T\mathbf{M}\mathbf{T}\widehat{\mathbf{q}}$ then $\mathbf{T_V}\widehat{\mathbf{q}} = \lambda\widehat{\mathbf{q}}$.

APPENDIX C

POWER CALCULATION

Representing harmonic forces and displacements in a complex form, makes all the calculation less tedious. However, computation of the power or the work done by these forces is not that straight forward. In chapter 2, we used the fact that the average power of a harmonic force with harmonic displacement equals to:

$$\frac{1}{2}\,\mathrm{Re}\left\{\left\langle \mathbf{F},\dot{\mathbf{q}}\right\rangle\right\}, \tag{180}$$

in which rather than a sinusoidal force and displacement, the harmonic force and displacement are represented by $\mathbf{F} = Fe^{i\omega t}$ and $\mathbf{q} = qe^{i(\omega t-\varphi)}$, respectively. In this part we investigate this relation. We use the phasor diagram of Fig. 39 for illustration.The real input power into the system equals to:

$$Power = F\cos(\omega t).\dot{q}\cos(\omega t-\varphi). \tag{181}$$

We can write 181 as:

$$\frac{F\dot{q}}{2}\left(\cos(2\omega t-\varphi)+\cos(\varphi)\right) \tag{182}$$

which is equal to

$$Power = \frac{F\dot{q}}{2}\cos\varphi + \frac{F\dot{q}}{2}\cos(2\omega t-\varphi). \tag{183}$$

By integrating the power over one period, the second term on the right hand side of eq. 183 vanishes. The second term dictates the fluctuation of the power; absorbing

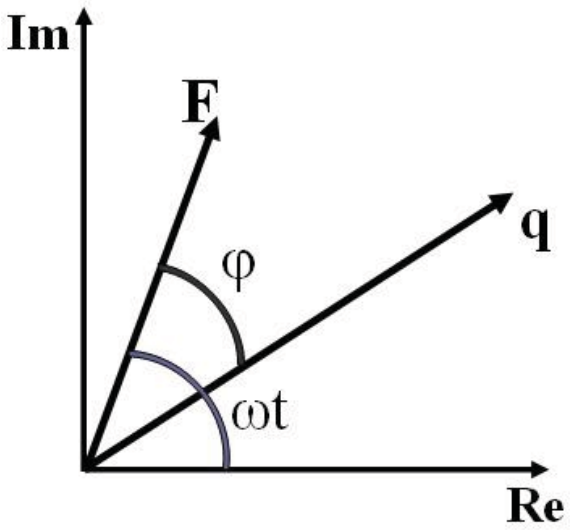

Figure 39: Phasor graph of force and displacement in a harmonic motion

at some instances and giving back in other instances. Thus, the average power over one period is:

$$\frac{\int_{one\ period}(\frac{F\dot{q}}{2}\cos\varphi + \frac{F\dot{q}}{2}\cos(2\omega t - \varphi))dt}{one\ period} = \frac{F\dot{q}}{2}\cos\varphi. \tag{184}$$

In complex plane we can write $\mathbf{F}$ and $\dot{\mathbf{q}}$ in Cartesian coordinates as:

$$\begin{aligned} \mathbf{F} &= a + bi, \\ \dot{\mathbf{q}} &= c + di. \end{aligned} \tag{185}$$

Then we have:

$$\frac{F\dot{q}}{2}\cos\varphi = \frac{ac + bd}{2}. \tag{186}$$

Also:

$$\left\langle \mathbf{F}, \dot{\mathbf{q}} \right\rangle = \mathbf{F}.\overline{\dot{\mathbf{q}}} = (a + bi)(c - di) = ac + bd + i(bc - ad). \tag{187}$$

Consequently,

$$\frac{\int_{one\ period} power}{one\ period} = \frac{1}{2}\,\mathrm{Re}\left\langle \mathbf{F}, \dot{\mathbf{q}} \right\rangle .$$

APPENDIX D

THE RELATION BETWEEN EIGENVALUES IN STATE-SPACE AND CONFIGURATION SPACE

In chapter IV, by transforming the equation of motion from the configuration space to the state-space form, we double the size of the coordinate vector and matrices. Hence we have to justify that during this operation, we do not introduce new eigenvalues; *i.e.*, the number of ω satisfying:

$$\overline{\mathbf{T}}^T(-\omega^2\mathbf{M}+i\omega\mathbf{C}+\mathbf{K})\mathbf{T}\widehat{\mathbf{q}}=\mathbf{0}, \tag{188}$$

and

$$\overline{\mathbf{T}}_S^T(i\omega\mathbf{M}^*+\mathbf{K}^*)\mathbf{T}_S\widehat{\mathbf{q}}_S=\mathbf{0}, \tag{189}$$

are the same. In eq. (188), $\mathbf{M},\mathbf{C}$ and $\mathbf{K}$ are mass, damping and stiffness matrices, respectively. In eq. (189), $\mathbf{M}^*$, $\mathbf{K}^*$ and $\widehat{\mathbf{q}}_S$ are defined as:

$$\mathbf{M}^* \triangleq \begin{bmatrix} \mathbf{0} & \mathbf{M} \\ \mathbf{K} & \mathbf{0} \end{bmatrix},\ \mathbf{K}^* \triangleq \begin{bmatrix} \mathbf{K} & \mathbf{C} \\ \mathbf{0} & -\mathbf{K} \end{bmatrix} \text{ and } \widehat{\mathbf{q}}_S \triangleq \begin{bmatrix} \mathbf{q}_i \\ \widetilde{\mathbf{q}} \\ \dot{\mathbf{q}}_i \\ \dot{\widetilde{\mathbf{q}}} \end{bmatrix}. \tag{190}$$

Also the transformation matrices are defined by:

$$\mathbf{T}_S = \begin{bmatrix} \mathbf{T} & \mathbf{0} \\ \mathbf{0} & \mathbf{T} \end{bmatrix} \text{ and } \overline{\mathbf{T}}_S^T = \begin{bmatrix} \overline{\mathbf{T}}^T & \mathbf{0} \\ \mathbf{0} & \overline{\mathbf{T}}^T \end{bmatrix}. \tag{191}$$

In order to satisfy the eqs. (188) and (189) for non-zero $\widehat{\mathbf{q}}$ and $\widehat{\mathbf{q}}_S$, the determinant of the left hand side operators should be zero:

$$\det(\overline{\mathbf{T}}^T(-\omega^2\mathbf{M}+i\omega\mathbf{C}+\mathbf{K})\mathbf{T}) = 0, \tag{192}$$

$$\det(\overline{\mathbf{T}}_S^T(i\omega\mathbf{M}^*+\mathbf{K}^*)\mathbf{T}_S) = 0. \tag{193}$$

Here, we show that these two conditions are equivalent. By expanding eq. (193), we have:

$$\det\left(\begin{bmatrix} \overline{\mathbf{T}}^T & \mathbf{0} \\ \mathbf{0} & \overline{\mathbf{T}}^T \end{bmatrix}\left(i\omega\begin{bmatrix} \mathbf{0} & \mathbf{M} \\ \mathbf{K} & \mathbf{0} \end{bmatrix}+\begin{bmatrix} \mathbf{K} & \mathbf{C} \\ \mathbf{0} & -\mathbf{K} \end{bmatrix}\right)\begin{bmatrix} \mathbf{T} & \mathbf{0} \\ \mathbf{0} & \mathbf{T} \end{bmatrix}\right) = 0, \tag{194}$$

which is equal to:

$$\det\left(\begin{bmatrix} \overline{\mathbf{T}}^T\mathbf{K} & \overline{\mathbf{T}}^T(i\omega\mathbf{M}+\mathbf{C}) \\ i\omega\overline{\mathbf{T}}^T\mathbf{K} & -\overline{\mathbf{T}}^T\mathbf{K} \end{bmatrix}\begin{bmatrix} \mathbf{T} & \mathbf{0} \\ \mathbf{0} & \mathbf{T} \end{bmatrix}\right) = 0, \tag{195}$$

and this can be simplified to:

$$\det\left(\begin{bmatrix} \overline{\mathbf{T}}^T\mathbf{K}\mathbf{T} & \overline{\mathbf{T}}^T(i\omega\mathbf{M}+\mathbf{C})\mathbf{T} \\ i\omega\overline{\mathbf{T}}^T\mathbf{K}\mathbf{T} & -\overline{\mathbf{T}}^T\mathbf{K}\mathbf{T} \end{bmatrix}\right) = 0. \tag{196}$$

It has been shown [98] that:

$$\forall\ \mathbf{A},\mathbf{B},\mathbf{C},\mathbf{D}\in\mathbb{C}^{n\times n};\ \det\left(\begin{bmatrix} \mathbf{A} & \mathbf{B} \\ \mathbf{C} & \mathbf{D} \end{bmatrix}\right) = \det(\mathbf{AD}-\mathbf{CB})\ \text{ when }\ \mathbf{AC}=\mathbf{CA}. \tag{197}$$

Since $\overline{\mathbf{T}}^T\mathbf{K}\mathbf{T}$ and $i\omega\overline{\mathbf{T}}^T\mathbf{K}\mathbf{T}$ obviously commute, we use this theorem to simplify eq. (196) as:

$$\det\left(-\left(\overline{\mathbf{T}}^T\mathbf{K}\mathbf{T}\right)^2-\left(i\omega\overline{\mathbf{T}}^T\mathbf{K}\mathbf{T}\right)\left(\overline{\mathbf{T}}^T(i\omega\mathbf{M}+\mathbf{C})\mathbf{T}\right)\right) = 0\ , \tag{198}$$

and this can be rephrased as:

$$-\det\left(\overline{\mathbf{T}}^T\mathbf{K}\mathbf{T}\right)\det\left(\overline{\mathbf{T}}^T\mathbf{K}\mathbf{T}+\overline{\mathbf{T}}^T(-\omega^2\mathbf{M}+i\omega\mathbf{C})\mathbf{T}\right)=0, \tag{199}$$

and in a more compact form:

$$\det\left(\overline{\mathbf{T}}^T\mathbf{K}\mathbf{T}\right)\det\left(\overline{\mathbf{T}}^T(-\omega^2\mathbf{M}+i\omega\mathbf{C}+\mathbf{K})\mathbf{T}\right)=0. \tag{200}$$

Comparing eq. (192) and (200), its deduced that transforming equation of motion from the configuration space to the state-space form would not introduce extra $\omega's$ to the solution.

APPENDIX E

SOME LINEAR ALGEBRA

E.1 Banded Matrix

A square matrix $\mathbf{A}_{n\times n} = (a_{ij})$ is called banded matrix with bandwidth $K_1 + K_2 + 1$ if [99]:

$$a_{ij} = 0 \quad \forall\ j < i - K_1 \text{ and } \forall\ j > i + K_2. \tag{201}$$

In a diagonal matrix, $K_1 = K_2 = 0$, and in a tridiagonal matrix we have $K_1 = 1$,

$K_2 = 1$. The stiffness matrix is banded for most of the systems. As we increase the number of interaction between neighbors, the bandwidth of the stiffness matrix increases accordingly.

E.2 Determinant

Let $p = (p_1, p_2, ...p_n)$ be one of $n!$ permutation of $(1, 2, ..., n)$. Determinant of an $n \times n$ matrix $\mathbf{A} = [a_{ij}]$ is defined by Leibniz formula to be the scalar:

$$\det(\mathbf{A}) = \sum_p \sigma(p) a_{1p_1} a_{2p_2} ... a_{np_n}, \tag{202}$$

in which the sum is taken over all the $n!$ permutation and

$$\sigma(p) = \begin{cases} 1 \text{ if } p \text{ is an even permutation of } (1, 2, ..., n) \\ -1 \text{ if } p \text{ is an odd permutation of } (1, 2, ..., n) \end{cases}. \tag{203}$$

By even/odd permutation, we mean the number of element swaps necessary to get $(p_1, p_2, ...p_n)$ from $(1, 2, ..., n)$ is even/odd. Note that each term in (202) contains exactly one entry from each row and each column of $\mathbf{A}$. For example of $(5, 3, 2, 4, 1, 7, 6)$ we can write:

$$(5, 3, 2, 4, 1, 7, 6) \rightarrow (5, 3, 2, 4, 1, 6, 7) \rightarrow (1, 3, 2, 4, 5, 6, 7) \rightarrow (1, 2, 3, 4, 5, 6, 7)\,. \quad (204)$$

We used three swaps and hence $\sigma(p) = -1$.

REFERENCES

[1] L.J. Gibson, M.F. Ashby, *Cellular Solids:Structure and properties*, 2nd ed. 1997, Cambridge University Press.

[2] "http://renraw.com/365/tag/bw/", accessed on October 15, 2010.

[3] N. G. Chopra, R. J. Luyken, et al. "Boron-Nitride Nanotubes," *Science*, vol. 269, no. 5226, pp. 966-967, 1995.

[4] M. Remskar, Z. Skraba, et al. "MoS2 as microtubes," *Applied Physics Letters*, vol. 69, no. 3, pp. 351-353, 1996.

[5] O. Stephan, P. M. Ajayan, et al. "Doping Graphitic and Carbon Nanotube Structures with Boron and Nitrogen," *Science*, vol. 266, no. 5191, pp. 1683-1685, 1994.

[6] M. Zhang, Y. Bando, et al. "Synthesis of nanotubes and nanowires of silicon oxide," *Journal of Materials Science Letters*, vol. 18, no. 23, pp. 1911-1913, 1999.

[7] C. Y. Li and T. W. Chou "Static and dynamic properties of single-walled boron nitride nanotubes," *Journal of Nanoscience and Nanotechnology*, vol. 6, no. 1, pp. 54-60, 2006.

[8] C. Y. Li and T. W. Chou "A structural mechanics approach for the analysis of carbon nanotubes," *International Journal of Solids and Structures*, vol. 40, no. 10, pp. 2487-2499, 2003.

[9] R. S. Lakes, "Deformation mechanisms in negative Poisson's ratio materials: structural aspects," *Journal of Materials Science*, vol. 26, no 9, pp. 2287-2292, 1991.

[10] K. E. Evans, "The design of doubly curved sandwich panels with honeycomb cores," *Composite Structures,* vol. 17, no 2, pp. 95-111, 1991.

[11] C. T. Herakovich,"Composite laminates with negative through-the-thickness Poisson's ratios," *Journal of composite materials*, vol.18, no 5, pp.447 -455, 1984

[12] Ruzzene, M., F. Scarpa, et al. "Wave beaming effects in two-dimensional cellular structures." Smart Materials & Structures 12(3): 363-372, 2003.

[13] "http://www.ipm.virginia.edu/newres/pcm.topo", accessed on August 20, 2010.

[14] R. Hempelmann, *Quasielastic neutron scattering and solid state diffusion*, Oxford University Press, 2000.

[15] S. Rols, Z. Benes, et al. "Phonon density of states of single-wall carbon nanotubes," *Physical Review Letters*, vol. 85, no. 24, pp. 5222-5225, 2000.

[16] A. Gruneis, R. Saito, et al. "Determination of two-dimensional phonon dispersion relation of graphite by Raman spectroscopy," *Physical Review B*, vol. 65, no. 15, pp. 7, 2002.

[17] R. A. Aziz , M. J. Slaman, et al. "Exchange Coulomb Potential-Energy Curves for He-He, and Related Physical Properties." *Molecular Physics* 77(2): 321-337, 1992.

[18] D. M. Ceperley "Path-Integrals in the Theory of Condensed Helium," *Reviews of Modern Physics*, vol. 67, no. 2, pp. 279-355, 1995.

[19] M. I. Baskes, M. Asta, et al. "Determining the range of forces in empirical many-body potentials using first-principles calculations," Philosophical Magazine a-Physics of Condensed Matter Structure Defects and Mechanical Properties, vol. 81, no. 4, pp. 991-1008, 2001.

[20] R. Aljishi and G. Dresselhaus "Lattice-Dynamical Model for Graphite," *Physical Review B*, vol. 26, no. 8, pp. 4514-4522, 1982.

[21] R. A. Jishi and M. S. Dresselhaus "Phonon Modes in Graphite, C-60, and C-60 Based Fibers," *Physical Review B*, vol. 45, no. 19, pp. 11305-11311, 1992.

[22] R. A. Jishi, L. Venkataraman, et al. "Phonon Modes in Carbon Nanotubules," *Chemical Physics Letters*, vol. 209, no. 1-2, pp. 77-82, 1993.

[23] T. Aizawa, R. Souda, et al. "Bond Softening in Monolayer Graphite Formed on Transition-Metal Carbide Surfaces," *Physical Review B*, vol. 42, no. 18, pp. 11469-11478, 1990.

[24] C. Oshima, T. Aizawa, et al. "Surface Phonon-Dispersion Curves of Graphite (001) Over the Entire Energy Region," *Solid State Communications*, vol. 65, no. 12, pp. 1601-1604, 1988.

[25] R Saito, G Dresselhaus, MS Dresselhaus, *Physical properties of carbon nanotubes*, Imperial College Press, 1998.

[26] M. T. Dove, *Introduction to Lattice Dynamics*, Cambridge University Press, 1 edition, 2005.

[27] M. Razeghi, *Fundamentals of Solid State Engineering*, 3rd edition, Springer-Verlag, 2009.

[28] L. Brillouin, *Wave Propagation in Periodic Structures*. New York: Dover Phoenix Editions, 1946.

[29] M. Cherchi "Bloch analysis of finite periodic microring chains." *Applied Physics B-Lasers and Optics* 80(1): 109-113, 2005

[30] Y. Tanaka, Y. Tomoyasu, et al. "Band structure of acoustic waves in phononic lattices: Two-dimensional composites with large acoustic mismatch." *Physical Review B* 62(11): 7387-7392, 2000.

[31] T. Miyashita "Sonic crystals and sonic wave-guides." *Measurement Science & Technology* 16(5): R47-R63, 2005.

[32] M. A. Heckl "Investigations on the Vibrations of Grillages and Other simple Beam Structures", *Journal of the Acoustical Society of America* 36(7): 1335-1343, 1964.

[33] D. J. Mead "Free wave propagation in periodically supported, infinite beams", *Journal of Sound and Vibration* 11(2): 181-197, 1970.

[34] D. J. Mead "A General theory of harmonic wave-propagation in linear periodic systems with multiple coupling", *Journal of Sound and Vibration*, vol. 27, pp. 235-260, 1973.

[35] G. Sengupta "Natural Flexural Waves And Normal Modes of Periodically-Supported Beams and Plates", *Journal of Sound and Vibration,* 13(1): 89-101, 1970.

[36] M. Ruzzene and A. Baz "Control of wave propagation in periodic composite rods using shape memory inserts," *Journal of Vibration and Acoustics-Transactions of the ASME,* vol. 122, no. 2, pp. 151-159, 2000.

[37] C. Pany and S. Parthan "Axial wave propagation in infinitely long periodic curved panels," *Journal of Vibration and Acoustics-Transactions of the ASME*, vol. 125, no. 1, pp. 24-30, 2003.

[38] F. Treyssede "Elastic waves in helical waveguides." *Wave Motion* 45(4): 457-470, 2008.

[39] F. Romeo, A. Paolone "Wave propagation in three-coupled periodic structures." *Journal of Sound and Vibration* 301(3-5): 635-648, 2007

[40] T. Kohrs, B. A. T. Petersson "Wave propagation in light weight profiles with truss-like cores: Wavenumber content, forced response and influence of periodicity perturbations." *Journal of Sound and Vibration* 304(3-5): 691-721, 2007

[41] D. Duhamel, B. R. Mace, et al. "Finite element analysis of the vibrations of waveguides and periodic structures." *Journal of Sound and Vibration* 294(1-2): 205-220, 2006.

[42] L. Houillon, M. N. Ichchou, et al. "Wave motion in thin-walled structures." *Journal of Sound and Vibration* 281(3-5): 483-507. 2005

[43] H. M. Saeed, F. Vestroni "Simulation of combined systems by periodic structures: The wave transfer matrix approach." *Journal of Sound and Vibration* 213(1): 55-73, 1998.

[44] A. Baz "Active control of periodic structures," *Journal of Vibration and Acoustics-Transactions of the ASME*, vol. 123, no. 4, pp. 472-479, 2001.

[45] M. ElRaheb "Frequency response of a two-dimensional trusslike periodic panel." *Journal of the Acoustical Society of America* 101(6): 3457-3465, 1997.

[46] D. J. Mead "Wave propagation in continuous periodic structures: Research contributions from Southampton, 1964-1995", *Journal of Sound and Vibration*, vol. 190, pp. 495-524, Feb 1996.

[47] R. M. Orris, and M. Petyt "Finite-Element Study of Harmonic Wave-Propagation in Periodic Structures", *Journal of Sound and Vibration* 33(2): 223-236, 1974.

[48] A. S. Phani, J. Woodhouse, and N. A. Fleck "Wave propagation in two-dimensional periodic lattices", *Journal of the Acoustical Society of America*, vol. 119, pp. 1995-2005, Apr 2006.

[49] A. Askar "Dispersion relation and wave solution for anharmonic lattices and Korteweg Delaunays Vries continua," *Proceedings of the Royal Society of London Series a-Mathematical Physical and Engineering Sciences*, vol. 334, no. 1596, pp. 83-94, 1973.

[50] G. Chakraborty and A. K. Mallik "Dynamics of a weakly non-linear periodic chain," *International Journal of Non-Linear Mechanics*, vol. 36, no. 2, pp. 375-389, 2001.

[51] J. M. Harrison, P. Kuchment, et al. "On occurrence of spectral edges for periodic operators inside the Brillouin zone," *Journal of Physics a-Mathematical and Theoretical*, vol. 40, no. 27, pp. 7597-7618, 2007.

[52] S. D. M. Adams, R. V. Craster, et al. "Bloch waves in periodic multi-layered acoustic waveguides," *Proceedings of the Royal Society a-Mathematical Physical and Engineering Sciences*, vol. 464, no. 2098, pp. 2669-2692, 2008.

[53] J.D. Patterson, B. C. Bailey, *Solid-State Physics: Introduction to the Theory*, Springer Berlin Heidelberg, 2009.

[54] F. Bloch "Über die Quantenmechanik der Elektronen in Kristallgittern." *Z. Physik* 52, 555-600, 1928.

[55] R. S. Langley "A note on the force boundary-conditions for 2-Dimensional periodic structures with corner freedoms", *Journal of Sound and Vibration*, vol. 167, pp. 377-381, Oct 1993.

[56] P. O. Lowdin, *Linear Algebra for Quantum Theory*, Wiley-Interscience, 1 edition, 1998.

[57] D. J. Griffiths, *Introduction to Quantum Mechanics,* Benjamin Cummings, 2 edition, 2004.

[58] J. J. Quinn, Kyung-Soo Yi, *Solid State Physics: Principles and Modern Applications*, Springer, 1 edition, 2009.

[59] "http://www.eng.fsu.edu/~dommelen/quantum/style_a/nt_diag.html#note:diag", accessed on November 4th, 2010.

[60] Steven G. Johnson, 2008 September 26, Personal correspondence.

[61] Y.Z. Wang, Y. Z., F. M. Li, et al. "Tuning of band gaps for a two-dimensional piezoelectric phononic crystal with a rectangular lattice.", Acta Mechanica Sinica 25(1): 65-71, 2009.

[62] Y.Z. Wang, Y. Z., F. M. Li, et al. "Elastic wave band gaps in magnetoelectroelastic phononic crystals.", *Wave Motion* 46(1): 47-56, 2009.

[63] C. Yilmaz, G. M. Hulbert, et al. "Phononic band gaps induced by inertial amplification in periodic media.", *Physical Review B* 76(5): 9, 2007.

[64] J. S. Jensen "Phononic band gaps and vibrations in one- and two-dimensional mass-spring structures.", *Journal of Sound and Vibration* 266(5): 1053-1078, 2003.

[65] S. Gonella, M. Ruzzene "Analysis of in-plane wave propagation in hexagonal and re-entrant lattices.", *Journal of Sound and Vibration* 312(1-2): 125-139, 2008.

[66] M. S. Kushwaha, , P. Halevi, et al. "Acoustic Band-Structure of Periodic Elastic Composites", *Physical Review Letters* 71(13): 2022-2025, 1993.

[67] Vasseur, J. O., P. A. Deymier, et al. "Absolute forbidden bands and waveguiding in two-dimensional phononic crystal plates." *Physical Review B* 77(8): 15, 2008.

[68] L. Meirovitch, *Fundamentals of Vibrations*, 1st ed. 2002, McGraw-Hill.

[69] D. J. Mead and S. Markus "Forced Vibration of a 3-Layer, Damped Sandwich Beam with Arbitrary Boundary Conditions," *Journal of Sound and Vibration*, vol. 10, no. 2, pp. 163-&, 1969.

[70] D. J. Mead "Wave-Propagation and Natural Modes in Periodic Systems .1. Mono-Coupled Systems," *Journal of Sound and Vibration*, vol. 40, no. 1, pp. 1-18, 1975.

[71] M. G. Faulkner and D. P. Hong "Free-Vibrations of a Mono-Coupled Periodic System," *Journal of Sound and Vibration*, vol. 99, no. 1, pp. 29-42, 1985.

[72] A. H. Vonflotow "Disturbance Propagation in Structural Networks," *Journal of Sound and Vibration*, vol. 106, no. 3, pp. 433-450, 1986.

[73] Y. Yong and Y. K. Lin "Propagation of Decaying Waves in Periodic and Piecewise Periodic Structures of Finite Length," *Journal of Sound and Vibration*, vol. 129, no. 1, pp. 99-118, 1989.

[74] E. Manconi and B. R. Mace "Wave characterization of cylindrical and curved panels using a finite element method," *Journal of the Acoustical Society of America*, vol. 125, no. 1, pp. 154-163, 2009.

[75] R. S. Langley, N. S. Bardell, et al. "The response of two-dimensional periodic structures to harmonic point loading: A theoretical and experimental study of a beam grillage," *Journal of Sound and Vibration*, vol. 207, no. 4, pp. 521-535, 1997.

[76] D. L. Yu, J. Y. Fang, et al. "Triply coupled vibrational band gap in a periodic and nonsymmetrical axially loaded thin-walled Bernoulli-Euler beam including the warping effect," Physics Letters A, vol. 373, no. 38, pp. 3464-3469, 2009.

[77] S. Mukherjee and E. H. Lee "Dispersion-Relations and Mode Shapes for Waves in Laminated Viscoelastic Composites by Variational Methods," *International Journal of Solids and Structures*, vol. 14, no. 1, pp. 1-13, 1978.

[78] R. Sprik and G. H. Wegdam "Acoustic band gaps in composites of solids and viscous liquids," *Solid State Communications*, vol. 106, no. 2, pp. 77-81, 1998.

[79] B. Merheb, P. A. Deymier, et al. "Elastic and viscoelastic effects in rubber/air acoustic band gap structures: A theoretical and experimental study," *Journal of Applied Physics*, vol. 104, no. 6, pp. 9, 2008.

[80] E. Tassilly "Propagation of Bending Waves in a Periodic-Beam," *International Journal of Engineering Science*, vol. 25, no. 1, pp. 85-94, 1987.

[81] J. Esteban and C. A. Rogers "Wave localization due to material damping," *Computer Methods in Applied Mechanics and Engineering*, vol. 177, no. 1-2, pp. 93-107, 1999.

[82] I. E. Psarobas "Viscoelastic response of sonic band-gap materials," *Physical Review B*, vol. 64, no. 1, pp. 4, 2001.

[83] M. I. Hussein "Theory of damped Bloch waves in elastic media," *Physical Review B*, vol. 80, no. 21, pp. 4, 2009.

[84] C. Y. Lee, M. J. Leamy, et al. "Frequency band structure and absorption predictions for multi-periodic acoustic composites," *Journal of Sound and Vibration*, vol. 329, no. 10, pp. 1809-1822, 2010.

[85] L. Meirovitch, *Computational Methods in Structural Dynamics*, Springer; 1 edition, 1980.

[86] O. Brand, H. Baltes "Micromachined Resonant Sensors - an Overview," *Sensors Update*, Volume 4, Issue 1, pp. 3-51, 1998.

[87] R. A. Buser, in: Sensors - A Comprehensive Survey, Volume 7, Bau, H. H., de Rooij, N. F., and Kloeck,

B. (eds.); Weinheim: VCH, pp. 205-284, 1994.

[88] K. Kokubun, M. Hirata, et al. "Frequency-Dependence of a Quartz Oscillator on Gas-Pressure," *Journal of Vacuum Science & Technology a-Vacuum Surfaces and Films*, vol. 3, no. 6, pp. 2184-2187, 1985.

[89] M. Christen "Air and Gas Damping of Quartz Tuning Forks," Sensors and Actuators, vol. 4, no. 4, pp. 555-564, 1983.

[90] M. V. Andres, K. W. H. Foulds, et al. "Nonlinear Vibrations and Hysteresis of Micromachined Silicon Resonators Designed as Frequency-Out Sensors," *Electronics Letters*, vol. 23, no. 18, pp. 952-954, 1987.

[91] Z. Cui, D. Y. Chen, et al. "Modelling and experiment of a silicon resonant pressure sensor," *Analog Integrated Circuits and Signal Processing*, vol. 32, no. 1, pp. 29-35, 2002.

[92] O. Paul, O. Brand, et al. "VACUUM GAUGING WITH COMPLEMENTARY METAL-OXIDE-SEMICONDUCTOR MICROSENSORS," Journal of Vacuum Science & Technology a-Vacuum Surfaces and Films, vol. 13, no. 3, pp. 503-508, 1995.

[93] F. Farzbod, M.J. Leamy "The treatment of forces in Bloch analysis," *Journal of Sound Vibration*, vol. 325, pp. 545–551, 2009.

[94] F. Farzbod, M.J. Leamy "Analysis of Bloch's Method and the Propagation Technique in Periodic Structures," *Journal of Vibration and Acoustics-Transactions of the ASME*, in press, 2010.

[95] K. Manktelow, M.J. Leamy, M. Ruzzene, "Multiple Scales Analysis of Wave-Wave Interactions in a Cubically Nonlinear Monoatomic Chain," *Journal of Nonlinear Dynamics*, DOI 10.1007/s11071-010-9796-1, 2010.

[96] C. D. Meyer, *Matrix Analysis and Applied Linear Algebra*, SIAM: Society for Industrial and Applied Mathematics, 2001.

[97] A. Rubio, J. Corkill, M. Cohen. "Theory of graphitic boron nitride nanotubes". *Physical Review B,* 49: 5081, 1994.

[98] Dennis S. Bernstein, *Matrix Mathematics: Theory, Facts, and Formulas with Application to Linear Systems Theory*; Princeton University Press, 2005.

[99] G. H. Golub and C. F. Van Loan, *Matrix Computations,* Johns Hopkins Studies in Mathematical Sciences, 3rd Edition, 1996.

[100] Y. Wang, J. J. Wang, et al. "A mixed-space approach to first-principles calculations of phonon frequencies for polar materials," *Journal of Physics-Condensed Matter*, vol. 22, no. 20, pp. 5, 2010.

[101] J. Serrano, A. Bosak, et al. "Vibrational properties of hexagonal boron nitride: Inelastic X-ray scattering and ab initio calculations," *Physical Review Letters*, vol. 98, no. 9, pp. 4, 2007.

[102] A. P. Seyranian, E. Lund, et al. "Multiple-Eigenvalues in Structural Optimization Problems," Structural Optimization, vol. 8, no. 4, pp. 207-227, 1994.